Durham E-Theses

Decomposition pathways of an S-nitroso sugar, S-nitroso dithiols and the reaction of S-nitrosothiols with iron complexes

Parkin, David

Decomposition Pathways of an *S*-Nitroso Sugar, *S*-Nitroso Dithiols and the Reaction of *S*-Nitrosothiols with Iron Complexes

By

David Parkin MSci (Hons.)

(Grey College)

A thesis submitted for the degree of Doctor of Philosophy in the Department of Chemistry, University of Durham.

November 2002

Abstract

Decomposition pathways of S-nitroso-1-thio-β-D-glucose tetraacetate were studied at physiological pH (pH 7.4) and compared with other low molecular weight S-nitrosothiols. Three large differences in reactivity were observed. A larger than expected rate of reaction for the thermal decomposition and reaction with cysteine was found. The second order rate constant obtained for the copper catalysed decomposition was very small compared with other more reactive S-nitrosothiols.

The decomposition pathways of the S-nitrosated derivatives of two 1,4 dithiols and a vicinal dithiol were studied. Rate of reaction via the thermal decomposition pathway was found to be much greater for the dinitrosated 1,4 dithiols than the dinitrosated vicinal dithiol. The mononitrosated 1,4 dithiols were found to be reasonably stable in acidic solution suggesting that an interaction between two S-nitroso groups on the same molecule could lead to a rapid decomposition. Conversely the mononitrosated vicinal thiol was found to decompose more rapidly than the analogous 1,4 dithiol compounds in acidic solution and at pH 7.4. The mononitrosated vicinal dithiol decomposed to form quantitative amounts of ammonia at pH 7.4. An interesting feature of the reactivity of the vicinal dithiol towards the S-nitrosothiol functional group was that the thiol form appeared to be an effective nucleophile as well as the thiolate ion forms. Other thiols have a negligible reactivity, except when deprotonated.

It has been found that S-nitrosothiols can transfer NO to an iron(+2) dithiol complex and iron dithiocarbamate complexes at pH 7.4. The iron complexes all have a high affinity for NO in aqueous solution. Primary S-nitrosothiols were found to be able to transfer directly NO^+ to the iron(+2) dithiol complex. However when S-nitrosoglutathione reacted with iron dithiocarbamate complexes NO appeared to be transferred. Evidence was also obtained that tertiary S-nitrosothiols could transfer NO to the iron(+2) dithiol complex. Clearly whether NO or NO^+ is transferred depends on the nature of the S-nitrosothiol and the iron complex. Currently iron(+2) dithiocarbamate complexes are used to detect NO, these findings suggest that the presence of S-nitrosothiols may compromise this experimental procedure.

Acknowledgements

Declaration

The material in this thesis is the result of research carried out in the Chemistry Department at the University of Durham between October 1999 and September 2002. It has not been submitted for any other degree and is the author's own work, except where acknowledged by reference.

Statement of Copyright

To my family.

Contents

Chapter 2: Decomposition Pathways of *S*-Nitroso-1-thio-*β*-D-glucose Tetraacetate.   37

Chapter 3: Decomposition Pathways of *S*-Nitroso Derivatives of Dithiols.

Chapter 1

Introduction

Chapter 1: Introduction

This chapter discusses why nitric oxide (NO) and *S*-nitrosothiol research has become popular in recent years, and summarises the chemistry of *S*-nitrosothiols. It also examines possible applications of *S*-nitrosothiols in medicine.

1.1 A Brief Summary of the Chemistry and Biochemistry of Nitric Oxide

Joseph Priestley discovered NO in 1772 when he reacted nitric acid with several metals.[1] The NO gas released was called nitrous air. For many years NO was considered mainly as an atmospheric pollutant, and is a product of the combustion of fossil fuels. In recent years NO has been found to be involved in many physiological functions, and in 1992 was named molecule of the year by Science magazine.[2]

1.1.1 The Structure and Stability of Nitric Oxide

NO is a neutral molecule which has an unpaired electron so it can be considered a free radical.[3] It is a relatively stable radical because the unpaired electron is delocalised over the structure. Figure 1.1 shows the resonance forms of NO.

$$\cdot N{=}O \longleftrightarrow N{-}O^{\cdot} \longleftrightarrow {}^{-}N{=}O^{+\cdot} \longleftrightarrow {}^{+}N{-}O^{-} \longleftrightarrow {}^{-}N{-}O^{+}$$
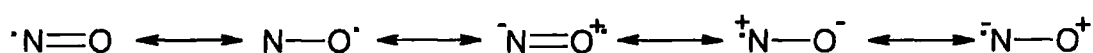
Figure 1.1 The different resonance forms of NO.

The nitrosonium cation NO^{+} is only found as a free species in aqueous solution in very acidic conditions, usually the N(III) species is present as nitrous acid / nitrite.[4] NO has a reduced form that is the nitroxyl anion NO^{-}, which is very unstable and has only been observed directly using pulse radiolysis.[5]

NO reacts with oxygen in aerobic aqueous solutions ultimately forming quantitative amounts of nitrite.[6] The rate equation for the reaction (see equation 1.1) was found to be unchanged over the pH range 1 to 13.[7] Despite arguments over the existence of the intermediate N_2O_3, the series of reactions shown in scheme 1.1 is accepted as the reaction profile.[8]

Rate = $k_3[NO]^2[O_2]$

Equation 1.1 The rate equation for the reaction of NO with oxygen.

$$2NO + O_2 \longrightarrow 2NO_2$$
$$NO_2 + NO \longrightarrow N_2O_3$$
$$N_2O_3 + H_2O \longrightarrow 2H^+ + 2NO_2^-$$
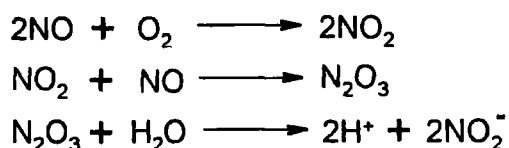
Scheme 1.1 The proposed reactions for NO oxidised to nitrite by oxygen.

It is well known that NO forms coordination complexes with transition metals to form nitrosyl metal complexes. The ligand NO can act as a one or three electron donor and also bridge metal centres. This results in several possible structures that are shown in figure 1.2.[3]
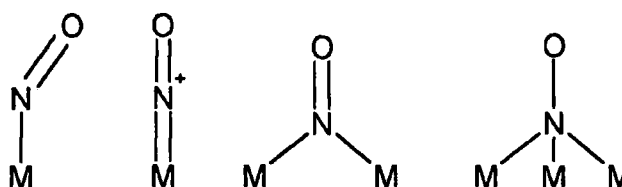
Figure 1.2 The possible coordination modes of NO in metal complexes.

1.1.2 The Discovery of the Endothelium Derived Relaxing Factor

In 1980 it was found that endothelial cells were required for the relaxation of arterial smooth muscle to take place.[9] This triggered research into what was being released by the endothelial cells to cause the relaxation of smooth muscle. The chemical being released was described as the endothelium derived relaxing factor, or EDRF.

NO was found to relax vascular smooth muscle in a similar way to the EDRF by two research groups in 1987.[10,11] Following this research it became evident that NO had an important role to play in how blood flow was controlled by the body.

1.1.3 Guanylate Cyclase

NO was found to be the signaling molecule for the relaxation of vascular smooth muscle. Studies have looked at the subsequent chemistry to determine the receptor for NO, and the mechanism of the next steps in the biological process.

It has been suggested that NO reacts with the iron centre of the protein guanylate cyclase activating the enzyme.[12] A six coordinate nitrosyl iron complex was proposed, followed by the detachment of the histidine from the iron centre. (see scheme 1.2) The release of the axial histidine group is believed to cause the activation of the enzyme.
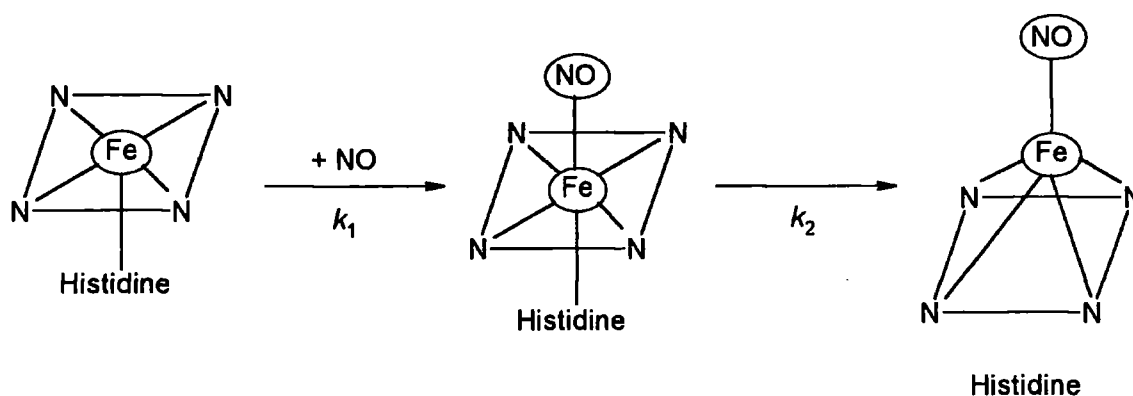
Scheme 1.2 The chemical processes that activate the enzyme guanylate cyclase.

The chemical kinetics of the two processes has been studied, and rate constants obtained were $k_1 = 1.4 \times 10^8$ dm^3 mol^{-1} s^{-1} and $k_2 = 2.4 \times 10^5$ dm^3 mol^{-1} s^{-1} for the second step at 4 °C.[13] It was found that both rate constants were NO dependent suggesting that a second NO molecule reacted with the protein. The release of the axial histidine group could occur by a slower NO independent process as well.

Guanylate cyclase catalyses the conversion of guanosine 5'-triphosphate to guanosine 3',5'-cyclic monophosphate (cGMP). The suggested mechanism is shown in scheme 1.3.[14] A proton is abstracted by the enzyme and this leads to internal nucleophilic attack. The histidine group detached from the iron centre could abstract the proton.
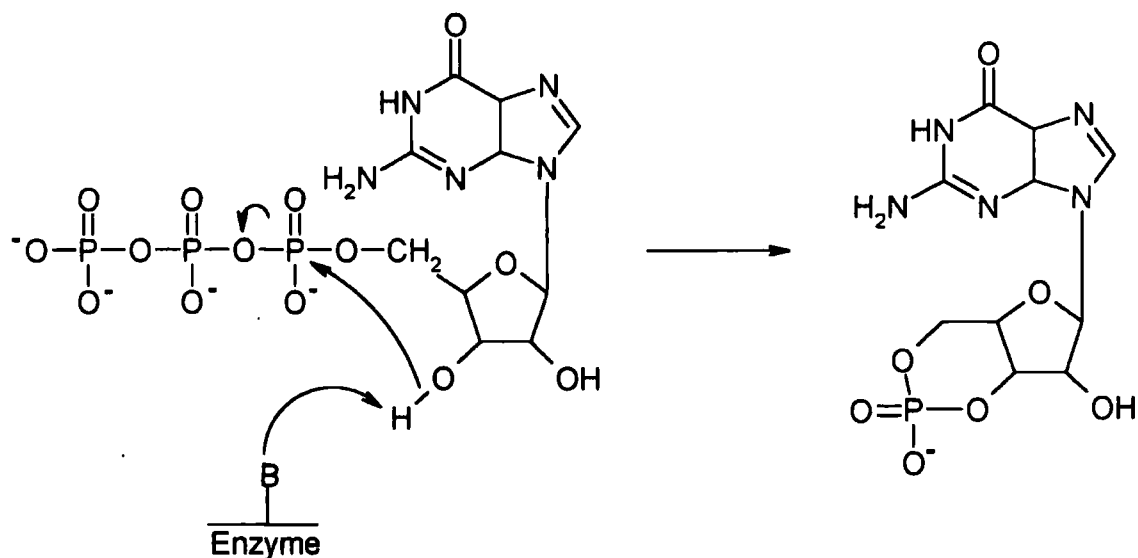
Scheme 1.3 The proposed mechanism for the guanylate cyclase catalysed conversion of guanosine 5'-triphosphate to cGMP.

1.1.4 The Biosynthesis of Nitric Oxide

NO is now known to be generated in the body by the conversion of L-arginine to L-citrulline.[15] N-Hydroxy-L-arginine has been identified as an intermediate in the process.[16] (see scheme 1.4) The reaction also requires oxygen and reduced nicotinamide adenine dinucleotide phosphate (NADPH). The enzyme responsible for the process is called NO synthase (NOS).
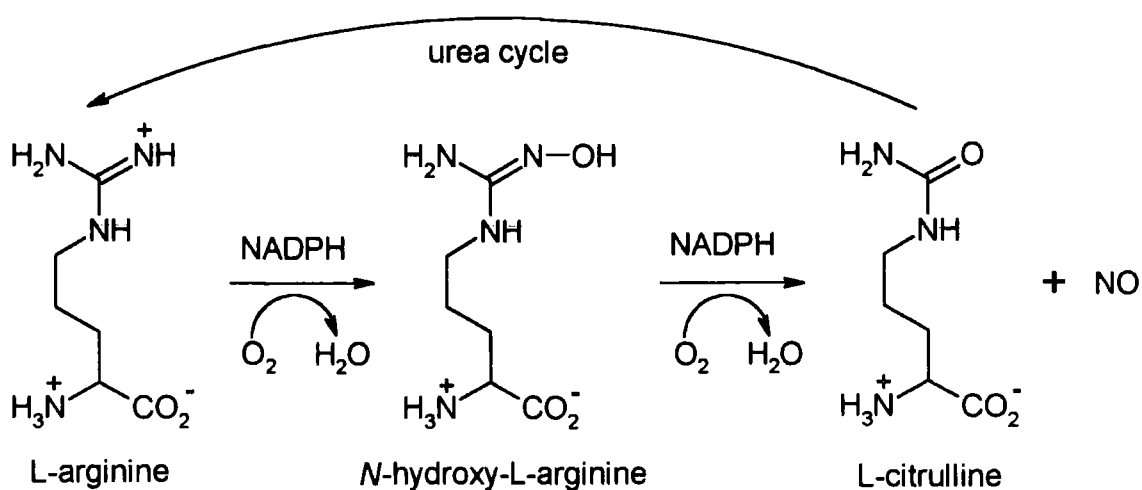
Scheme 1.4 The proposed reactions for the formation of NO from L-arginine.

A study found that when NOS was purified, free NO could not be detected.[17] The addition of the thiol glutathione (GSH) and neocuproine lead to the formation of S-nitrosoglutathione (GSNO) in solution. In a separate experiment when GSH and copper(+2) ions were present free NO was detected. Copper-S-nitrosothiol chemistry is explained in section 1.3.2 The concentration of glutathione in cells has been estimated[18] as 5×10^{-3} M so this could be a physiologically relevant process. This is evidence that NO synthase could form S-nitrosothiols rather than free NO *in vivo*.

1.1.5 The Multiple Roles of Nitric Oxide in the Body

NO is believed to have many roles in the body. For example it has been found that in addition to effecting vasodilation, NO can cause the inhibition of platelet aggregation.[19] Other functions include NO acting as a neurotransmitter in the nervous system and high concentrations being released by macrophages in the immune system to kill bacteria and tumour cells.[20,21]

The activation of the enzyme guanylate cyclase by NO is believed to be the initial step when inhibition of platelet aggregation occurs and is also involved in the function of NO as a neurotransmitter. Macrophages are believed to release NO that then reacts with superoxide to form the strong oxidant peroxynitrite.[22]

1.1.6 The Similarities in the Biological Activity of Nitric Oxide and S-Nitrosothiols

The concentration of S-nitrosothiols in human plasma has been estimated as 7×10^{-6} M.[23] It was found that 96 % was accounted for by S-nitroso proteins of which 82 % was S-nitroso-serum albumin. The remainder is likely to have been low molecular weight S-nitrosothiols, such as GSNO and S-nitrosocysteine.

GSNO and S-nitrosocysteine have been added to human plasma to determine what could happen to low molecular weight S-nitrosothiols *in vivo*.[24] After fifteen minutes both S-nitrosothiols decomposed to less than ten percent of their original concentration. Nearly all the S-nitrosothiol recovered after the reaction was found to be S-nitroso-serum albumin. It

was suggested that serum albumin may act as an NO store and NO is transported to where it is required in the body by low molecular weight thiols.

NO and a series of other vasodilators have been found to require the presence of thiol for vasodilation to occur.[25] The fact that S-nitrosothiols have been found to cause the relaxation of vascular smooth muscle suggests that S-nitrosothiols could be an intermediate in the biological process.

S-Nitrosothiols have also been found to initiate the inhibition of platelet aggregation.[26] It has been suggested that S-nitrosothiol intermediates might be involved *in vivo* in the NO reactions.

1.2 Synthesis and Physical Properties of S-Nitrosothiols

The study of S-nitrosothiol chemistry requires a method for the formation of the S-nitrosothiol and a way of observing the compound in solution. The structure of the S-nitrosothiol functional group is shown in figure 1.3 where R can be a range of organic substituents.

$$R-S-N=O$$
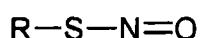
Figure 1.3 The generic structure of S-nitrosothiols.

1.2.1 Methods of Detecting S-Nitrosothiols in Solution

IR analytical techniques can be used to detect characteristic bond frequencies, the nitrogen oxygen bond has a stretching vibration in the region of $1480 - 1530$ cm^{-1} and there is a carbon sulfur bond vibration in the region $600 - 730$ cm^{-1}.[27]

S-Nitrosothiols give characteristic UV / Vis absorbance spectra in solution. There is an absorption peak around 340 nm ($n_o{\rightarrow}\pi^*$) with an extinction coefficient approximately 1000 dm^3 mol^{-1} cm^{-1} and a peak at around 540nm or 590 nm ($n_N{\rightarrow}\pi^*$) with an extinction coefficient approximately 20 dm^3 mol^{-1} cm^{-1}.[28] The exact position of the absorbance maximum for the ($n_N{\rightarrow}\pi^*$) transition, and the ^{15}N NMR chemical shifts in a 3 : 1 D_2O :

CD_3CN solvent mixture for a range of S-nitrosothiols have been published.[29] A correlation between the reduction potential and the ^{15}N NMR chemical shift (using 98 % enriched $Na^{15}NO_2$ as a reference) of several S-nitrosothiols was obtained. This was explained in terms of an electron deficiency at the nitrogen atom making a reduction more favourable.

Primary and secondary S-nitrosothiols are known to be red in colour whereas the tertiary ones are green. It has been suggested that this is due to the preferred conformation of the S-nitrosothiols.[30] Primary and secondary S-nitrosothiols prefer the syn orientation and tertiary ones prefer the anti orientation. The syn and anti structures are shown in figure 1.4.
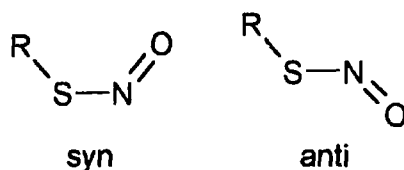
Figure 1.4 The structures of the syn and anti conformations of S-nitrosothiols.

1.2.2 Methods of Forming S-Nitrosothiols in Solution

S-Nitrosothiols can readily be formed by the nitrosation of thiols. A nitrosation reaction occurs when NO^+ is added to a compound. There are several possible nitrosating agents that can be used to nitrosate a thiol group.

1.2.2.1 S-Nitrosation Using Nitrous Acid

The acid catalysed nitrosation of thiols with nitrous acid has been studied.[31] (see scheme 1.5) The rate equation was established and is shown in equation 1.2.

$$RSH + HNO_2 \xrightarrow{H^+} RSNO + H_2O$$
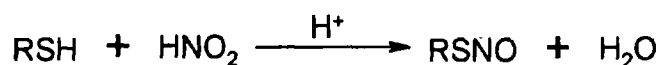
Scheme 1.5 Chemical equation for the acid catalysed nitrosation of thiols by nitrous acid.

Rate $= k_3[RSH][H^+][HNO_2]$

Equation 1.2 Rate equation for the acid catalysed nitrosation of thiol by nitrous acid.

The addition of the nucleophiles Cl⁻, Br⁻ and SCN⁻ (X⁻) catalysed the reactions. This was rationalised in terms of the generation and reaction of the corresponding nitrosyl species XNO in solution (see scheme 1.6), for which the equilibrium constants have been independently determined.

$$HNO_2 + X^- + H^+ \rightleftharpoons XNO + H_2O$$
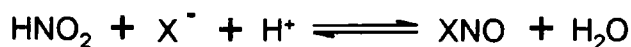
Scheme 1.6 Formation of the XNO species in solution.

An explanation for the greater reaction rates in the presence of the nucleophiles (X⁻) is that larger concentrations of XNO are present. The proposed mechanism for the reaction is shown in scheme 1.7.

Uncatalysed,   Catalysed,
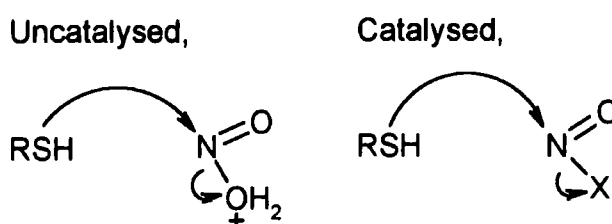
Scheme 1.7 Mechanism for the nitrosation of thiol by nitrous acid and a XNO species.

1.2.2.2 S-Nitrosation Using Peroxynitrous Acid

When peroxynitrite was used to oxidise thiol in acidic solution the reaction formed an S-nitrosothiol and disulfide.[32] Kinetic data for the formation of S-nitrosothiol were obtained to determine the reaction mechanism.[33]

When peroxynitrite was reacted with thiol in excess, third order rate constants were obtained. They were found to correlate well with the rate constants obtained for the reaction of the corresponding thiol with nitrous acid using the rate equation shown in equation 1.2. This suggested that peroxynitrite was oxidising thiol to yield the disulfide and nitrite anion and this was becoming protonated, which lead to nitrosation of the thiol by nitrous acid.

When the acidity of the reaction solutions was increased it became evident that two nitrosation processes were taking place. This was explained in terms of an additional

reaction in which the thiol reacts with a protonated form of peroxynitrous acid that then formed a S-nitrosothiol. The proposed mechanism is shown in scheme 1.8.
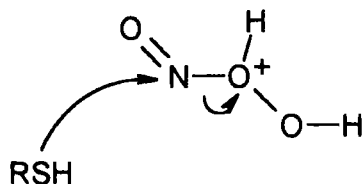
Scheme 1.8: Proposed mechanism for S-nitrosothiol formation from thiol and peroxynitrous acid.

1.2.2.3 S-Nitrosation Using Alkyl Nitrites

Alkyl nitrites are the oxygen analogues of S-nitrosothiols and their generic structure is shown in figure 1.5. The big advantage using an alkyl nitrite as a nitrosating agent is that the reaction does not have to be performed in acidic conditions.

$$R—O—N{=}O$$

Figure 1.5 Generic structure of alkyl nitrites.

It has been found that thiol reacts with a range of alkyl nitrites to form S-nitrosothiols.[34] A plot of rate constant against pH gave an S shaped curve suggesting that the reaction mechanism involved nucleophilic attack by the thiolate anion. A rate equation (see equation 1.3) and mechanism (see scheme 1.9) for the reactions was determined.

Rate = k_2[RONO][RS⁻]

Equation 1.3 Rate equation for the reactions of thiol with alkyl nitrites.
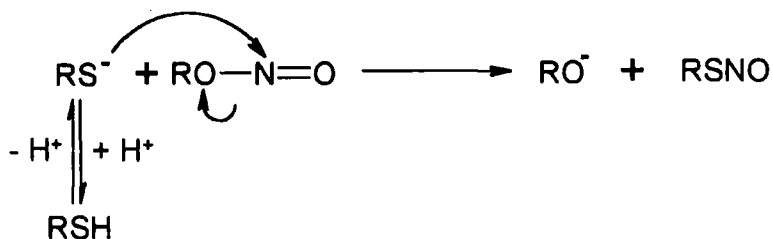
Scheme 1.9 Mechanism for the reactions of thiol with alkyl nitrites.

1.2.2.4 *S*-Nitrosation Using Dinitrogen Trioxide

The formation of *S*-nitrosothiol in solutions containing NO, oxygen and thiol has been studied at physiological pH.[35] It was suggested that NO oxidation occurred leading to the formation of N_2O_3 which then nitrosated the thiol. The proposed reactions are shown in scheme 1.10.

$$2NO + O_2 \longrightarrow 2NO_2$$
$$NO_2 + NO \longrightarrow N_2O_3$$
$$N_2O_3 + RSH \longrightarrow RSNO + NO_2^- + H^+$$
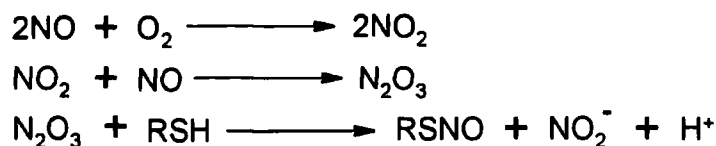
Scheme 1.10 The proposed reactions for *S*-nitrosothiol formation in solutions containing NO and oxygen at pH 7.4.

The rate constant for the reaction of glutathione with N_2O_3 was $6.6 \times 10^7 \, dm^3 \, mol^{-1} \, s^{-1}$.

1.2.3 Proposed Mechanisms for *S*-Nitrosothiol Formation in the Body

Studies have attempted to explain how *S*-nitrosothiols are formed in the body. It has been suggested that copper(+2) ions and the copper containing protein ceruloplasmin can catalyse the formation of *S*-nitrosothiols.[36] The proposed mechanism is that copper in the protein complexes NO and oxidises it so that it can react with thiol. Oxygen is then reduced by copper(+1) to form water. (see scheme 1.11)

$$4Cu^+ + O_2 + 4H^+ \longrightarrow 4Cu^{2+} + 2H_2O$$
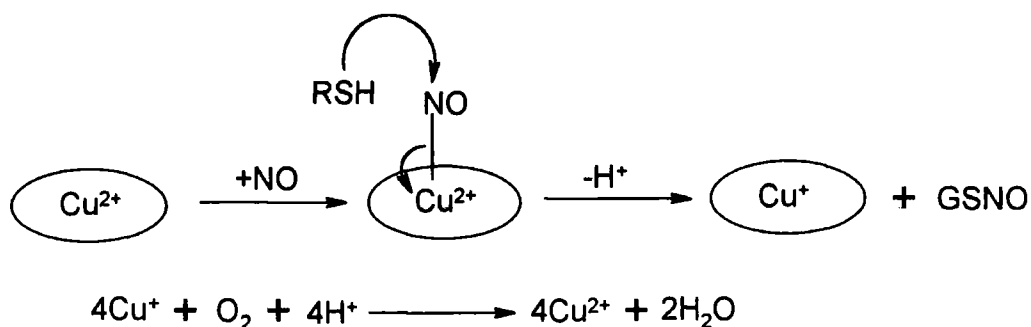
Scheme 1.11 Proposed reactions for the catalysed formation of a *S*-nitrosothiol by ceruloplasmin.

Any copper catalysed formation of S-nitrosothiol must occur faster than the copper catalysed decomposition process (see section 1.3.2) for any significant quantities of S-nitrosothiol to be generated. It has been found that the build up of copper(+1) during the reaction does destabilise the S-nitrosothiol product.[37] S-Nitroso-bovine serum albumin was found to be much less sensitive to decomposition and the product could be detected using UV / Vis spectroscopy.

It has been suggested that the protein serum albumin is involved in the formation of S-nitrosothiols.[38] The third order reaction which involves the oxidation of NO by oxygen to form the nitrosating agent N_2O_3 would be very slow in physiological conditions because of the low concentrations of oxygen and NO present. If NO and oxygen were attracted to the core of serum albumin the high local concentrations of the reactants could make the reaction viable in the body. This could occur because NO and oxygen are both hydrophobic so could be attracted to the interior of proteins from the aqueous phase.

1.3 Decomposition Pathways of S-Nitrosothiols

S-Nitrosothiols have been found to be biologically active compounds and it is widely believed that the decomposition of the compounds causes the effects observed. In recent years reactions involving S-nitrosothiols have been studied to understand what factors affect their lifetime in aqueous solution, and determine possible reaction pathways that could occur *in vivo*.

1.3.1 Thermal / Photolytic Decomposition of S-Nitrosothiols

It was found that when several S-nitrosothiols were irradiated with visible light ($\lambda > 408$ nm) thiyl radicals were produced, and could be trapped in the solution using 5,5'-dimethyl-1-pyrroline N-oxide and detected using EPR.[39] When EPR spectra were taken in the dark and during copper ion catalysed decay (see section 1.3.2) no thiyl radicals were detected. The photolysis of GSNO has been found to be close to a first order process.[40]

A mechanism has been proposed for the photolytic decomposition of S-nitrosothiols in aerobic conditions.[41] (see scheme 1.12) Laser flash photolysis was used to study the different steps of the reaction.

$$RSNO \longrightarrow RS^{\bullet} + NO$$

$$RS^{\bullet} + O_2 \longrightarrow RSOO^{\bullet} \xrightarrow{RSNO} RSSR + NO + O_2$$

$$RS^{\bullet} + RSNO \longrightarrow RSSR + NO$$
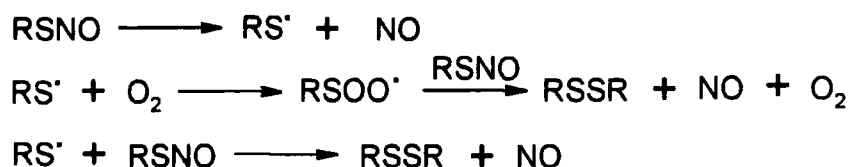
Scheme 1.12 Proposed mechanism for the photolytic decomposition of S-nitrosothiols.

The products of the thermal decomposition of S-nitrosothiols are disulfide and NO. It is assumed that the thermal and photolytic reaction mechanisms are very similar. The thermal reaction for S-nitrosothiols is generally a very slow process at room temperature.

Very few S-nitrosothiols can be prepared and stored as a solid in a pure form. However S-nitroso-N-acetylpenicillamine (SNAP) can be prepared as a solid and stored in a fridge over a long period of time.[42] It has been suggested that the improved thermal stability of SNAP as a solid compared to S-nitroso-N-acetylcysteine is because the geminal methyl groups on SNAP could sterically hinder thiyl radical dimerisation and reaction with other S-nitrosothiols.[43]

One method found to increase the photochemical decomposition of GSNO has been to add a photosensitiser.[44] The Rose Bengal (RB) photosensitiser has an absorbance that overlaps with GSNO at 559 nm. Excitation of a solution containing GSNO and RB at 550 nm caused a larger than expected increase in production of NO and thiyl radicals. The proposed mechanism for increased rate of decomposition is shown in scheme 1.13.

$$RB \xrightarrow{\text{hv}/\Delta} RB^*$$

$$RB^* + GSNO \longrightarrow GSNO^* + RB$$

$$GSNO^* \longrightarrow GS^{\cdot} + NO$$
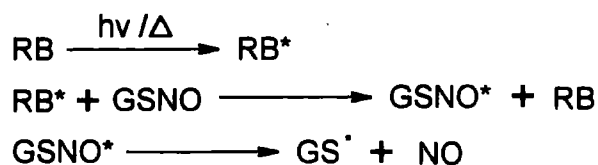
Scheme 1.13 Proposed mechanism for the increased rate of GSNO decomposition via the photolytic pathway in the presence of RB.

1.3.2 Metal Ion Induced Decomposition of S-Nitrosothiols

Initial work on S-nitrosothiols found that they could decompose spontaneously in aqueous solution at physiological pH (pH 7.4). It has been found that several metal ions can cause their decomposition and they are Cu^{2+}, Fe^{2+}, Hg^{2+} and Ag^+.

1.3.2.1 S-Nitrosothiol Decomposition Catalysed by Copper Ions

The addition of the metal ion chelator EDTA was found to stabilise S-nitrosothiols in solution. It has been found that copper(+2) ions catalyse the decomposition of S-nitrosothiols at physiological pH.[45] Chemical and rate equations were determined for the reaction (see scheme 1.14 and equation 1.3) and the products of the reaction were found to be NO and disulfide. A much slower reaction was also found to occur that was believed to be the thermal reaction.

$$2RSNO \xrightarrow{Cu^{2+}} RSSR + 2NO$$
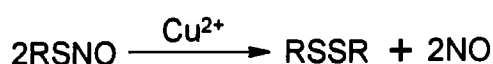
Scheme 1.14 Chemical equation for the copper catalysed decomposition of S-nitrosothiols.

Rate $= k_2[\text{RSNO}][\text{Cu}^{2+}] + k_1[\text{RSNO}]$

Equation 1.3 Rate equation for the copper catalysed decomposition of S-nitrosothiols.

The difference in second order rate constants obtained was initially explained by postulating possible copper S-nitrosothiol coordination complexes. S-Nitrosothiols with favourable coordination sites decompose much faster than those with less favourable ones.

For example the structures of six S-nitrosothiols are shown in figure 1.6 with k_2 values obtained for the copper reaction shown in table 1.1.

GSNO

S-Nitrosothiomalic acid S-Nitrosocysteine S-Nitrosohomocysteine

SNAP   S-Nitrosopenicillamine
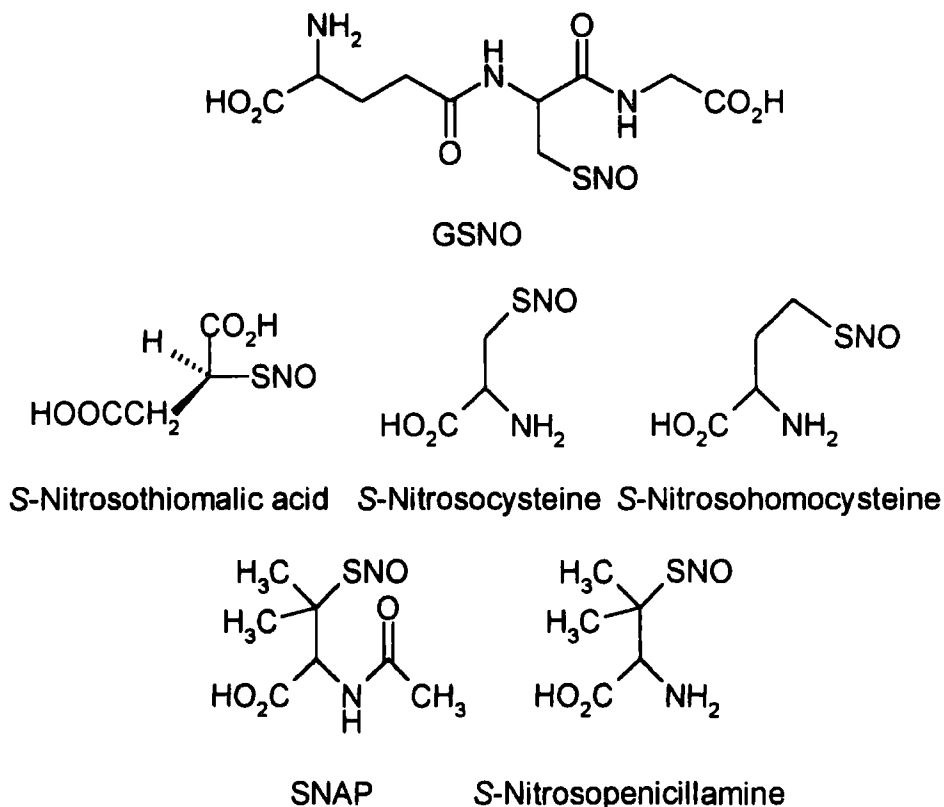
Figure 1.6 Structure and names of some S-nitrosothiols.

S-Nitrosothiol	$k_2 / \mathrm{dm^3\ mol^{-1}\ s^{-1}}$
GSNO	0
S-Nitrosothiomalic acid	1 100 ± 60
S-Nitrosocysteine	24 500 ± 500
S-Nitrosohomocysteine	16 ± 0.5
SNAP	20 ± 1
S-Nitrosopenicillamine	67 000 ± 2 000

Table 1.1 Second order rate constants obtained for the copper catalysed decomposition of some S-nitrosothiols.

The difference in reactivity of the S-nitrosothiols towards copper was explained by the presence of six membered complexes with copper. (see figure 1.7) For example the rate

15

constant obtained for *S*-nitrosohomocysteine could have been smaller than *S*-nitrosocysteine because a less favourable seven membered intermediate formed.
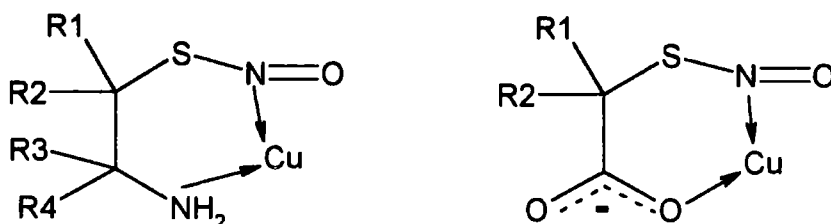
Figure 1.7 Suggested *S*-nitrosothiol copper reaction intermediates.

The presence of the acetyl group on the nitrogen in SNAP and the use of a carboxylic acid group in *S*-nitrosothiomalic acid decreased reactivity. This could be because less electron density was available for metal complexation due to electron delocalisation. It appears that reactivity is increased by the presence of *gem* methyl groups in *S*-nitrosopenicillamine: methyl groups are electron donating, which could make metal complexation more favourable. However this explanation does not take into account the thiol dependence on rate of decomposition and possible copper(+2) complexation by disulfide which are both explained later.

It has been found that the addition of the specific copper(+1) chelator neocuproine stabilises *S*-nitrosothiols at pH 7.4.[46] This observation has been used to explain why zero order reactions and induction periods were observed in the copper catalysed decomposition of *S*-nitrosothiols. Zero order reaction profiles and induction periods were observed when the reduction of copper ions was rate limiting. The free thiol initially required to reduce copper ions is probably present due to the slight reversibility of *S*-nitrososation of thiols.[47] When thiol concentrations are reduced by performing nitrosation reactions with an excess of nitrous acid, the copper catalysed decomposition is hindered at pH 7.4.

The mechanism for the reduction of copper(+2) ions by thiol in aqueous solution has been studied independently.[48] No evidence of thiyl radical formation was observed during the reactions. It was suggested that the reaction occurred via the dimerisation of copper(+2) thiolate complexes leading to the formation of a copper(+1) thiolate complex and disulfide. The proposed mechanism is shown in scheme 1.15.
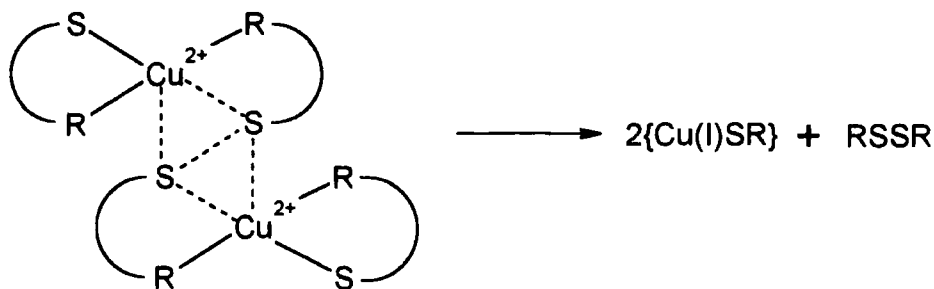
Scheme 1.15 Proposed mechanism for the reduction of copper(+2) by thiol.

The chemical reactions in scheme 1.16 describe how copper ions could catalyse the decomposition of S-nitrosothiols at pH 7.4. It has been shown that when S-nitrosothiols are reduced electrochemically, thiol and NO are the products of the reaction.[49] This would explain the copper(+1) interaction with S-nitrosothiols.

$$2\{Cu(II)(SR)_2\} \longrightarrow 2\{Cu(I)(SR)\} + RSSR$$
$$\{Cu(I)(SR)\} + RSNO \longrightarrow \{Cu(II)(SR)_2\} + NO$$
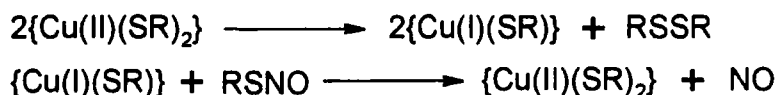
Scheme 1.16 Proposed chemical reactions for the copper catalysed decomposition of S-nitrosothiols.

Several studies have found that the rate of the copper decomposition is dependent on the concentration of thiol present.[46,50,51] It can affect the rate of reaction in two ways. The thiol can increase the rate of decomposition by increasing the rate of reduction of copper(+2) ions or decrease the rate by complexing copper ions. In some cases both these effects occur at different thiol concentrations.

The S-nitrosothiol GSNO is stable at millimolar concentrations at pH 7.4 when there is no added copper or thiol present. However it has been found that when the concentration of the GSNO is lowered to micromolar concentrations quantitative amounts of NO are rapidly generated and can be detected using an NO electrode.[52] This was explained by complexation of copper(+2) by glutathione disulfide (GSSG) at high GSNO concentrations. The proposed structure of the complex is shown in figure 1.8.[53] (the formation constant for the Cu(II) : (GSSG) 1 : 1 complex is $K = 10^{14}\ dm^3\ mol^{-1}$).[54]
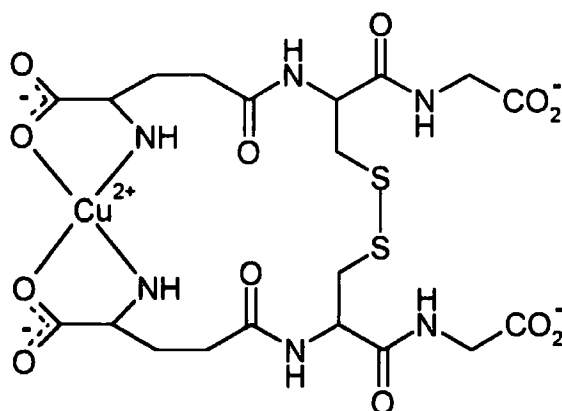
Figure 1.8 Proposed structure of the copper(+2) GSSG complex.

When the *S*-nitroso derivatives of bovine and human serum albumin were formed at pH 7.4 both were found to be relatively stable.[55] Like GSNO, when their concentrations were reduced to micromolar levels they both rapidly decomposed and generated NO. It was believed that this effect was due to copper complexation at high protein concentrations.

Another method has been found to promote the copper ion catalysed decomposition of GSNO at pH 7.4. The addition of ascorbic acid at low concentrations (ie. below 1×10^{-4} M) has been shown to decompose GSNO in the presence of GSSG.[56] This was found to be a metal ion dependent process with NO and GSSG being identified as the products of the reaction. Ascorbic acid appeared to make available the copper ions complexed to GSSG. This could be a physiologically relevant process because ascorbic acid is present in the body and the concentration in the blood has been measured as $0.2 \times 10^{-5} - 8.5 \times 10^{-5}$ M.[57]

There is about 0.1g of copper per 75 kg body weight, however very little is present as free hydrated Cu^{2+} ions. In an attempt to discover whether the copper catalysed process could be promoted by bound copper sources, copper complexes found in the body were reacted with *S*-nitrosothiols.[58] Copper bound to two histidine molecules, the tripeptide Gly-Gly-His or human serum albumin were found to be available for the decomposition of *S*-nitrosothiols. Rates of reaction were found to be lower than expected with an equivalent amount of free copper. The copper containing enzyme ceruloplasmin was also found to decompose *S*-nitrosothiols at low concentrations.

18

There is another report in the literature of a copper containing enzyme decomposing an *S*-nitrosothiol. It was found that copper, zinc superoxide dismutase decomposed GSNO at low concentrations in a thiol and copper ion dependent process at physiological pH.[59]

It has been found that the biological activity of GSNO is a copper(+1) dependent process. The presence of neocuproine significantly decreased the ability of GSNO and SNAP to relax vascular smooth muscle.[60] Neocuproine and bathocuproine sulfonate (BCS), both copper(+1) chelators have been found to hinder the anti-aggregatory activity of GSNO on human platelets.[61]

In another study platelets were pre-treated with BCS before being reintroduced to BCS free buffer.[62] When GSNO was added there was no biological activity suggesting that an enzyme was either copper(+1) dependent or deactivated by BCS via another method.

1.3.2.2 *S*-Nitrosothiol Decomposition Catalysed by Iron Ions

It has been claimed that iron(+2) ions can catalyse the decomposition of *S*-nitrosothiols at physiological pH via the formation of dinitrosyl iron complexes.[63] The products of the reaction were detected using EPR but no rate equation or rate constants have been determined for the process.

The products of the reaction of *S*-nitrosocysteamine with iron(+2) ions have been characterised using a variety of methods at pH 7.8 in anaerobic conditions.[64] It was found that the product of the reaction was dependent on the concentration of thiol present. Solutions containing iron(+2) with cysteamine in two or twenty fold excess were reacted with *S*-nitrosocysteamine and different nitrosyl iron complexes were believed to form.

RSNO
+ RSH (2 fold excess)   Fe²⁺   RSNO
+ RSH (20 fold excess)
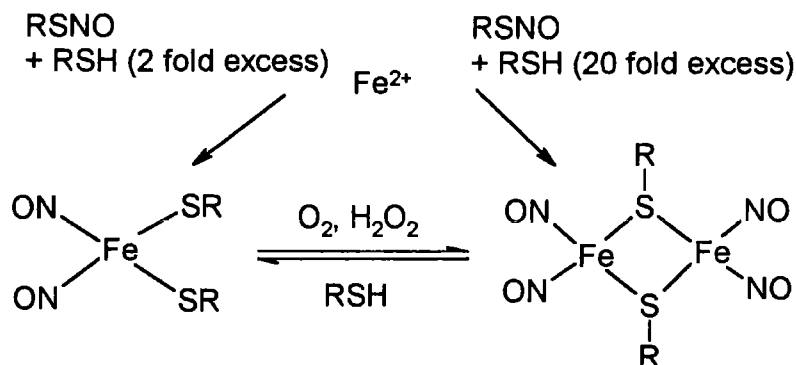
Scheme 1.17 Possible reactions involving iron(+2), cysteamine and S-nitrosocysteamine.

1.3.2.3 The Reaction of S-Nitrosothiols with Mercury and Silver Ions

The reaction of mercury(+2) ions with S-nitrosothiols and thiols has been used as a quantitative test for the two chemical species.[65] A kinetic study into the mercury(+2) reaction with S-nitrosothiols in aqueous solution yielding thiol bound to mercury(+2) and nitrous acid has been undertaken.[66] The rate equation found when using $HgCl_2$ is shown in equation 1.4. When $Hg(NO_3)_2$ was used reactions were so fast that reaction profiles could not be obtained. This was explained by the fact that there was much less dissociation of $HgCl_2$ in aqueous solution leading to lower concentrations of Hg^{2+} present.

$$Rate = k_2[HgCl_2][RSNO]$$

Equation 1.4 Rate equation for the reaction of mercury(+2) ions with S-nitrosothiols.

Reactions were performed in anaerobic conditions so that any NO formed could be detected using an NO electrode. No NO was detected so the formation of nitrous acid could not be accounted for by formation of NO in the solutions. The proposed mechanism is shown in scheme 1.18.

Scheme 1.18 Proposed mechanism for the mercury(+2) ion reaction with S-nitrosothiols.

The mechanism is very similar to the one postulated for the acid catalysed hydrolysis of S-nitrosothiols.[67] At high acidity it was believed that the sulfur atom became protonated which lead to hydrolysis that could be observed in the presence of a nitrite trap.

Silver(+1) ions are known to have a high affinity for thiol and were found to decompose S-nitrosothiols as well. It was believed that the reaction mechanism was similar to the mercury reaction.

1.3.3 The Reaction of S-Nitrosothiols with Nucleophiles

S-Nitrosothiols have been found to react with a range of nucleophiles, the general mechanism is shown in scheme 1.19 and the rate equation is shown in equation 1.4.

Scheme 1.19 General mechanism for the reaction of S-nitrosothiols with nucleophiles.

Rate = k_2[X⁻][RSNO]

Equation 1.4 General rate equation for the reaction of S-nitrosothiols with nucleophiles.

1.3.3.1 Reaction of S-Nitrosothiols with Oxygen Nucleophiles

Ascorbic acid has been found to decompose S-nitrosothiols by two different pathways.[56] At low ascorbic acid concentrations, copper normally unavailable for the copper catalysed decomposition was found to decompose S-nitrosothiols. When ascorbic acid was present at much higher concentrations it reacted with S-nitrosothiols yielding thiol, NO and dehydroascorbic acid. Two nucleophilic sites are present on the ascorbic acid molecule so the reaction occurs in a 2 : 1 S-nitrosothiol : ascorbic acid stoichiometric ratio. The nitrosated ascorbic acid rapidly decomposes to form NO and the reaction scheme is shown in scheme 1.20.
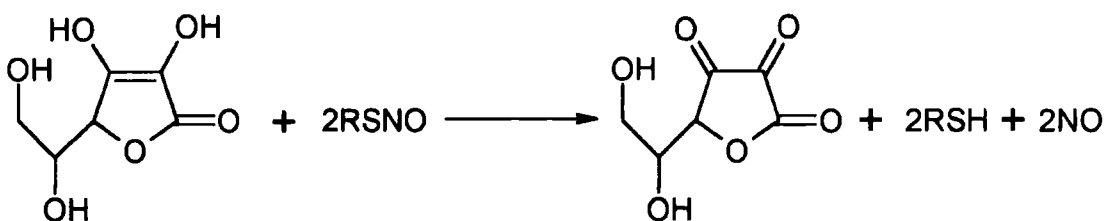
Scheme 1.20 The reaction scheme for the nucleophilic attack by ascorbic acid on an S-nitrosothiol.

An equation for the rate constant dependence on pH using the three different forms of ascorbic acid (H_2A, HA^- and A^{2-}) was derived. When rate constants were determined at different pH values it was found that the dianion reacted most readily at pH 7.4 and the fully protonated molecule did not contribute significantly during the reactions.

Another oxygen nucleophile that has been studied is hydrogen peroxide. It has been found that S-nitrosothiols react with hydrogen peroxide to form peroxynitrite in aqueous solution.[68] (see scheme 1.21) The rate of reaction increased with pH indicating that the deprotonated form of hydrogen peroxide was the reactive species.
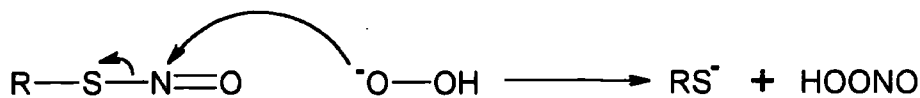
Scheme 1.21 Proposed reaction between S-nitrosothiols and hydrogen peroxide.

S-Nitrosopenicillamine has been found to undergo alkaline hydrolysis and was expected to form nitrite via the reaction proposed in scheme 1.22.[69] However nitrite was only found in

fifty percent yield. It was suggested that nucleophilic attack at the sulfur of the *S*-nitrosothiol group might have occurred leading to NO⁻ formation.

$$RSNO + {}^-OH \longrightarrow RS^- + NO_2^- + H^+$$

Scheme 1.22 Proposed chemical reaction between *S*-nitrosopenicillamine and hydroxide ions leading to nitrite formation. ·

1.3.3.2 Reaction of *S*-Nitrosothiols with Nitrogen Nucleophiles

The reaction of *S*-nitrosothiols with different nitrogen nucleophiles has been studied.[69] As expected, secondary amines reacted with *S*-nitrosothiols to form the corresponding nitrosamines. Primary aliphatic amines gave diazonium ions.

With primary amines the rates of reaction deviated from the expected kinetic model at high concentrations of amine. The formation of the complex in figure 1.9 was used to explain why rates of reaction did not increase as amine concentration was further increased. Scheme 1.23 shows the reactions suggested for *S*-nitrosothiols reacting with primary amines at high concentration.
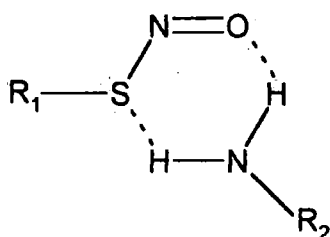
Figure 1.9 The proposed *S*-nitrosothiol primary amine complex.

$$RSNO + R'NH_2 \rightleftharpoons \{(RSNO)(R'NH_2)\} \quad \text{rapid equilibrium}$$
$$RSNO + R'NH_2 \longrightarrow RS^- + R'N_2^+ + H_2O \quad \text{slow reaction}$$
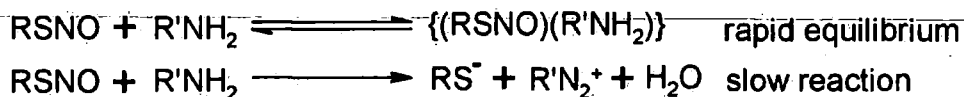
Scheme 1.23 Proposed reaction scheme for *S*-nitrosothiols reacting with primary amines at high concentration.

1.3.3.3 Reaction of *S*-Nitrosothiols with Sulfur Nucleophiles

It has been found that NO^+ can be transferred directly between *S*-nitrosothiols and thiols in a transnitrosation reaction.[70] (see scheme 1.24) The rate constant dependence on pH suggested that the reaction occurred by nucleophilic attack of the thiolate anion. It is possible that these reactions could occur *in vivo*.
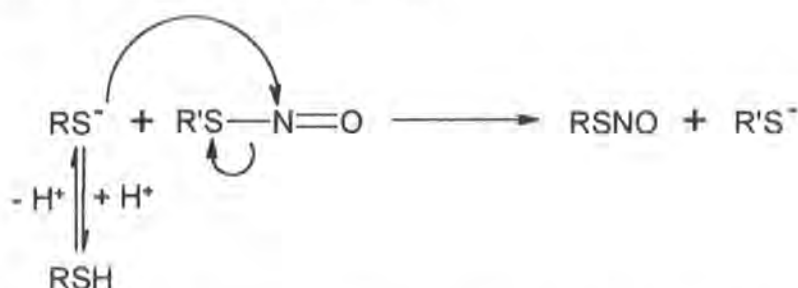
Scheme 1.24 Proposed mechanism for a transnitrosation reaction between an S-nitrosothiol and a thiol.

The rate equation for a transnitrosation reaction between an *S*-nitrosothiol and a thiol has been determined and is shown in equation 1.5.[71] Introducing an electron withdrawing group on the *S*-nitrosothiol was found to increase the rate of reaction, thus confirming that reaction was one of nucleophilic attack by RS^-.

Rate = $k_2[RS^-][R'SNO]$

Equation 1.5 Rate equation for a transnitrosation reaction between an S-nitrosothiol and a thiol.

Equilibrium constants for some transnitrosation reactions have been determined using HPLC techniques.[72] It was found that the equilibrium between GSNO and cysteine favoured GSNO and the equilibrium between GSH and *S*-nitroso-bovine serum albumin favoured the protein. This helps explain why the addition of GSNO or *S*-nitrosocysteine to human plasma rapidly leads to the formation of *S*-nitroso proteins.

The rates of formation and decomposition of *S*-nitroso-bovine serum albumin in transnitrosation reactions have been studied. The second order rate constants (k_2) for the

reaction of S-nitroso-bovine serum albumin with several thiols have been determined at pH 7.4.[73] A plot of $\log(k_2 \,/\, dm^3 \, mol^{-1} \, s^{-1})$ against pK_a of the thiols showed a negative linear correlation. This is logical because the larger the pK_a of the thiol, the less thiolate anion would be present, so the rate constant would be smaller.

Bovine serum albumin has been reacted with several low molecular weight S-nitrosothiols to identify what factors determine the rate of reaction.[74] Two of the lowest second order rate constants obtained were for GSNO and S-nitroso-3-mercaptopropionate. It was suggested that a sterically bulky S-nitrosothiol or one carrying a negative charge would be hindered from reacting with the protein.

There is a much slower reaction that can take place between an S-nitrosothiol and a sulfur nucleophile. It has been shown that when GSH is present in excess with GSNO a slow decomposition occurs at pH 7.4.[75] Ammonia and disulfide were found to be major products of the reaction. The change in product of the S-nitrosothiol reaction with thiol was explained by an alternative set of reactions occurring shown in scheme 1.25.
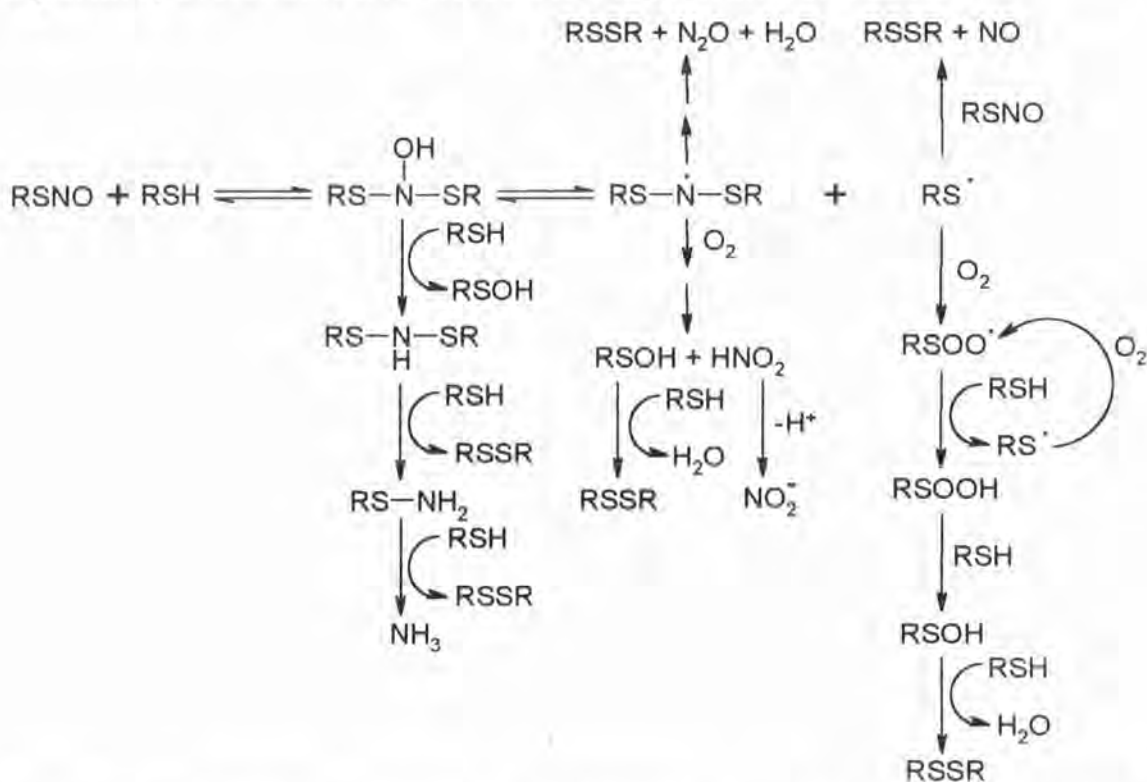
Scheme 1.25 Proposed mechanism for S-nitrosothiol reacting with thiol leading to ammonia formation.

A kinetic study of the decomposition of S-nitrosothiols at high thiol concentration has been undertaken.[76] The reaction was found to be metal ion independent and the rate equation shown in equation 1.6 was determined. Second order rate constants found were much smaller than the ones obtained for transnitrosation reactions. A much slower reaction was also observed, believed to be the thermal reaction. The rate of reaction was found to be dependent on pH in a similar way to transnitrosation reactions indicating that the rate determining step was a nucleophilic attack by thiolate anions.

$$\text{Rate} = k_2[\text{RS}^-][\text{RSNO}] + k_1[\text{RSNO}]$$

Equation 1.6 Rate equation for S-nitrosothiol decomposition at high thiol concentrations.

The sulfur-containing product of the reaction was found to be disulfide and the nitrogen containing products were found to be mostly nitrite and ammonia. At lower thiol concentrations nitrite was found as the major product but as thiol concentration was increased ammonia became the major product of the reaction with a corresponding decrease in yield of nitrite.

An alternative reaction mechanism has been suggested for the decomposition of S-nitrosothiols at high thiol concentrations (see scheme 1.26).[77,78] It has been proposed that the initial step is nucleophilic attack at the sulfur atom by the thiolate anion leading to disulfide and NO^- formation.
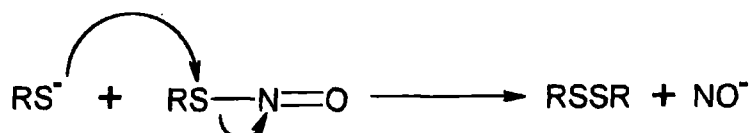
Scheme 1.26 Alternative initial reaction proposed for S-nitrosothiol decomposition at high thiol concentrations.

Second order rate constants for a range of sulfur nucleophiles (not including thiols) reacting with S-nitrosothiols have been measured.[79] Sulfite was found to react with a variety of S-nitrosothiols solely as SO_3^{2-} and the reactions shown in scheme 1.27 were proposed. The rate of reaction was found to be pH dependent in a similar way to the other reactions involving sulfur nucleophiles.

26

$$RSNO + SO_3^{2-} + H^+ \longrightarrow RSH + ONSO_3^-$$
$$ONSO_3^- + SO_3^{2-} + H^+ \longrightarrow HON(SO_3^-)_2.$$
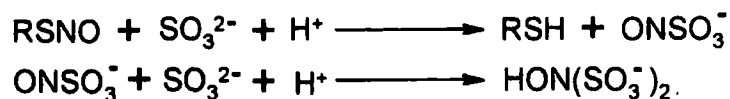
Scheme 1.27 Proposed reactions for the decomposition of S-nitrosothiols by sulfite.

1.3.4 Decomposition of S-Nitrosothiols by Enzymes

The stability of S-nitrosothiols has been studied in the presence of enzymes found in the body. Chemical reactions for the decompositions observed have been proposed.

1.3.4.1 Decomposition of S-Nitrosothiols by Glutathione Peroxidase

A study found that the selenium-containing enzyme glutathione peroxidase decomposed GSNO catalytically but not SNAP.[80] However selenocystamine and selenocystine were found to be able to decompose catalytically both SNAP and GSNO. NO was detected as a product of the reactions using an NO electrode.

When selenocystamine and selenocystine were reacted with SNAP and GSNO at pH 7.4 it was found that a rapid decomposition occurred. The reaction was metal ion independent and required the presence of thiol. This suggested that an intermediate was formed by the reaction of thiol with the diselenides. Diselenides react with thiol to produce selenols and they were found to generate NO when reacted with S-nitrosothiols. The proposed mechanism for the decomposition is shown in scheme 1.28.

$$R'Se-SeR' + RSH \rightleftharpoons RS-SeR' + R'SeH$$
$$RS-SeR' + RSH \rightleftharpoons RS-SR + R'SeH$$
$$2RSNO \xrightarrow[RSH]{R'Se-SeR'} RSSR + 2NO$$
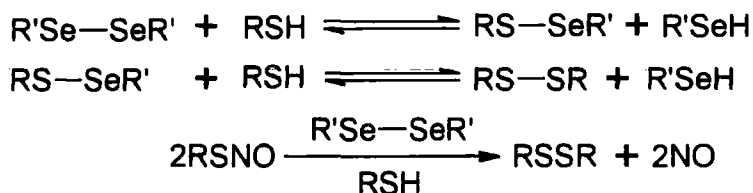
Scheme 1.28 Proposed catalytic decomposition of S-nitrosothiols by diselenides.

1.3.4.2 Decomposition of S-Nitrosothiols by Xanthine Oxidase

The reaction of superoxide with GSNO and S-nitrosocysteine at pH 7.8 has been studied using the superoxide generator xanthine oxidase.[81] It was found that superoxide reacted with S-nitrosothiols in a 2 : 1 stoichiometric ratio giving the rate equation shown in equation 1.7.

Rate = $k_2[O_2^-][RSNO]$

Equation 1.7 Rate equation for the reaction of superoxide with S-nitrosothiols.

The k_2 value obtained for S-nitrosocysteine was 76 900 dm^3 mol^{-1} s^{-1} and for GSNO it was 12 800 dm^3 mol^{-1} s^{-1} at 25°C. The nitrite and nitrate found as products of the reaction accounted for more than 90 % of the nitrogen-containing product.

Decomposition of S-nitrosothiols by xanthine oxidase in aerobic and anaerobic conditions has been studied.[82] The proposed reactions (see scheme 1.29) in aerobic conditions correlate well with the data obtained in the kinetic study for the reaction of superoxide with S-nitrosothiols. A k_2 value for the reaction of superoxide with GSNO at 25 °C was found to be 10 000 dm^3 mol^{-1} s^{-1}.

$$RSNO + O_2^{\cdot-} + H^+ \longrightarrow RSH + NO + O_2$$
$$O_2^{\cdot-} + NO \longrightarrow ONOO^-$$

Scheme 1.29 Proposed reaction mechanism for S-nitrosothiol decomposition by xanthine oxidase in aerobic conditions at pH 7.4.

The nitrite and nitrate products of the reaction could be present from the decomposition of peroxynitrite. Peroxynitrite has been found to be able to decompose to form nitrate and nitrite in aqueous solution and the reactions are shown in scheme 1.30.[83]

Isomerisation,

$$ONOO^- \longrightarrow NO_3^-$$

Decomposition,

$$2ONOO^- \longrightarrow 2NO_2^- + O_2$$
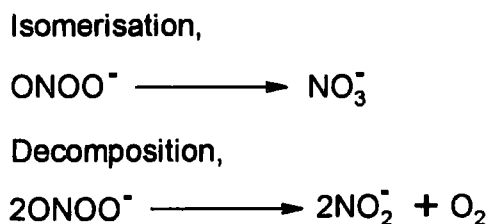
Scheme 1.30 Proposed formation of nitrate and nitrite from the peroxynitrite anion.

S-Nitrosocysteine but not GSNO was found to react with xanthine oxidase in anaerobic conditions.[82] It was suggested that the S-nitrosothiol formed a complex with the enzyme then accepted an electron leading to the formation of NO and thiol. The proposed reactions for this process are shown in scheme 1.31.

$$Mo^{4+} \xrightarrow{-2e} Mo^{6+}$$

$$2RSNO \xrightarrow{+2e} 2RS^- + 2NO$$
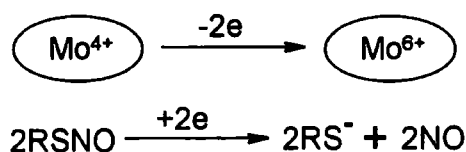
Scheme 1.31 Proposed mechanism for the superoxide independent decomposition of S-nitrosocysteine by xanthine oxidase.

Superoxide dismutase was found to inhibit the decomposition by xanthine oxidase of S-nitrosocysteine in aerobic conditions. It was believed that S-nitrosocysteine mainly decomposed via the superoxide dependent process. All experiments were carried out in the presence of the metal ion chelator diethylenetriaminepentaacetic acid.

1.4 Therapeutic Applications of S-Nitrosothiols

S-Nitrosothiols are found in the body and are believed to be responsible for the transport and storage of NO. In recent years attempts have been made to utilise the biological activity of S-nitrosothiols for the treatment of disease.

1.4.1 Use of S-Nitrosothiols in Patients

In spite of the intense interest in the biological properties of S-nitrosothiols, there are few reports of clinical trials. The S-nitrosothiol GSNO has been used to inhibit platelet

aggregation (i.e. blood clotting) during coronary angioplasty.[84] GSNO could be used at concentrations where no vasodilation effects were observed. Coronary angioplasty is the medical procedure where a balloon is inflated in a blood vessel to restore or improve blood flow past a constriction.

There has been one case of GSNO being used to treat a form of pre-eclampsia.[85] A woman suffering from high blood pressure before and after giving birth was given an intravenous infusion of GSNO. Shortly afterwards her blood pressure became normal.

1.4.2 Possible Treatment of Heart Disease Using S-Nitrosothiols

The organic nitrate, glyceryl trinitrate (see figure 1.10) has been used for many years as a treatment for angina sufferers. It is administered orally to relieve heart pain caused by inadequate blood supply to the heart by dilating blood vessels. However over time the treatment can become ineffective due to nitrate tolerance. An enzyme (mitochondrial aldehyde dehydrogenase) has been isolated that can generate NO from glyceryl trinitrate, it was depleted by repeated dosage.[86]

$$\begin{array}{l} -O-NO_2 \\ -O-NO_2 \\ -O-NO_2 \end{array}$$
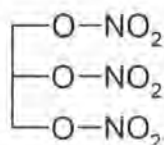
Figure 1.10 Chemical structure of glyceryl trinitrate.

It has been found that the use of S-nitrosothiols to relax rat vascular muscle does not lead to such a tolerance.[87] In fact S-nitrosothiols were able to relax rat vascular muscle that had acquired a nitrate tolerance. S-Nitrosocaptopril has been found to decrease artery blood pressure in living rats when administered orally or intravenously.[88]

1.4.3 S-Nitrosothiols as Anti Tumour Agents

The most effective breast cancer drug adriamycin like several other anti tumour drugs has been found to stimulate NO production *in vivo*.[89] Theoretically using an S-nitrosothiol to generate NO in the vicinity of a tumour could produce the same effect.

30

When GSNO was photolysed it was found that there was an enhanced toxic effect on leukemia cells observed.[40] There is the possibility that the use of a photosensitiser to release NO from S-nitrosothiols could enhance NO production by photolysis in specific areas of the body.[44]

1.4.4 Possible Medicinal Uses for Sugar Bonded to S-Nitrosothiols

A series of S-nitrosothiols that contain SNAP linked with glucose in various conformations have been synthesised.[90] The glyco-S-nitrosothiols were found to be more stable than SNAP at pH 7.4 with respect to copper mediated decomposition and also when EDTA was present.

The compound N-(S-nitroso-N-acetylpenicillamine)-2-amino-2-deoxy-1,3,4,6,-tetra-O-acetyl-β-D-glucopyranose named RIG200 (see figure 1.11) has been used in biological experiments.[91] RIG200 was found to induce vasodilation over a longer period of time than SNAP on rat arteries. This was attributed to the improved stability of RIG200 over SNAP in the presence of copper ions.
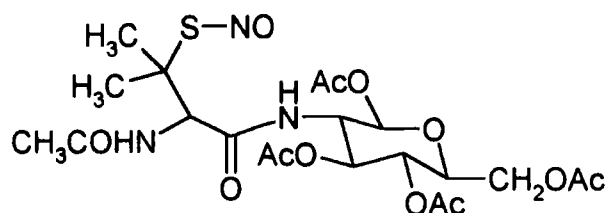
Figure 1.11 Structure of RIG200.

An interesting feature of the biological activity of RIG200 was the effect it had on arterial muscle that had the endothelium layer removed. When endothelium cells were removed the arterial tissue appeared to retain RIG200, which did not occur when they were present. This could prove useful because the S-nitrosothiol could act as a substitute for areas of vascular muscle where endothelial cells have been removed.

Glyco-S-nitrosothiols have been found to be more effective at killing human prostate cancer cells *in vitro* compared to SNAP.[92] An explanation for this could be the increased uptake of sugars by malignant tissue.[93] Compounds which contained fructose conjugated with SNAP

were found be more effective at killing cancer cells than glyco-S-nitrosothiols. Improved strategies for the synthesis of the fructose containing compounds have been published.[94]

Some diseases are now looked at in terms of NO metabolic dysfunction. For example patients with asthma[95] and chronic bronchitis[96] have been found to have higher than normal concentrations of NO in their breath. Controlling the chemistry of NO in the body may be one method by which these diseases and others may be treated in the future.

1.5 References

1) E. W. Ainscough and A. M. Brodie, *J. Chem. Educ.*, 1995, **72**, 686.

2) E. Culotta and D. E. Koshland, *Science*, 1992, **258**, 1862.

3) M. Fontecave and J. L. P. Pierre, *Bull. Soc. Chim. Fr.*, 1994, **131**, 620.

4) M. N. Hughes, *Biochim. Biophys. Acta*, 1999, **1411**, 263.

5) M. Grätzel, S. Taniguchi and A. Henglein, *Ber. Bunsenges. Phys. Chem.*, 1970, **74**, 1003.

6) D. A. Wink, J. F. Darbyshire, R. W. Nims, J. E. Saavedra and P. C. Ford, *Chem. Res. Toxicol.*, 1993, **6**, 23.

7) H. H. Awad and D. M. Stanbury, *Int. J. Chem. Kinet.*, 1993, **25**, 375.

8) A. R. Butler and D. L. H. Williams, *Chem. Soc. Rev.*, 1993, 233.

9) R. F. Furchgott and J. V. Zawadzki, *Nature*, 1980, **288**, 373.

10) R. M. J. Palmer, A. G. Ferrige and S. Moncada, *Nature*, 1987, **327**, 524.

11) L. J. Ignarro, G. M. Buga, K. S. Wood, R. E. Byrns and G. Chaudhuri, *Proc. Natl. Acad. Sci. USA*, 1987, **84**, 9265.

12) A. J. Hobbs, *TiPS*, 1997, **18**, 484.

13) Y. Zhao, P. E. Brandish, D. P. Ballou and M. A. Marletta, *Proc. Natl. Acad. Sci. USA*, 1999, **96**, 14753.

14) P. D. Senter and F. Eckstein, *J. Biol. Chem.*, 1983, **258**, 6741.

15) S. Moncada, R. M. J. Palmer and E. A. Higgs, *Biochem. Pharmacol.*, 1989, **38**, 1709.

16) D. J. Stuehr, N. S. Kwoon, C. F. Nathan and O. W. Griffith, *J. Biol. Chem.*, 1991, **266**, 6259.

17) B. Mayer, S. Pfeiffer, A. Schrammel, D. Koesling, K. Schmidt and F. Brunner, *J. Biol. Chem.*, 1998, **273**, 3264.

18) G. E. Schulz, 'Principles of Protein Structure', Springer-Verlag, New York, 1979, 53.

19) M. W. Radomski, R. M. J. Palmer and S. Moncada, *Br. J. Pharmacol.*, 1987, **92**, 639.

20) C. R. Triggle, *Pharmaceutical News*, 1994, **1**, 9.

21) S. Moncada, R. M. J. Palmer and E. A. Higgs, *Pharmacol. Rev.*, 1991, **43**, 109.

22) H. Ischiropoulos, L. Zhu and J. S. Beckman, *Arch. Biochem. Biophys.*, 1992, **298**, 446.

23) J. S. Stamler, O. Jaraki, J. Osborne, D. I. Simon, J. Keaney, J. Vita, D. Singel, C. R. Valeri and J. Loscalzo, *Proc. Natl. Acad. Sci. USA*, 1992, **89**, 7674.

24) D. Jourd'heuil, K. Hallén, M. Feelisch and M. B. Grisham, *Free Radic. Biol. Med.*, 2000, **28**, 409.

25) L. J. Ignarro, H. Lippton, J. C. Edwards, W. H. Baricos, A. L. Hyman, P. J. Kadowitz and C. A. Gruetter, *J. Pharmacol. Exp. Ther.*, 1981, **218**, 739.

26) B. T. Mellion, L. J. Ignarro, C. B. Myers, E. H. Ohlstein, B. A. Ballot, A. L. Hyman and P. J. Kadowitz, *Mol. Pharmacol.*, 1983, **23**, 653.

27) S. Oae and K. Shinhama, *Org. Prep. Proceed. Int.*, 1983, **15**, 165.

28) J. Barrett, D. F. Debenham and J. Glauser, *Chem. Commun.*, 1965, 248.

29) K. Wang, Y. Hou, W. Zhang, M. B. Ksebati, M. Xian, J. P. Cheng and P. G. Wang, *Bioorg. Med. Chem. Lett.*, 1999, **9**, 2897.

30) M. D. Bartberger, K. N. Houk, S. C. Powell, J. D. Mannion, K. Y. Lo, J. S. Stamler and E. J. Toone, *J. Am. Chem. Soc.*, 2000, **122**, 5889.

31) P. A. Morris and D. L. H. Williams, *J. Chem. Soc., Perkin Trans. 2*, 1988, 513.

32) L. Grossi, P. C. Montevecchi and S. Strazzari, *Eur. J. Org. Chem.*, 2001, 131.

33) P. J. Coupe and D. L. H. Williams, *J. Chem. Soc., Perkin Trans. 2*, 2001, 1595.

34) H. M. S. Patel and D. L. H. Williams, *J. Chem. Soc., Perkin Trans. 2*, 1990, 37.

35) M. Keshive, S. Singh, J. S. Wishnok, S. R. Tannenbaum and W. M. Dean, *Chem. Res. Toxicol.*, 1996, **9**, 988.

36) K. Inoue, T. Akaike, Y. Miyamoto, T. Okamoto, T. Sawa, M. Otagiri, S. Suzuki, T. Yoshimura and H. Maeda, *J. Biol. Chem.*, 1999, **274**, 27069.

37) G. Stubauer, A. Giuffrè and P. Sarti, *J. Biol. Chem.*, 1999, **274**, 28128.

38) O. Rafikova, R. Rafikov and E. Nudler, *Proc. Natl. Acad. Sci. USA*, 2002, **99**, 5913.

39) R. J. Singh, N. Hogg, J. Joseph and B. Kalyanaraman, *J. Biol. Chem.*, 1996, **271**, 18596.

40) D. J. Sexton, A. Muruganandam, D. J. McKenney and B. Mutus, *Photochem. Photobiol.*, 1994, **59**, 463.

41) P. D. Wood, B. Mutus and R. W. Redmond, *Photochem. Photobiol.*, 1996, **64**, 518.

42) L. Field, R. V. Dilts, R. Ravichandran, P. G. Lenhert and G. E. Carnahan, *J. Chem. Soc., Chem. Commun.*, 1978, 249.

43) N. Bainbridge, A. R. Butler and C. H. Görbitz, *J. Chem. Soc., Perkin Trans. 2*, 1997, 351.

44) R. J. Singh, N. Hogg, J. Joseph and B. Kalyanaraman, *FEBS Lett.*, 1995, **360**, 47.

45) S. C. Askew, D. J. Barnett, J. McAninly and D. L. H. Williams, *J. Chem. Soc., Perkin Trans. 2*, 1995, 741.

46) A. P. Dicks, H. R. Swift, D. L. H. Williams, A. R. Butler, H. H. Al-Sa'doni and B. G. Cox, *J. Chem. Soc., Perkin Trans. 2*, 1996, 481.

47) P. H. Beloso and D. L. H. Williams, *J. Chem. Soc., Chem. Commun.*, 1997, 89.

48) B. C. Gilbert, S. Silvester and P. H. Walton, *J. Chem. Soc., Perkin Trans. 2*, 1999, 1115.

49) Y. Hou, J. Wang, F. Arias, L. Echegoyen and P. G. Wang, *Bioorg. Med. Chem. Lett.*, 1998, **8**, 3065.

50) A. P. Dicks, P. H. Beloso and D. L. H. Williams, *J. Chem. Soc., Perkin Trans. 2*, 1997, 1429.

51) A. C. F. Gorren, A. Schrammel, K. Schmidt and B. Mayer, *Arch. Biochem. Biophys.*, 1996, **330**, 219.

52) D. R. Noble and D. L. H. Williams, *Nitric Oxide: Biol. Chem.*, 2000, **4**, 392.

53) K, Varnagy, I. Sovago, and H. Kozlowski, *Inorg. Chim. Acta*, 1988, **151**, 117.

54) M. Micheloni, P. M. May and D. R. Williams, *J. Inorg. Nucl. Chem.*, 1978, **40**, 1209.

55) D. R. Noble and D. L. H. Williams, *J. Chem. Soc., Perkin Trans. 2*, 2001, 13.

56) A. J. Holmes and D. L. H. Williams, *J. Chem. Soc., Perkin Trans. 2*, 2000, 1639.

57) T. M. Devlin, 'Textbook of Biochemistry', 3rd Ed., Wiley, New York, 1992, 321.

58) A. P. Dicks and D. L. H. Williams, *Chem. Biol.*, 1996, **3**, 655.

59) D. Jourd'heuil, F. S. Laroux, D. Kang, A. M. Miles, D. A. Wink and M. B. Grisham, *Methods Enzymol.*, 1999, **301**, 220.

60) H. H. Al-Sa'doni, I. L. Megson, S. Bisland, A. R. Butler and F. W. Flitney, *Br. J. Pharmacol.*, 1997, **121**, 1047.

61) M. P. Gordge, D. J. Meyer, J. Hothersall, G. H. Neild, N. N. Payne and A. Noronha-Dutra, *Br. J. Pharmacol.*, 1995, **114**, 1083.

62) M. P. Gordge, J. S. Hothersall, G. H. Field and A. A. Noronha Dutra, *Br. J. Pharmacol.*, 1996, **119**, 533.

63) A. F. Vanin, *Biochem. (Moscow)*, 1998, **63**, 782.

64) S. Costanzo, S. Ménage, R. Purrello, R. P. Bonomo and M. Fontecave, *Inorg. Chim. Acta*, 2001, **318**, 1.

65) B. Saville, *Analyst*, 1958, **83**, 670.

66) H. R. Swift and D. L. H. Williams, *J. Chem. Soc., Perkin Trans. 2*, 1997, 1933.

67) S. S. Al-Kaabi, D. L. H. Williams, R. Bonnett and S. L. Ooi, *J. Chem. Soc., Perkin Trans. 2*, 1982, 227.

68) P. J. Coupe and D. L. H. Williams, *J. Chem. Soc., Perkin Trans. 2*, 1999, 1057.

69) A. P. Munro and D. L. H. Williams, *J. Chem. Soc., Perkin Trans. 2*, 1999, 1989.

70) D. J. Barnett, J. McAninly and D. L. H. Williams, *J. Chem. Soc., Perkin Trans. 2*, 1994, 1131.

71) D. J. Barnett, A. Rios and D. L. H. Williams, *J. Chem. Soc., Perkin Trans. 2*, 1995, 1279.

72) N. Hogg, *Anal. Biochem.*, 1999, **272**, 257.

73) K. Wang, Z. Wen, W. Zhang, M. Xian, J. P. Cheng and P. G. Wang, *Bioorg. Med. Chem. Lett.*, 2001, **11**, 433.

74) H. Zhang and G. E. Means, *Anal. Biochem.*, 1996, **237**, 141.

75) S. P. Singh, J. S. Wishnok, M. Keshive, W. M. Deen and S. R. Tannenbaum, *Proc. Natl. Acad. Sci. USA*, 1996, **93**, 14428.

76) A. P. Dicks, E. Li, A. P. Munro, H. R. Swift and D. L. H. Williams, *Can. J. Chem.*, 1998, **76**, 789.

77) P. S. Y. Wong, J. Hyun, J. M. Fukuto, F. N. Shirota, E. G. DeMaster, D. W. Shoeman and H. T. Nagasawa, *Biochem.*, 1998, **37**, 5362.

78) T. Komiyama and K. Fujimori, *Bioorg. Med. Chem. Lett.*, 1997, **7**, 175.

79) A. P. Munro and D. L. H. Williams, *J. Chem. Soc., Perkin Trans. 2*, 2000, 1794.

80) Y. Hou, Z. Guo, J. Li and P. G. Wang, *Biochem. Biophys. Res. Commun.*, 1996, **228**, 88.

81) S. Aleryani, E. Milo, Y. Rose and P. Kostka, *J. Biol. Chem.*, 1998, **273**, 6041.

82) M. Trujillo, M. N. Alvarez, G. Peluffo, B. A. Freeman and R. Radi, *J. Biol. Chem.*, 1998, **273**, 7828.

83) J. O. Edwards and R. C. Plumb, *Prog. Inorg. Chem.*, 1993, **41**, 599.

84) E. J. Langford, A. S. Brown, R. J. Wainwright, A. J. de Belder, M. R. Thomas, R. E. A. Smith, M. W. Radomski, J. F. Martin and S. Moncada, *Lancet*, 1994, **344**, 1458.

85) A. de Belder, C. Lees, J. Martin, S. Moncada and S. Campbell, *Lancet*, 1995, **345**, 124.

86) Z. Chen, J. Zhang and J. S. Stamler, *Proc. Natl. Acad. Sci. USA*, 2002, **99**, 8306.

87) M. R. Miller, I. L. Megson, M. J. Roseberry, F. A. Mazzei, A. R. Butler and D. J. Webb, *Eur. J. Pharmacol.*, 2000, **403**, 111.

88) L. Jia and R. C. Blantz, *Eur. J. Pharmacol.*, 1998, **354**, 33.

89) D. S. Lind, M. I. Kontaridis, P. D. Edwards, M. D. Josephs, L. L. Moldawer and E. M. Copeland, III, *J. Surg. Res.*, 1997, **69**, 283.

90) J. Ramirez, L. Yu, J. Li, P. G. Braunschweiger and P. G. Wang, *Bioorg. Med. Chem. Lett.*, 1996, **6**, 2575.

91) I. L. Megson, I. R. Greig, G. A. Gray, D. J. Webb and A. R. Butler, *Br. J. Pharmacol.*, 1997, **122**, 1617.

92) Y. Hou, J. Wang, P. R. Andreana, G. Cantauria, S. Tarasia, L. Sharp, P. G. Braunschweiger and P. G. Wang, *Bioorg. Med. Chem. Lett.*, 1999, **9**, 2255.

93) M. Hatanaka, *Biochim. Biophys. Acta*, 1974, **355**, 77.

94) Y. Hou, X. Wu, W. Xie, P. G. Braunschweiger and P. G. Wang, *Tet. Lett.*, 2001, **42**, 825.

95) B. Gaston, S. Sears, J. Woods, J. Hunt, M. Ponaman, T. McMahon and J. S. Stamler, *Lancet*, 1998, **351**, 1317.

96) F. M. Delen, J. M. Sippel, M. L. Osborne, S. Law, N. Thukkani and W. E. Holden, *Chest*, 2000, **117**, 695.

Chapter 2

Decomposition Pathways of S-Nitroso-1-thio-β-D-glucose Tetraacetate

Chapter 2: Decomposition Pathways of *S*-Nitroso-1-thio-*β*-D-glucose Tetraacetate

2.1 Introduction

Studies into the biological activity of *S*-nitrosothiols found that *S*-nitroso-*β*-D-thioglucose (SNTG) inhibited platelet aggregation[1] and *S*-nitrosothio-*β*-D-galactopyranose (SNGP) induced vasodilation.[2] A study attempted to find a *S*-nitroso sugar stable as a solid so that biological testing could be performed using it.[3] Transdermal delivery of SNAG was found to induce vasodilation in a human volunteer. The structures of the three S-nitroso sugars are shown in figure 2.1.

Figure 2.1 Structure of three *S*-nitroso sugars.

In this chapter decomposition pathways of SNAG are studied to determine if there are any significant differences in the reactivity of SNAG compared to other low molecular weight *S*-nitrosothiols.

2.2 Nitrosation of 1-Thio-*β*-D-glucose Tetraacetate

The nitrosation of 1-thio-*β*-D-glucose tetraacetate was studied to determine the conditions required to form the corresponding *S*-nitrosothiol.

38

2.2.1 Determination of UV / Vis Spectroscopic Parameters

A method for making SNAG in the laboratory had to be found because it could not be purchased commercially. SNAG was generated *in situ* by the 1 : 1 stoichiometric addition of thiol with $NaNO_2$ in acidic conditions. The thiol was first dissolved in acetonitrile due to its poor solubility in aqueous conditions. The final percentage volume of acetonitrile was ten percent.

When the thiol was reacted with different concentrations of nitrous acid the absorbance levelled off after the 1 : 1 stoichiometric ratio was passed. This showed that when generating SNAG *in situ* a 1 : 1 nitrous acid thiol mixture would yield a near quantitative amount of *S*-nitrosothiol.

After the conditions for generating SNAG *in situ* had been determined the absorbance maxima and extinction co-efficients were calculated. SNAG was prepared by reacting equimolar quantities of thiol and sodium nitrite in a solution containing ten percent acetonitrile and 0.2 M perchloric acid. Table 2.1 shows the absorbance of various [SNAG] at 345 nm.

[SNAG] / M	Absorbance
0.2×10^{-3}	0.08
0.4×10^{-3}	0.17
0.6×10^{-3}	0.25
0.8×10^{-3}	0.35
1.0×10^{-3}	0.43

Table 2.1 Absorbance at 345 nm for various solutions of SNAG.

$$A = \varepsilon cl$$

Equation 2.1 The Beer-Lambert law.

The extinction co-efficients for SNAG were calculated using the Beer-Lambert law (equation 2.1) where A is absorbance, ε is the extinction co-efficient, c is the concentration of the absorbing species and l is the pathlength of the cell. The extinction co-efficients were calculated by plotting absorbance against concentration and measuring the gradient of the graph. Plots gave a near zero y axis intercept because no absorbing species would be present. Figure 2.2 shows the data plotted from table 2.1.
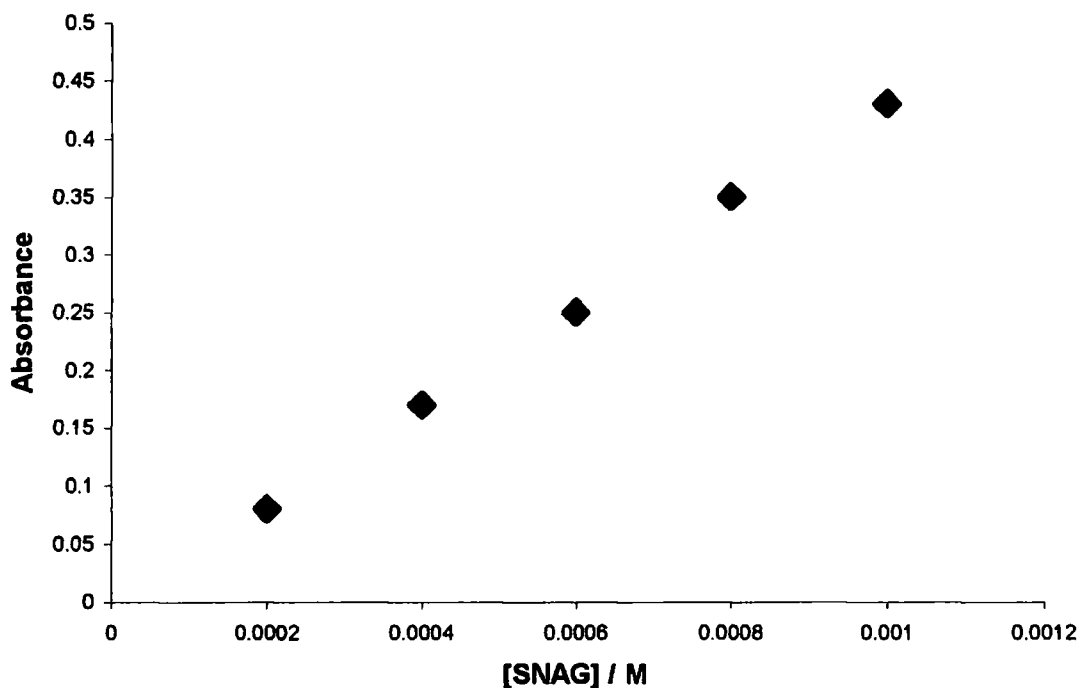
Figure 2.2 Absorbance of SNAG at 345 nm plotted against concentration.

Absorbance maxima were observed at 345 and 558 nm giving the extinction co-efficients $\varepsilon_{345nm} = 440 \pm 8$ dm^3 mol^{-1} cm^{-1} and $\varepsilon_{558nm} = 10$ dm^3 mol^{-1} cm^{-1}.

No significant error for the extinction co-efficient at 558 nm is reported because it was calculated from only three readings. When SNAG was made at the concentration required to determine the absorbance accurately at 558 nm a rapid decomposition occurred, probably via the thermal / photolytic decomposition pathway.

2.2.2 S-Nitrosation Kinetics of 1-Thio-β-D-glucose Tetraacetate

Kinetics for the nitrosation of the thiol group on the sugar were measured. The general rate equation for S-nitrosation of thiols has been determined.[4] (equation 2.2) The chemical equation for the reaction is shown in scheme 2.1.

Rate = k_3[RSH][H$^+$][HNO$_2$]

Equation 2.2 Rate equation for the acid catalysed S-nitrosation of a thiol.

$$RSH \ + \ HNO_2 \ \xrightarrow[k_3]{H^+} \ RSNO \ + \ H_2O$$
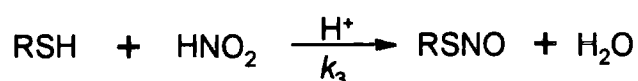
Scheme 2.1 Chemical equation for the nitrosation of a thiol.

The reaction was followed by increase in absorbance at 345 nm using an excess of sodium nitrite. All experiments gave good individual first order plots. The first order rate constants obtained from the reaction solutions are shown in table 2.2.

[NaNO$_2$] / M	[RSH] / M	k_{obs} / s^{-1}
1.0×10^{-2}	1×10^{-3}	0.194
1.2×10^{-2}	1×10^{-3}	0.243
1.4×10^{-2}	1×10^{-3}	0.316
1.6×10^{-2}	1×10^{-3}	0.380
1.8×10^{-2}	1×10^{-3}	0.410
2.0×10^{-2}	1×10^{-3}	0.465

Table 2.2 Concentration of sodium nitrite and thiol in each solution and psuedo first order rate constants obtained in the presence of 0.2 M perchloric acid at 25 °C.

The first order rate constants obtained were plotted against sodium nitrite concentration from table 2.2. The gradient of the graph shown in figure 2.3 is equal to k_3[H$^+$], therefore the third order rate constant for S-nitrosation was found to be $k_3 = 137 \pm 7$ dm^6 mol^{-2} s^{-1}. The graph has a near zero intercept.
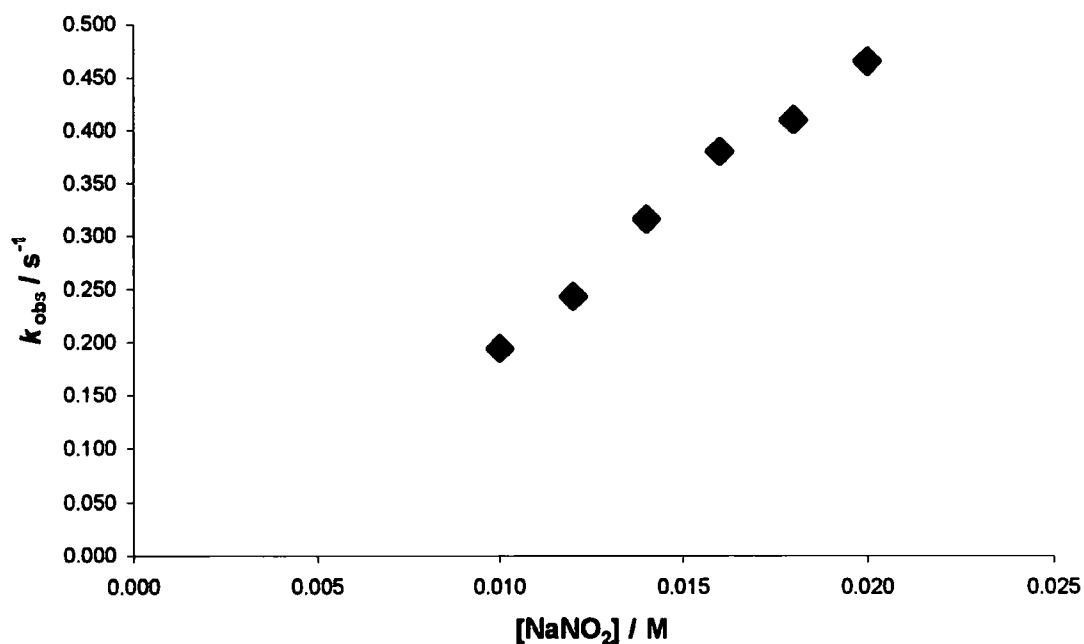
Figure 2.3 First order rate constants obtained plotted against sodium nitrite concentration.

Third order rate constants for S-nitrosation of a range of thiols have been collated.[5] They varied between $213 - 4760$ dm^6 mol^{-2} s^{-1} and are similar to the value obtained in this study.

When generating SNAG *in situ* for experimental work the acid concentration was lowered to 0.02 M. This was because reactions were to be carried out at specific pH values so lowering the acid concentration meant buffers would maintain pH more effectively.

2.3 Investigation into the Thermal / Photolytic Decomposition Pathway

S-Nitrosothiols can decompose to their corresponding disulfide and nitric oxide via a thermal / photolytic pathway. It has been found that the rate of photolytic decomposition with respect to the S-nitrosothiol is first order.[6] A reaction mechanism for the photolytic pathway has been suggested and is shown in scheme 2.2.[7] It is assumed that the thermal decomposition proceeds by a similar mechanism giving the same products.

$$RSNO \xrightarrow{hv / \Delta} RS^{\bullet} + NO$$

$$RS^{\bullet} + O_2 \longrightarrow RSOO^{\bullet} \xrightarrow{RSNO} RSSR + NO + O_2$$

$$RS^{\bullet} + RSNO \longrightarrow RSSR + NO$$
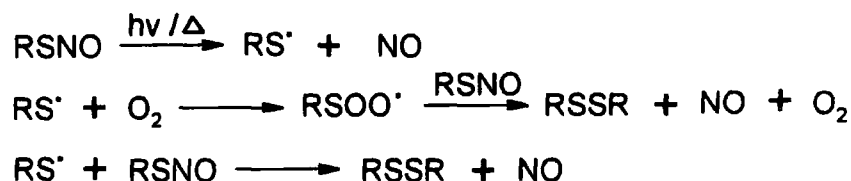
Scheme 2.2 Proposed series of reactions for the photochemical decomposition of *S*-nitrosothiols.

2.3.1 Thermal Decomposition of SNAG at Different Temperatures

When SNAG was generated *in situ* in the laboratory at high enough concentration the *S*-nitrosothiol decomposed rapidly, forming a precipitate believed to be the disulfide. The thermal decomposition was measured and first order rate constants were obtained. Reactions were carried out at different temperatures to determine whether at body temperature the lifetime of the *S*-nitrosothiol significantly decreased.

Reactions were followed by measuring absorbance at 345 nm for twenty four hours. The concentration of SNAG used was 5×10^{-4} M and 1×10^{-4} M EDTA was present to suppress the copper ion mediated decomposition. Reactions were studied in 0.2 M perchloric acid and 0.15 M phosphate buffer (pH 7.4) and first order rate constants obtained are shown in table 2.3.

Temperature / K	k_{obs} / s^{-1}	
	pH 7.4	0.2 M H$^+$
298	$3.51 \times 10^{-5} \pm 0.06 \times 10^{-5}$	$2.41 \times 10^{-5} \pm 0.01 \times 10^{-5}$
303	$4.21 \times 10^{-5} \pm 0.07 \times 10^{-5}$	$3.28 \times 10^{-5} \pm 0.02 \times 10^{-5}$
308	$4.99 \times 10^{-5} \pm 0.05 \times 10^{-5}$	$4.20 \times 10^{-5} \pm 0.04 \times 10^{-5}$
313	$7.76 \times 10^{-5} \pm 0.07 \times 10^{-5}$	$5.23 \times 10^{-5} \pm 0.02 \times 10^{-5}$
318	$11.08 \times 10^{-5} \pm 0.10 \times 10^{-5}$	$6.10 \times 10^{-5} \pm 0.02 \times 10^{-5}$

Table 2.3 First order rate constants obtained for the decomposition of SNAG in acid and at pH 7.4 at different temperatures.

The rate of decomposition at physiological pH was found to be a little greater than in acidic solution. This can be explained by a hydrolysis reaction occurring at pH 7.4 that is shown in scheme 2.3.[8] In acidic solution even if hydrolysis took place nitrous acid would reform the S-nitrosothiol. The rate equations describing the decompositions at different pH have been derived. (equation 2.3)

$$RSNO \ + \ ^\cdot OH \longrightarrow RSH \ + \ NO_2^-$$

Scheme 2.3 Chemical equation for the hydrolysis of S-nitrosothiols.

In 0.2 M H^+, Rate = $k_{thermal}$[RSNO].

In pH 7.4 buffer, Rate = $(k_{thermal} + k_{hydrolysis})$[RSNO].

Equation 2.3 Rate equations for the decomposition of SNAG in 0.2 M $HClO_4$ and pH 7.4 buffer.

Using the rate constants determined in acidic solution for thermal decomposition at different temperatures, SNAG activation parameters could be calculated using the Eyring equation. (equation 2.4) k_T is the rate constant at temperature T, h is the Planck constant, k_B is the Boltzmann constant, $\Delta S^{\ominus\ddagger}$ is the entropy of activation, $\Delta H^{\ominus\ddagger}$ is the enthalpy of activation and R is the gas constant.

$$\ln\left(\frac{k_T h}{k_B T}\right) = \frac{\Delta S^{\ominus\ddagger}}{R} - \frac{\Delta H^{\ominus\ddagger}}{RT}$$

Equation 2.4 The Eyring equation.

The values required to determine the activation parameters were calculated and are shown in table 2.4. A plot of $\ln(k_T h/k_B T)$ against T^{-1} was linear (see figure 2.4) and the value of $\Delta H^{\ominus\ddagger}$ and $\Delta S^{\ominus\ddagger}$ determined from the gradient and intercept respectively.

T^{-1} / K^{-1}	$\ln(k_T h/k_B T)$
0.003354	-40.091
0.003299	-39.799
0.003245	-39.568
0.003193	-39.365
0.003143	-39.227

Table 2.4 Values calculated for the Eyring plot.
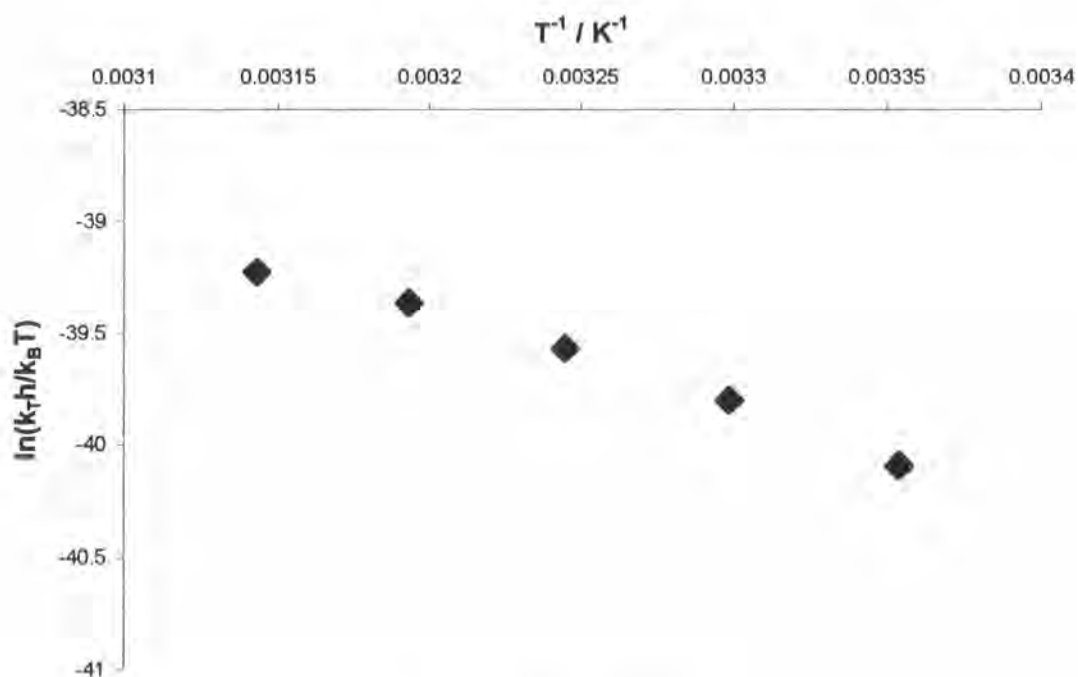
Figure 2.4 The Eyring plot drawn from data in table 2.4.

The activation parameters were found to be $\triangle H^{\ominus\ddagger} = 34 \pm 2$ kJ mol^{-1} and $\triangle S^{\ominus\ddagger} = -218 \pm 7$ J K^{-1} mol^{-1}. An interesting point concerning these values was the increase of order at the transition state, consistent with the reaction of a radical with SNAG being in the rate limiting step.

2.3.2 Product Analysis of the Thermal / Hydrolysis Reaction

SNAG at pH 7.4 in the presence of EDTA decomposed by a hydrolysis and thermal reaction. NO formed would rapidly oxidize to form nitrite ions quantitatively[9,10], which are also the product of the hydrolysis reaction. Using a Griess test (see scheme 2.4) concentrations of nitrite ions in aqueous solution can be determined very accurately.[11]

Solutions of N-(1-naphthyl)ethylenediamine (NNED) and sulfanilamide (SUL) were prepared using 0.4 M perchloric acid. Nitrite ions at acidic pH form nitrous acid, which nitrosates SUL leading to the diazotisation of the amine group. A purple azo dye forms when the coupling agent NNED is added to the solution and the extinction co-efficient of the azo dye is measured at 535 nm to calibrate the test. The measured absorbance and final concentration of reactants is shown in table 2.5.
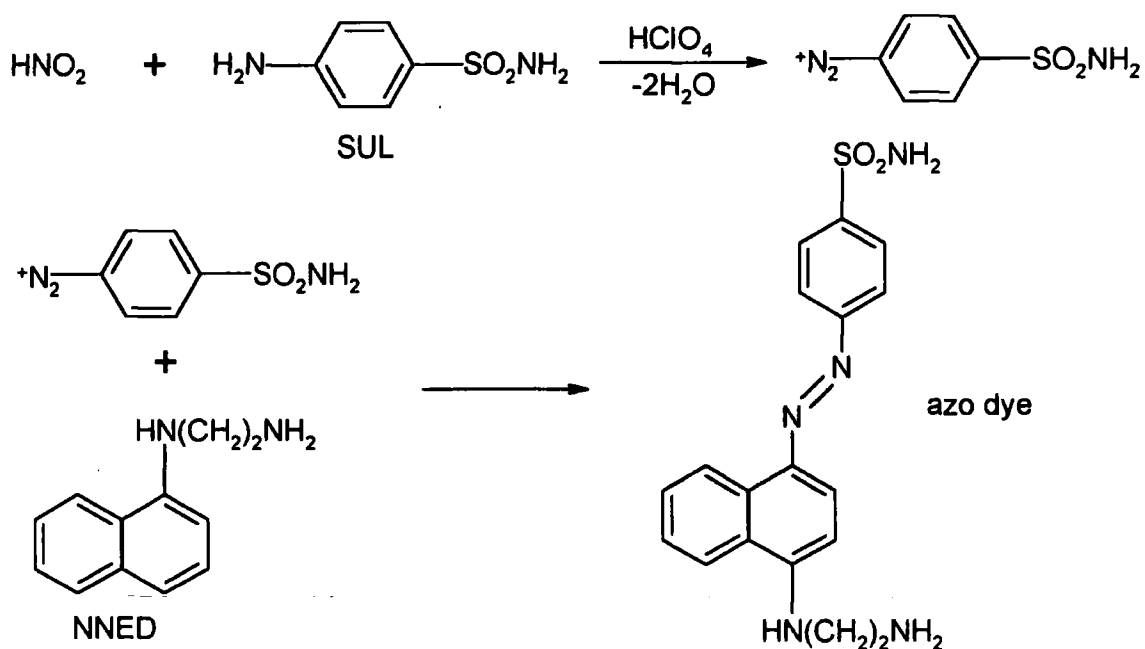
Scheme 2.4 The chemical reactions used in the Griess test.

[NNED] / M	[SUL] / M	[HClO₄] / M	[NaNO₂] / M	Absorbance
0.002	0.08	0.32	0.6×10^{-5}	0.29
0.002	0.08	0.32	1.2×10^{-5}	0.57
0.002	0.08	0.32	1.8×10^{-5}	0.85
0.002	0.08	0.32	2.4×10^{-5}	1.11
0.002	0.08	0.32	3.0×10^{-5}	1.38

Table 2.5 Absorbance at 535 nm due to the azo dye formed with various [NaNO₂].

The extinction co-efficient was calculated as described in section 2.2.1 using the data in table 2.5. The value calculated was $\varepsilon_{535nm} = 45\,300 \pm 420$ dm^3 mol^{-1} cm^{-1} and this was found to be a reproducible result. The Griess reaction for several nitrosatable compounds and a range of coupling agents has been studied.[12] The extinction co-efficient reported for this system is $\varepsilon_{535nm} = 27\,000$ dm^3 mol^{-1} cm^{-1} which is significantly lower than the experimental value found in this study.

A reaction solution containing 5×10^{-4} M SNAG, 1×10^{-4} M EDTA and 0.15 M phosphate buffer (pH 7.4) was analysed for nitrite after the S-nitrosothiol had fully decomposed. The nitrite yield from the reaction was found to be 98 %.

2.3.3 Thermal Decomposition of some other S-Nitrosothiols

The thermal decomposition of S-nitrosopenicillamine, S-nitrosocysteine, S-nitroso-N-acetylpenicillamine (SNAP) and S-nitrosoglutathione (GSNO) was studied. This was so that data obtained using SNAG could be compared with other S-nitrosothiols. Reaction solutions containing 5×10^{-4} M S-nitrosothiol, 1×10^{-4} M EDTA and 0.2 M perchloric acid were made up. The absorbance at 340 nm was measured over twenty four hours.

No change in absorbance was observed in the GSNO solution and the absorbance due to S-nitrosocysteine only decreased by 0.01. This suggests that the light used by the spectrometer to obtain absorbance values is not strong enough to trigger a photochemical decomposition, and the thermal reaction is very slow at 25 °C.

The thermal stability of primary S-nitrosothiols has been studied and initial rates of reaction were determined at 25 °C.[13] When unbuffered solutions of GSNO and S-nitrosocysteine were analysed, first order rate constants were obtained which appeared to be dependent on concentration. This study has found that in the dark these S-nitrosothiols are stable over long periods of time.

The rate of decomposition for the tertiary S-nitrosothiols over twenty four hours was more significant and are shown in figure 2.5. The reaction profile for S-nitrosopenicillamine assuming a first order process gave a value $k = 7.1 \times 10^{-6} \pm 0.1 \times 10^{-6}$ s^{-1}. For SNAP an induction period was observed but the remainder of the reaction profile treated as a first order model gave the rate constant $k = 7.3 \times 10^{-6} \pm 0.1 \times 10^{-6}$ s^{-1}.
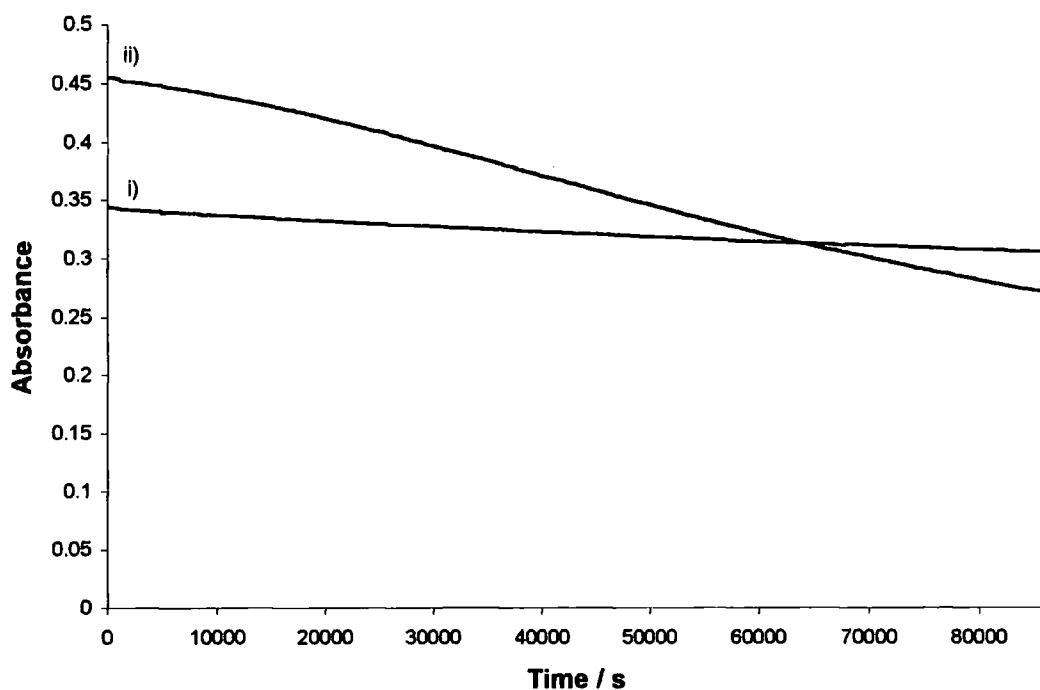
Figure 2.5 Absorbance at 340 nm measured over twenty four hours for i) S-nitrosopenicillamine and ii) SNAP at 25 °C.

The first order rate constants reported must be considered only as estimates since the full reaction profile was not taken into account in the calculations.

2.3.4 Effect of Added Disulfide on S-Nitrosothiol Decomposition

The presence of disulfide can have a large effect on the rate of copper catalysed S-nitrosothiol decomposition at pH 7.4.[14] Disulfide was added to tertiary S-nitrosothiol solutions to find out if disulfide affected the thermal reaction as well.

The thermal decomposition of 5×10^{-4} M S-nitrosopenicillamine was followed at 340 nm for twenty four hours with penicillamine disulfide concentrations between 5×10^{-3} M and 1×10^{-2} M. The presence of disulfide had no effect on the rate of decomposition of the S-nitrosothiol.

The experiment was repeated with SNAP using a lower concentration of disulfide due to its poorer solubility. The disulfide was prepared and characterised as described in section 6.2.3.
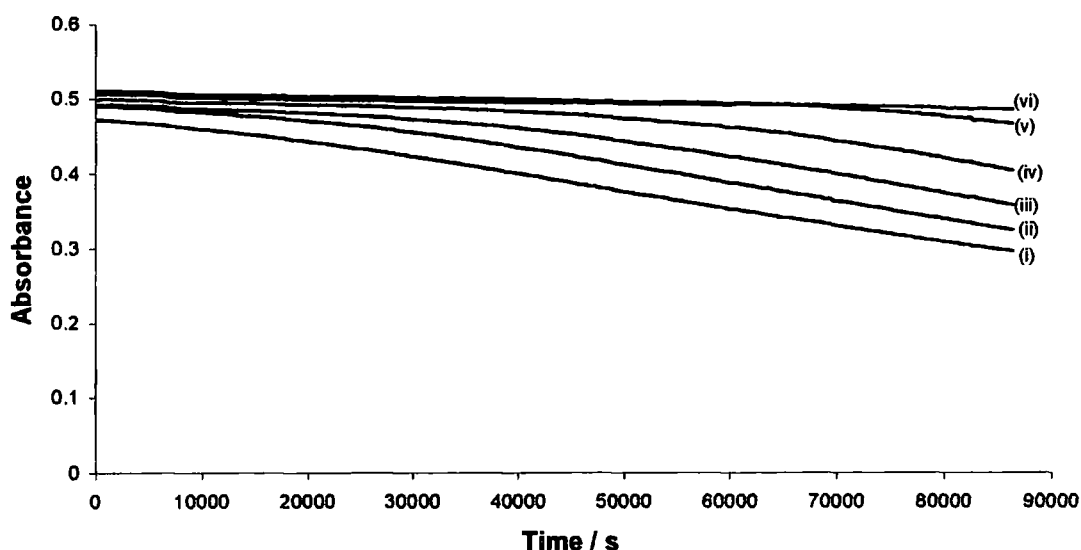
Figure 2.6 Decomposition followed at 340 nm of 5×10^{-4} M SNAP with i) 5×10^{-4}, ii) 6×10^{-4}, iii) 7×10^{-4}, iv) 8×10^{-4}, v) 9×10^{-4} and vi) 1×10^{-3} M NAP disulfide, 0.2 M perchloric acid and 1×10^{-4} M EDTA at 25 °C.

The addition of disulfide to a solution of SNAP decreased the rate of decomposition and this is shown in figure 2.6. This may arise if the product of the thermal reaction reacts with the disulfide to generate the S-nitrosothiol. Studies have described a process where NO in

the presence of oxygen reacts with disulfide leading to the formation of an *S*-nitrosothiol.[15,16]

Lifetimes of *S*-nitrosothiols in a UV / Vis spectrometer are not representative of their lifetime unprotected in a laboratory. This is because photolysis can occur due to sunlight and fluorescent lighting that will lead to an increase in the rate of decomposition.[6]

2.4 Investigation into the Copper(+2) Catalysed Decomposition Pathway

It has been found that copper(+2) ions decompose *S*-nitrosothiols catalytically at pH 7.4.[17] Further experiments looking at the reaction mechanism found that copper(+1) was a intermediate in the process.[18] The rate equation has been determined for the copper ion induced decomposition for a number of reactants. (equation 2.5)

$$\text{Rate} = k_2[\text{Cu}^{2+}][\text{RSNO}] + k_1[\text{RSNO}]$$

Equation 2.5 Rate equation for the copper catalysed decomposition of *S*-nitrosothiols.

The effect of the addition of copper(+2) on the life time of SNAG at pH 7.4 has been studied.[3] However no rate constants were reported.

2.4.1 Effect of Added Copper(+2) on the Rate of Decomposition

The addition of copper ions dramatically increased the rate of decomposition of SNAG at pH 7.4. (see figure 2.7) The decrease in absorbance at 345 nm was followed over time, and the decomposition reactions exhibited first order kinetics.
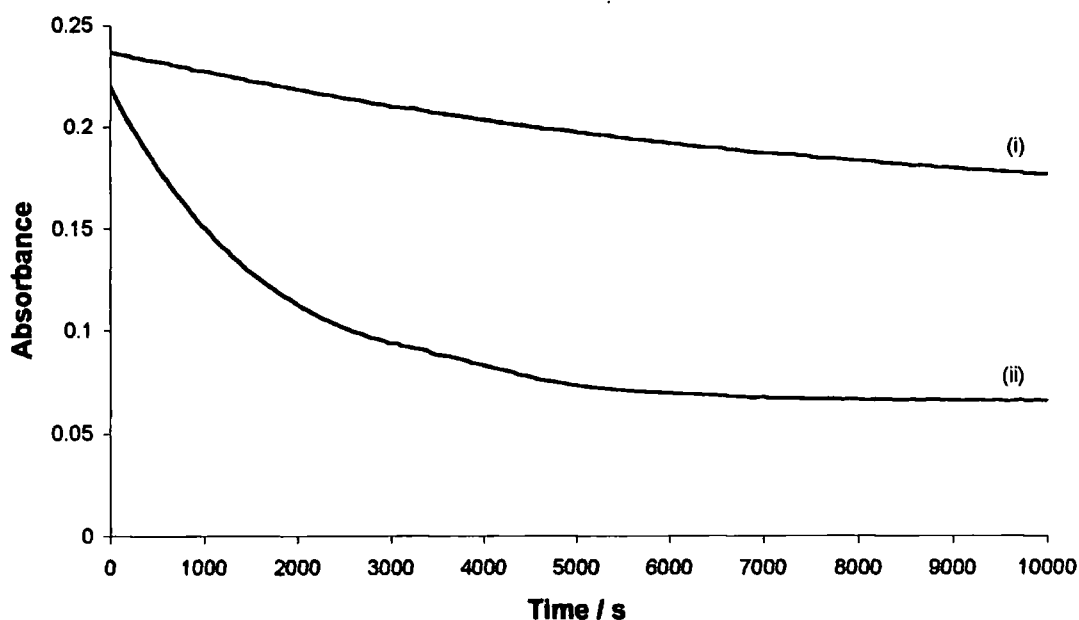
Figure 2.7 5×10^{-4} M SNAG in 0.15 M phosphate buffer (pH 7.4) with i) 1×10^{-4} M EDTA or ii) 1×10^{-5} M copper(+2) at 25 °C.

Initial work on the copper reaction found no significant rate of reaction dependence on copper at low concentration. The copper concentration was increased until a change could be observed, but this was accompanied by copper phosphate precipitation. Use of TRIS buffer instead of phosphate eliminated this problem and the results are shown in table 2.6.

[SNAG] / M	[Cu^{2+}] / M	k_{obs} / s^{-1}
5×10^{-4}	5×10^{-4}	$1.875 \times 10^{-3} \pm 0.006 \times 10^{-3}$
5×10^{-4}	6×10^{-4}	$1.914 \times 10^{-3} \pm 0.006 \times 10^{-3}$
5×10^{-4}	7×10^{-4}	$1.965 \times 10^{-3} \pm 0.008 \times 10^{-3}$
5×10^{-4}	8×10^{-4}	$1.994 \times 10^{-3} \pm 0.005 \times 10^{-3}$
5×10^{-4}	9×10^{-4}	$2.083 \times 10^{-3} \pm 0.005 \times 10^{-3}$

$k_2 = 0.50 \pm 0.05$ dm^3 mol^{-1} s^{-1}.

Table 2.6 Concentrations of SNAG and copper(+2) in the presence of 0.15 M TRIS buffer (pH 7.4) and first order rate constants obtained at 25 °C.

51

2.4.2 Effect of Ascorbic Acid on the Copper Catalysed Decomposition

Ascorbic acid is present *in vivo*, with concentrations in the blood having been measured as $0.2 \times 10^{-5} - 8.5 \times 10^{-5}$ M.[19] The presence of ascorbic acid at low concentrations can have a dramatic effect on the stability of GSNO at pH 7.4.[20] Ascorbic acid makes available copper(+2) bound to glutathione disulfide, the copper(+1) generated then reacts with the *S*-nitrosothiol. The copper decomposition of SNAG was investigated in the presence of ascorbic acid. The reaction was followed by decrease in absorbance at 345 nm and first order rate constants were obtained which are shown in table 2.7.

[SNAG] / M	[Cu²⁺] / M	[Ascorbic Acid] / M	k_{obs} / s⁻¹
5×10^{-4}	1×10^{-5}	0	$6.04 \times 10^{-4} \pm 0.03 \times 10^{-4}$
5×10^{-4}	1×10^{-5}	5×10^{-5}	$7.42 \times 10^{-4} \pm 0.05 \times 10^{-4}$
5×10^{-4}	1×10^{-5}	1×10^{-4}	$8.46 \times 10^{-4} \pm 0.09 \times 10^{-4}$

Table 2.7 Concentration of SNAG, copper(+2) and ascorbic acid with first order rate constants obtained in the presence of phosphate buffer (pH 7.4) at 25 °C.

The addition of a reducing agent did not significantly increase the rate of *S*-nitrosothiol decomposition. If the efficiency of copper reduction were the rate limiting factor here zero order reaction profiles would be observed. A slight increase in rate of reaction was found probably because the copper ion decomposition goes via copper(+1) intermediates.

2.4.3 Product Analysis of the Copper Catalysed Decomposition

Nitric oxide and disulfide are generated by the copper induced decomposition of an *S*-nitrosothiol,[17] so the Griess test was used as described in section 2.3.2. A reaction solution containing 5×10^{-4} M SNAG, 1×10^{-5} M copper(+2) and 0.15 M phosphate buffer (pH 7.4) was analysed for nitrite after the *S*-nitrosothiol had fully decomposed. The nitrite yield from the reaction was found to be 90 %.

2.4.4 Possible Reaction Intermediates in the Copper Catalysed Decomposition

The decomposition of two other S-nitroso sugars, 2-acetamido-2-deoxy-S-nitroso-1-thio-β-D-glucopyranose-3,4,6-triacetate (GPSNO) and SNTG has been studied previously.[21] The structures are shown in figure 2.1 and 2.8. It was found that GPSNO like SNAG was stable as a solid. The kinetic work concentrated mainly on the copper ion induced decomposition.
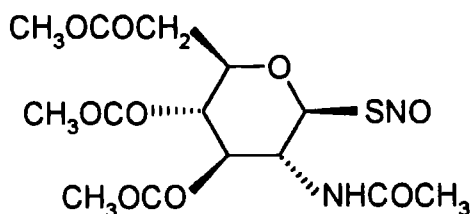
Figure 2.8 Structure of GPSNO.

Second order rate constants for the copper decomposition of a range of S-nitrosothiols have been calculated.[17] When reactions were observed the values ranged from 16 dm^3 mol^{-1} s^{-1} to 270 000 dm^3 mol^{-1} s^{-1}. The rate constant calculated for SNAG is much smaller.

The addition of copper ions to solutions of GPSNO and SNTG at pH 7.4 increased the rate of decomposition of the S-nitrosothiols but first order reaction profiles were not observed.[21] The addition of copper ions to SNAG had a less dramatic effect on the rate of decomposition. This could be due to GPSNO and SNTG having more favourable binding sites for copper(+1) ions and these proposed intermediates are shown in figure 2.9.

i)   ii)
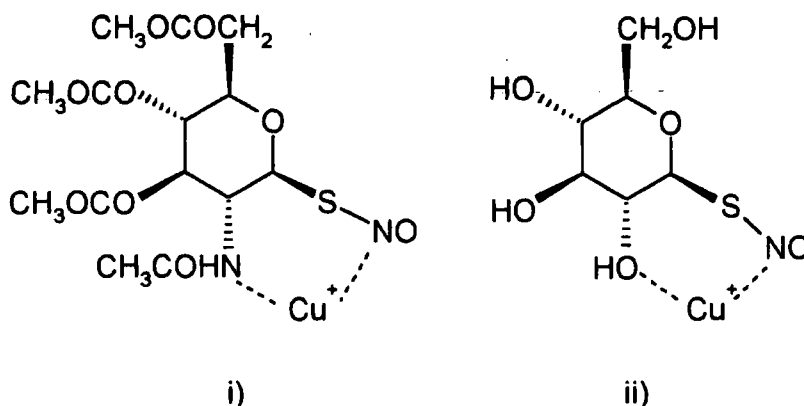
Figure 2.9 Proposed copper(+1) intermediates with i) GPSNO and ii) SNTG.

The copper binding sites could also explain why the copper decomposition of GPSNO and SNTG does not fit a first order model or go to completion at low copper concentrations. GSNO is a relatively stable S-nitrosothiol at pH 7.4 and its stability is attributed to the fact that glutathione disulfide complexes copper(+2) ions.[14] It is possible that the disulfide of the two S-nitroso sugars can complex copper(+2) ions as well. Two complex structures are proposed in figure 2.10.
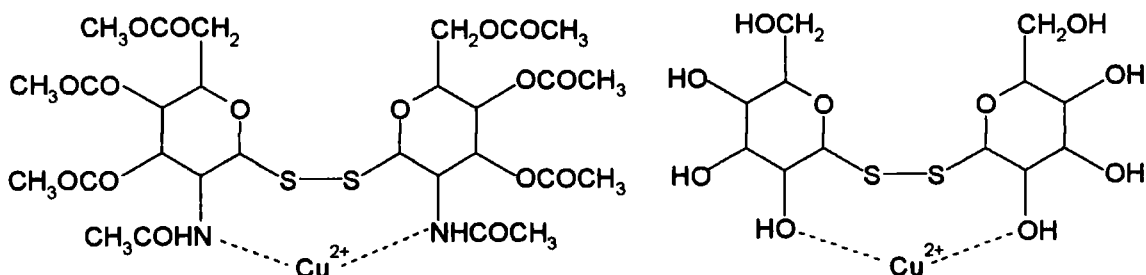
Figure 2.10 Proposed copper(+2) ion complexes with the disulfides of the S-nitroso sugars.

2.5 Investigation into the Transnitrosation Pathway

SNAG can release NO at physiological pH via the thermal / photolytic and copper reaction. An S-nitrosothiol can also deliver NO^+ by transnitrosation to another thiol group and the chemical equation is shown in scheme 2.5.

$$R'SH + RSNO \rightleftharpoons R'SNO + RSH$$

Scheme 2.5 The chemical equation for a transnitrosation reaction between thiol and a S-nitrosothiol.

The transnitrosation reaction has been studied for a number of S-nitrosothiols but not previously using an S-nitroso sugar as the NO^+ carrier.[22] A rate equation was determined for the reaction. (see equation 2.6)

Rate = k_2[R'SH][RSNO]

Equation 2.6 The rate equation for the forward reaction of a transnitrosation reaction between thiol and a S-nitrosothiol.

Cysteine was chosen as the thiol for reaction with SNAG because it is a component of glutathione and human serum albumin. All three thiols are found in the body.

2.5.1 Reaction of SNAG with Cysteine

To determine whether a reaction between these two compounds could be followed easily the extinction co-efficient of S-nitrosocysteine at 345 nm was measured. The method used is described in section 2.2.1. S-Nitrosocysteine was generated *in situ* then diluted down. UV / Vis spectra of the solutions were obtained and the measured absorbance is shown in table 2.8.

[S-Nitrosocysteine] / M	Absorbance at 345 nm
0.0002	0.135
0.0004	0.269
0.0006	0.396
0.0008	0.526
0.0010	0.665

$\varepsilon_{345nm} = 659 \pm 6 \ dm^3 \ mol^{-1} \ cm^{-1}$.

Table 2.8 Concentration of S-nitrosocysteine and absorbance at 345 nm.

The extinction co-efficient of SNAG at 345 nm is 219 $dm^3 \ mol^{-1} \ cm^{-1}$ less than S-nitrosocysteines. Therefore when SNAG reacted with cysteine an increase in absorbance at 345 nm was expected.

When cysteine was reacted with SNAG in excess at physiological pH it was expected that the potentially reversible reaction would be driven in the forward direction. The metal ion chelator EDTA was used to rule out the possibility of a copper ion reaction component. A rapid increase in absorbance at 345 nm was observed and first order rate constants were determined from the reaction profiles. (see table 2.9)

[SNAG] / M	[Cysteine] / M	k_{obs} / s^{-1}
5×10^{-4}	0.005	148
5×10^{-4}	0.006	174
5×10^{-4}	0.007	209
5×10^{-4}	0.008	229
5×10^{-4}	0.009	269
5×10^{-4}	0.010	287

$k_2 = 29\ 000 \pm 1\ 200\ dm^3\ mol^{-1}\ s^{-1}$.

Table 2.9 Concentration of SNAG and cysteine in the presence of 0.075 M phosphate buffer (pH 7.4) and 1×10^{-4} M EDTA with first order rate constants obtained at 25 °C.

A plot of observed first order rate constant against cysteine concentration from the data in table 2.9 gave a straight line that is shown in figure 2.11. The gradient of the line is equal to the second order rate constant for the forward reaction of the transnitrosation reaction.
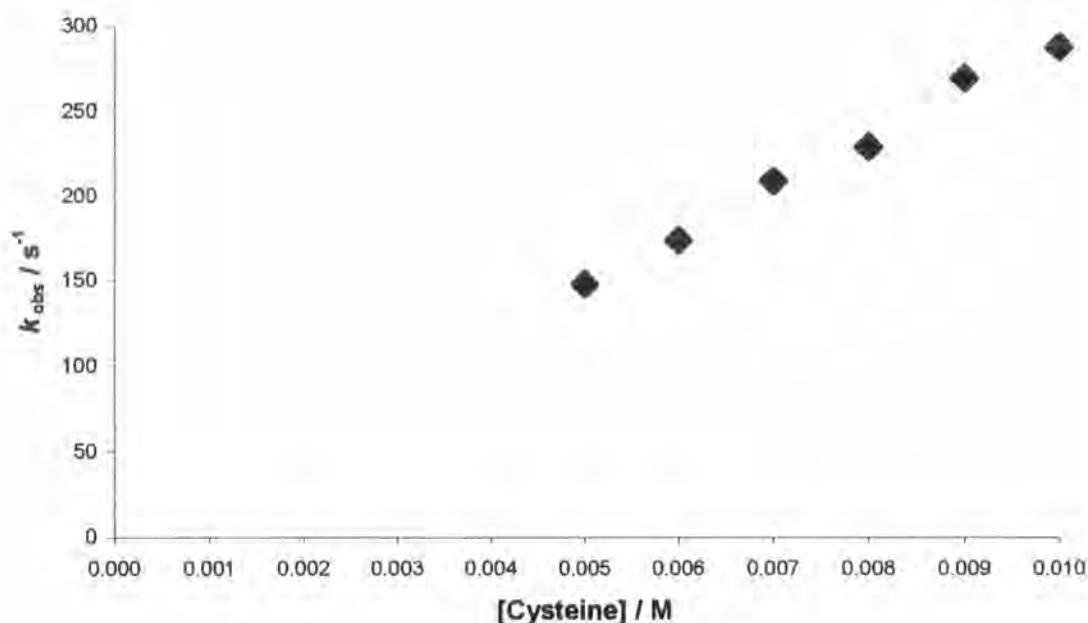
Figure 2.11 First order rate constants plotted against cysteine concentration.

2.5.2 pH Dependence of the Transnitrosation Reaction

The rate constant for a transnitrosation reaction has been found to increase with increasing pH confirming that the reaction occurred via nucleophilic attack by the thiolate anion.[22] The rate constant dependence on pH was studied for the reaction of SNAG with cysteine.

The second order rate constant was determined for the reaction at different pH values by using different phosphate buffer solutions. The pH of the reaction solutions was measured after the reaction had taken place so that an exact value could be obtained. The data collected are shown in table 2.10.

pH	k_2 / dm^3 mol^{-1} s^{-1}
5.83	1070 ± 20
6.38	3600 ± 70
6.91	10 630 ± 510
7.35	27 940 ± 940
7.41*	29 000 ± 1 200
7.62	43 910 ± 1 060

* data from table 2.9.

Table 2.10 Kinetic data obtained for the reaction of SNAG with cysteine in the presence of 1×10^{-4} M EDTA and 0.075 M phosphate buffers at various pH values at 25 °C.

The expression for the second order rate constant (k_2) assuming reaction takes place only via the cysteine anion (RS$^-$) is shown in equation 2.7. K_a is the acid dissociation constant for cysteine and k_{A^-} is the second order rate constants for the reaction of the thiolate anion with the S-nitrosothiol.

$$k_2 = \left(\frac{(k_{A^-} K_a)}{([H^+] + K_a)} \right)$$

Equation 2.7 Hypothesised second order rate constant dependence on pH for the transnitrosation reaction.

The data in table 2.10 were fitted to equation 2.7 using the modelling package Scientist.[23] A full pH curve unfortunately could not be obtained because the reaction became too fast for stopped flow techniques at higher pH. Decreasing the concentration of reactants in order to slow the reaction would lead to the already small absorbance change becoming insignificant.

The pK_a of the thiol group in cysteine was taken as 8.4.[24]
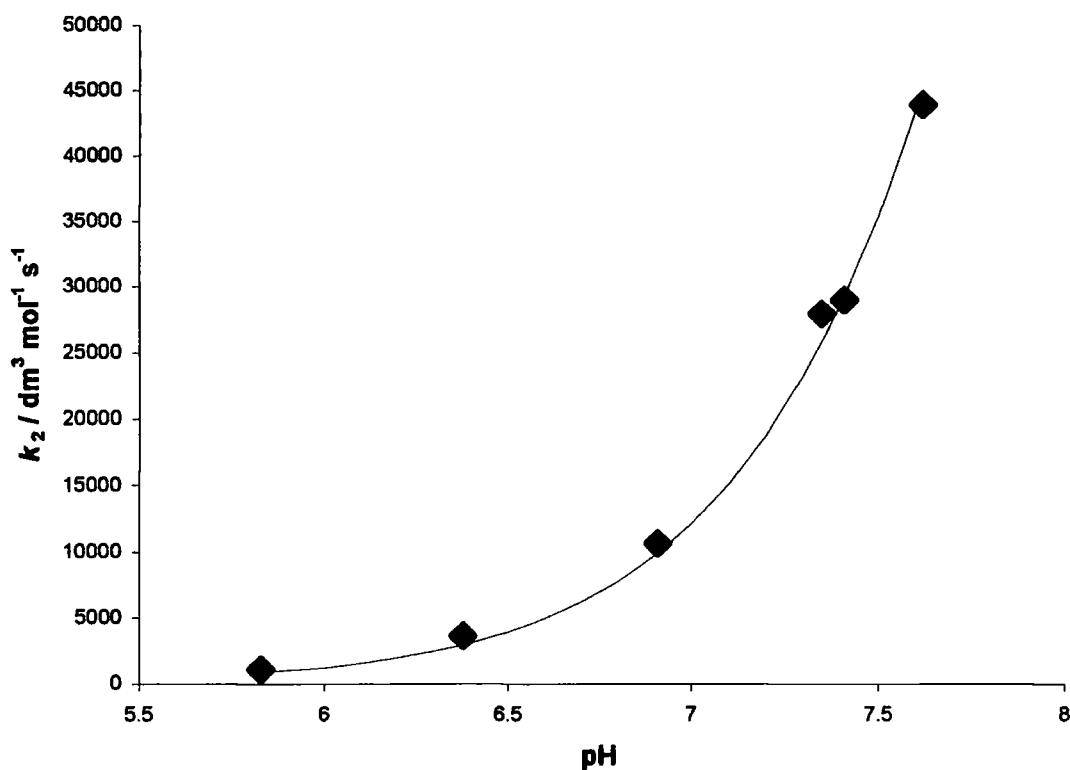
Figure 2.12 Data in table 2.10, (♦) fitted to equation 2.7. (the solid line)

Equation 2.7 fitted the experimental data well (see figure 2.12) over the pH range studied and a value for k_{A^-} was obtained, $k_{A^-} = 316\ 000 \pm 6\ 000\ dm^3\ mol^{-1}\ s^{-1}$. This confirms that the transnitrosation reaction occurs by nucleophilic attack of the thiolate anion.

2.5.3 Reaction of Cysteine with other S-Nitrosothiols

Second order rate constants were determined for the transnitrosation reaction of cysteine with other low molecular weight S-nitrosothiols at pH 7.4. This was to determine whether the rate constant found using SNAG as the NO^+ donor and cysteine as the nucleophile was a typical value.

EDTA was used again to remove any copper ion component from the rate constants determined. The plateau of the first order reaction profiles could not be obtained because the product decomposed due to the much slower high thiol reaction.[25]

Cysteine was reacted in excess with S-nitroso-N-acetylcysteine (SNAC), S-nitrosocaptopril (SNOCAP) and SNAP at pH 7.4 and second order rate constants were determined. The reactions were monitored by following absorbance at 340 nm over time. The extinction co-efficients of the three S-nitrosothiols and S-nitrosocysteine have been measured at 340 nm[26] and are shown in table 2.11 so the absorbance change could be predicted.

S-Nitrosothiol	ε_{340nm} / dm^3 mol^{-1} cm^{-1}
S-Nitrosocysteine	855 ± 47
SNAC	920 ± 29
SNAP	956 ± 20
SNOCAP	1108 ± 24

Table 2.11 Extinction co-efficients of SNAC, SNOCAP, SNAP and S-nitrosocysteine at 340 nm.

[SNAC] / M	[Cysteine] / M	k_{obs} / s^{-1}
5x10^{-4}	0.005	0.103
5x10^{-4}	0.006	0.123
5x10^{-4}	0.007	0.136
5x10^{-4}	0.008	0.159
5x10^{-4}	0.009	0.168
5x10^{-4}	0.010	0.187

$k_2 = 16.5 \pm 0.8$ dm^3 mol^{-1} s^{-1}.

Table 2.12 Concentration of SNAC and cysteine in the presence of 1x10^{-4} M EDTA and 0.075 M phosphate buffer (pH 7.4) at 25 °C.

[SNOCAP] / M	[Cysteine] / M	k_{obs} / s^{-1}
5x10^{-4}	0.005	0.0377
5x10^{-4}	0.006	0.0417
5x10^{-4}	0.007	0.0432
5x10^{-4}	0.008	0.0457
5x10^{-4}	0.009	0.0493
5x10^{-4}	0.010	0.0518

$k_2 = 2.7 \pm 0.1$ dm^3 mol^{-1} s^{-1}.

Table 2.13 Concentration of SNOCAP and cysteine in the presence of 1x10^{-4} M EDTA and 0.075 M phosphate buffer (pH 7.4) at 25 °C.

[SNAP] / M	[Cysteine] / M	k_{obs} / s^{-1}
5x10^{-4}	0.005	0.0681
5x10^{-4}	0.006	0.0788
5x10^{-4}	0.007	0.0910
5x10^{-4}	0.008	0.1040
5x10^{-4}	0.009	0.1130
5x10^{-4}	0.010	0.1210

$k_2 = 10.9 \pm 0.4$ dm^3 mol^{-1} s^{-1}.

Table 2.14 Concentration of SNAP and cysteine in the presence of 1x10^{-4} M EDTA and 0.075 M phosphate buffer (pH 7.4) at 25 °C.

The second order rate constants found when other low molecular weight S-nitrosothiols were reacted with cysteine are shown in tables 2.12 – 2.14. When SNAG was used as the NO$^+$ donor the second order rate constant for the reaction with cysteine was found to be much larger. (see table 2.9)

2.6 Discussion

The parent thiol of SNAG was reacted with nitrous acid and the product gave a characteristic S-nitroso UV / Vis spectra with peaks at 345 and 558 nm. Despite the thiol having to be dissolved using an acetonitrile water mixture to help improve solubility the reaction was similar to other thiol nitrosations studied.

Three large differences in the reactivity of SNAG compared to other low molecular weight S-nitrosothiols were found. The slow copper catalysed decomposition, the faster than expected thermal / photolytic reaction and the very fast transnitrosation reaction with cysteine.

SNAG like many other S-nitrosothiols undergoes a copper catalysed decomposition at pH 7.4. However the second order rate constant obtained for the reaction was smaller than those obtained for other S-nitrosothiols in previous studies. This could be due to the lack of a favourable Cu^{+} co-ordination site on the SNAG molecule, or the possibility exists that Cu^{2+} is largely complexed within the SNAG molecule.

The study into the thermal / photochemical decomposition found that SNAG decomposed faster via this pathway compared to other low molecular weight S-nitrosothiols. However even at body temperature this reaction takes several hours to go to completion. A slow hydrolysis reaction at pH 7.4 was also observed.

There is one large difference in the structure of SNAG compared with other low molecular weight S-nitrosothiols looked at in this study. The S-nitroso functional group is bonded to a heterocyclic ring.

It is known that when an electron withdrawing group is present on an S-nitrosothiol the rate constant for a transnitrosation reaction is increased.[27] The oxygen atom in close proximity to the S-nitrosothiol group in SNAG is likely to be responsible for the large rate constant found for the reaction with cysteine. When S-nitroso sugars were reacted with the nucleophile sulfite larger rate constants were found compared with other low molecular S-nitrosothiols.[28]

62

SNAG has been found to be more effective at delivering NO^+ in the presence of thiol rather than NO at pH 7.4. Rates of reaction for several decomposition pathways are very different to those found for other S-nitrosothiols looked at in this study. The chemical properties of SNAG described here hopefully can be utilised in nitric oxide based biological experiments in the future.

2.7 References

1) B. T. Mellion, L. J. Ignarro, C. B. Myers, E. H. Ohlstein, B. A. Ballott, A. L. Hyman and P. J. Kadowitz, *Mol. Pharmacol.*, 1983, **23**, 653.

2) W. R. Mathews and S. W. Kerr, *J. Pharamcol. Exp. Ther.*, 1993, **267**, 1529.

3) A. R. Butler, R. A. Field, I. R. Greig, F. W. Flitney, S. K. Bisland, F. Khan and J. J. F. Belch, *Nitric Oxide: Biol. Chem.*, 1997, **1**, 211.

4) P. A. Morris and D. L. H. Williams, *J. Chem. Soc., Perkin Trans. 2*, 1988, 513.

5) D. L. H. Williams, 'Nitrosation', Cambridge University Press, Cambridge, 1988, 176.

6) D. J. Sexton, A. Muruganandam, D. J. McKenny and B. Mutus, *Photochem. Photobiol.*, 1994, **59**, 463.

7) P. D. Wood, B. Mutus and R. W. Redmond, *Photochem. Photobiol.*, 1996, **64**, 518.

8) A. P. Munro and D. L. H. Williams, *J. Chem. Soc., Perkin Trans. 2*, 1999, 1989.

9) D. A. Wink, J. F. Darbyshire, R. W. Nims, J. E. Saavedra and P. C. Ford, *Chem. Res. Toxicol.*, 1993, **6**, 23.

10) H. H. Awad and D. M. Stanbury, *Int. J. Chem. Kinet.*, 1993, **25**, 375.

11) J. P. Griess, *Ber. Dtsch. Chem. Ges.*, 1879, **12**, 426.

12) J. B. Fox, Jr., *Anal. Chem.*, 1979, **51**, 1493.

13) M. G. de Oliveira, S. M. Shishido, A. B. Seabra and N. H. Morgon, *J. Phys. Chem. A*, 2002, **106**, 8963.

14) D. R. Noble and D. L. H. Williams, *Nitric Oxide: Biol. Chem.*, 2000, **4**, 392.

15) S. Oae, D. Fukushima and Y. H. Kim, *Chem. Lett.*, 1978, 279.

16) N. Tsutsumi, T. Itoh and A. Ohsawa, *Chem. Pharm. Bull.*, 2000, **48**, 1524.

17) S. C. Askew, D. J. Barnett, J. McAninly and D. L. H. Williams, *J. Chem. Soc., Perkin Trans. 2*, 1995, 741.

18) A. P. Dicks, H. R. Swift, D. L. H. Williams, A. R. Butler, H. H. Al-Sa'doni and B. G. Cox, *J. Chem. Soc., Perkin Trans. 2*, 1996, 481.

19) T. M. Devlin, 'Textbook of Biochemistry', 3rd Ed., Wiley, New York, 1992, 321.

20) A. J. Holmes and D. L. H. Williams, *J. Chem. Soc., Perkin Trans. 2*, 2000, 1639.

21) A. P. Munro and D. L. H. Williams, *Can. J. Chem.*, 1999, 77, 550.

22) D. J. Barnett, J. McAninly and D. L. H. Williams, *J. Chem. Soc., Perkin Trans. 2*, 1994, 1131.

23) Scientist, version 2.02, Micromath Scientific Software, Salt Lake City, UT, USA. www.micromath.com

24) D. D. Perrin, 'Dissociation Constants of Organic Bases in Aqueous Solution', Butterworths, London, 1965.

25) A. P. Dicks, E. Li, A. P. Munro, H. R. Swift and D. L. H. Williams, *Can. J. Chem.*, 1998, 76, 789.

26) D. J. Barnett, Ph.D. thesis, University of Durham, 1994, 77.

27) D. J. Barnett, A. Rios and D. L. H. Williams, *J. Chem. Soc., Perkin Trans. 2*, 1995, 1279.

28) A. P. Munro and D. L. H. Williams, *J. Chem. Soc., Perkin Trans. 2*, 2000, 1794.

Chapter 3

Decomposition Pathways of *S*-Nitroso Derivatives of Dithiols

Chapter 3: Decomposition Pathways of *S*-Nitroso Derivatives of Dithiols

3.1 Introduction

Studies have found that introducing nitric oxide (NO), *S*-nitrosothiols and other NO donors to proteins can have a large effect on their biological activity. The proteins studied contain multiple thiol groups some of which are in close proximity to each other and some are vicinal thiol groups. After addition of the compounds to creatine kinase[1], protein kinase C[2] and type I adenylyl cyclase[3] the proteins were deactivated.

The processes were reversed by reacting a dithiol with the proteins, which is used for the cleavage of low molecular weight[4,5] and protein[6,7] disulfide bonds. The presence of intramolecular disulfide bonds could be explained by the formation of *S*-nitroso dithiol intermediates that decompose at pH 7.4.

Dithiothreitol (DTT), dithioerythritol (DTE) and 2,3-dimercapto-1-propanesulfonic acid (DMPS) were used as models for proteins with multiple thiol groups. The structures of the dithiols are shown in figure 3.1. DMPS contains a vicinal dithiol group.
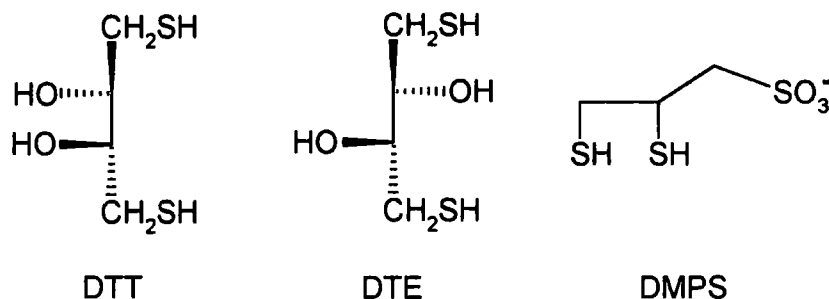
Figure 3.1 The structure of three dithiols.

This chapter looks at the chemistry of the *S*-nitrosated dithiols shown in figure 3.1.

66

3.2 Nitrosation of DTT, DTE and DMPS

To study the S-nitroso dithiols they first had to be generated *in situ* using nitrous acid and the corresponding dithiol.

3.2.1 Determination of UV / Vis Spectroscopic Parameters

Slightly different procedures for generating mono-S-nitroso and di-S-nitroso dithiols are described in the literature.[8] To generate di-S-nitroso compounds a 2 : 1 nitrite : dithiol stoichiometric ratio in acidic conditions was used, the ratio was changed to 1 : 10 for mono nitrosations. The thiols were initially nitrosated using these methods to determine absorbance maxima and extinction coefficients using the Beer-Lambert law (see section 2.2.1) so that reactions could be followed using UV / Vis spectroscopy.

The reaction stoichiometry of DTT with nitrous acid was studied to check that no further nitrous acid was required to form di-S-nitroso DTT quantitatively. Absorbance values at 333 nm were taken immediately after solutions were made up because of the instability of the di-S-nitroso compound. Concentrations used and absorbances recorded are shown in table 3.1. It was found that increasing the nitrous acid concentration beyond a 2 : 1 ratio did not bring about a large increase in absorbance which is shown in figure 3.2. The slight increase in absorbance could be due to nitrous acid formation.

$[NaNO_2]$ / M	[DTT] / M	Absorbance at 333nm
2.5×10^{-4}	5×10^{-4}	0.30
5.0×10^{-4}	5×10^{-4}	0.57
7.5×10^{-4}	5×10^{-4}	0.83
10.0×10^{-4}	5×10^{-4}	0.96
12.5×10^{-4}	5×10^{-4}	0.97
15.0×10^{-4}	5×10^{-4}	0.98

Table 3.1 Concentration of sodium nitrite and dithiothreitol in solution with absorbance measured at 333 nm in the presence of 0.2 M perchloric acid.
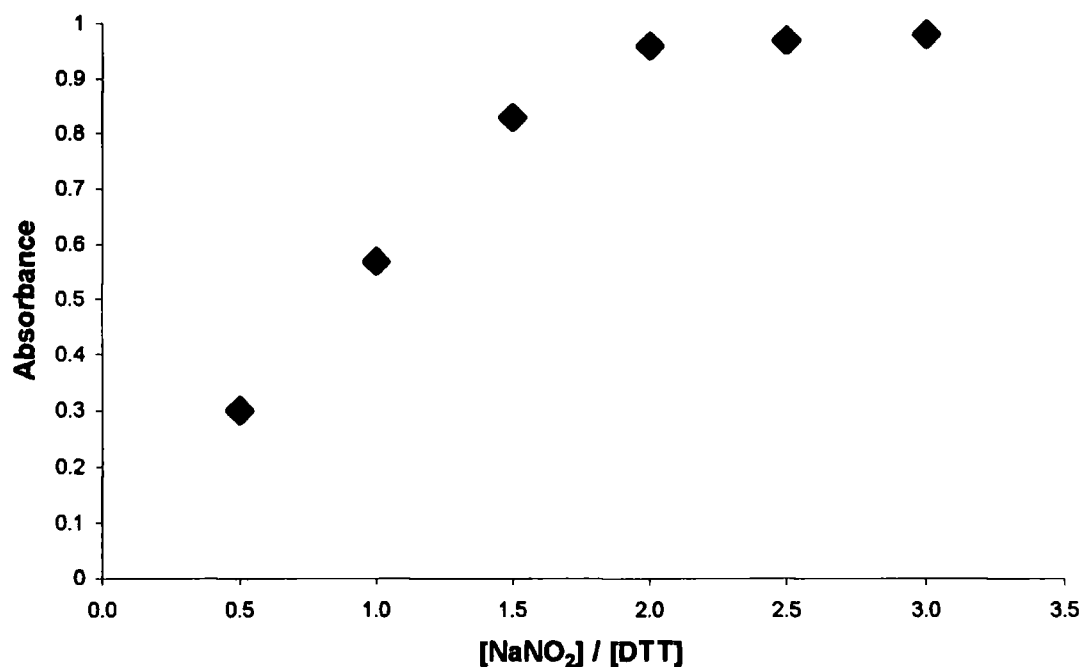
Figure 3.2 Absorbance at 333 nm plotted against [NaNO₂] / [DTT] in the presence of 0.2 M perchloric acid.

The absorbance value obtained at the highest sodium nitrite concentration corresponds to an extinction co-efficient ε_{333nm} = 1 960 dm^3 mol^{-1} cm^{-1}. Another absorbance maximum was observed at 543 nm and an approximate extinction coefficient was determined as ε_{543nm} = 33 dm^3 mol^{-1} cm^{-1}. When DTE was dinitrosated, very similar absorbance maxima and extinction coefficients were found.

Concentration / M	Absorbance (338 nm)	Absorbance (548 nm)
0.0002	0.324	0.010
0.0004	0.660	0.019
0.0006	0.995	0.026
0.0008	1.337	0.032
0.0010	1.694	0.040

Table 3.2 Concentration of di-S-nitroso DMPS and absorbance values measured.

68

Di-S-nitroso DMPS was found to be more stable, and absorbance maxima could be measured using UV / Vis spectra. (see table 3.2) The extinction coefficients determined were ε_{338nm} = 1 709 ± 13 dm^3 mol^{-1} s^{-1} and ε_{548nm} = 37 ± 1 dm^3 mol^{-1} s^{-1}.

Mono-S-nitroso compounds were generated *in situ* using 0.02 M perchloric acid. The ten fold excess of dithiol over sodium nitrite meant the reaction went readily at the lower acid concentration. A solution of the S-nitrosothiol was made up and diluted and UV / Vis spectra were taken of the resulting solutions. The absorbance maxima and values measured are shown in table 3.3.

Concentration / M	Mono-S-nitroso DTT		Mono-S-nitroso DTE		Mono-S-nitroso DMPS	
	Abs. (333 nm)	Abs. (544 nm)	Abs. (333 nm)	Abs. (544 nm)	Abs. (336 nm)	Abs. (545 nm)
0.0004	0.413	0.008	0.434	0.005	0.314	0.006
0.0008	0.848	0.014	0.858	0.016	0.639	0.013
0.0012	1.271	0.020	1.313	0.022	0.975	0.018
0.0016	1.702	0.028	1.746	0.029	1.313	0.027
0.0020	2.126	0.041	2.176	0.038	1.663	0.037

Table 3.3 Concentration of mono-S-nitroso DTT, DTE and DMPS with measured absorbance values.

The absorbance values for the weaker peak are small but still have a linear dependence with respect to concentration therefore the extinction coefficients are reported.

The extinction coefficients were found to be for mono-S-nitroso DTT ε_{333nm} = 1 070 ± 3 dm^3 mol^{-1} cm^{-1} and ε_{544nm} = 20 ± 2 dm^3 mol^{-1} cm^{-1}, for mono-S-nitroso DTE ε_{333nm} = 1 093 ± 6 dm^3 mol^{-1} cm^{-1} and ε_{544nm} = 20 ± 1 dm^3 mol^{-1} cm^{-1} and for mono-S-nitroso DMPS ε_{336nm} = 843 ± 6 dm^3 mol^{-1} cm^{-1} and ε_{545nm} = 19 ± 1 dm^3 mol^{-1} cm^{-1}.

The extinction coefficients found for the mono-S-nitroso compounds are roughly half the value for the corresponding di-S-nitroso compound.

3.2.2 Kinetics of DTT, DTE and DMPS S-Nitrosation

The kinetics for the nitrosation of thiol groups in dithiols were measured assuming the general rate equation determined for acid catalysed S-nitrosation.[9] (see equation 3.1) The chemical equation for the reaction is shown in scheme 3.1. When nitrous acid was reacted with DTT and DTE the formation of the nitrosated thiols was followed by their UV / Vis absorbance at 333 nm. The reaction profiles fitted a first order model when [HNO$_2$] >> [dithiol].

Rate = k_3[H$^+$][RSH][HNO$_2$]

Equation 3.1 Rate equation for the acid catalysed S-nitrosation of a thiol.

$$\text{RSH} \;+\; \text{HNO}_2 \;\xrightarrow[\;k_3\;]{\text{H}^+}\; \text{RSNO} \;+\; \text{H}_2\text{O}$$
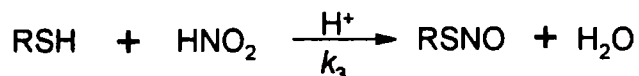
Scheme 3.1 Chemical equation for the nitrosation of a thiol group by nitrous acid.

The concentration of DTT and sodium nitrite in the reaction solutions and the first order rate constants obtained are shown in table 3.4. The plot of observed rate constant against nitrite concentration was found to be linear and is shown in figure 3.3. The gradient is equal to k_3[H$^+$].

[DTT] / M	[NaNO$_2$] / M	k_{obs} / s^{-1}
0.0005	0.005	2.54
0.0005	0.006	3.20
0.0005	0.007	3.91
0.0005	0.008	4.52
0.0005	0.009	5.23
0.0005	0.010	5.89

$k_3 = 3\ 350 \pm 27$ dm^6 mol^{-2} s^{-1}.

Table 3.4 Concentration of sodium nitrite and DTT with first order rate constants obtained in the presence of 0.2 M perchloric acid at 25 °C.
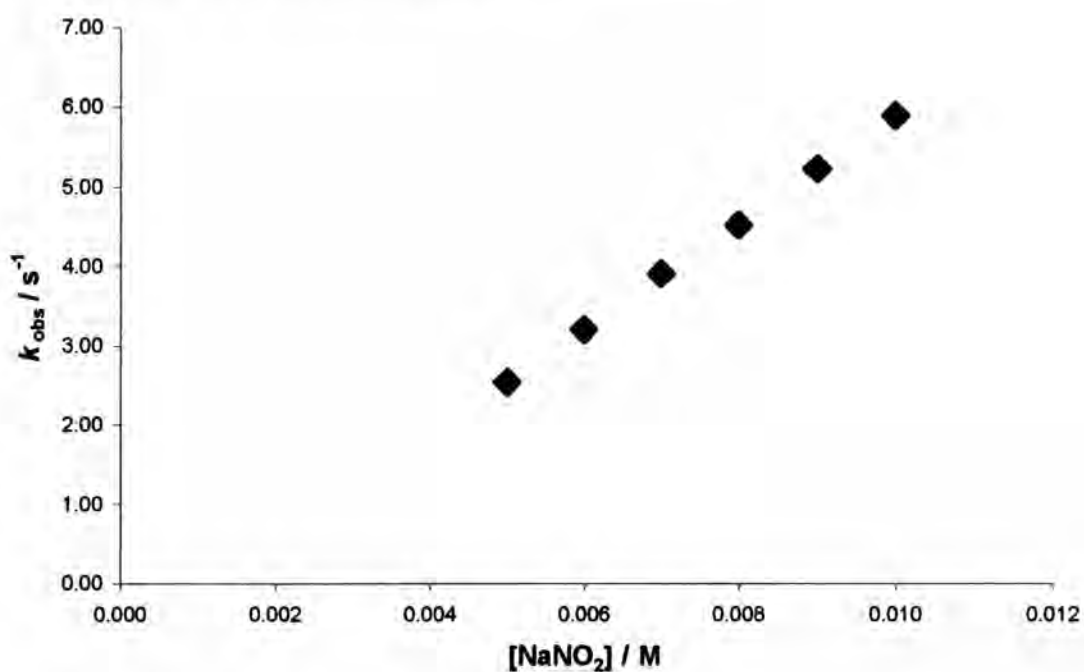
Figure 3.3 Observed rate constant plotted against sodium nitrite concentration for the nitrosation of DTT in the presence of 0.2 M perchloric acid at 25 °C.

The experiment was repeated with DTE and first order rate constants were also obtained and these are shown in table 3.5.

[DTE] / M	[NaNO$_2$] / M	k_{obs} / s^{-1}
0.0005	0.005	2.68
0.0005	0:006	3.37
0.0005	0.007	4.06
0.0005	0.008	4.73
0.0005	0.009	5.45
0.0005	0.010	6.07

$k_3 = 3\ 409 \pm 27\ \text{dm}^6\ \text{mol}^{-2}\ \text{s}^{-1}$.

Table 3.5 Concentration of sodium nitrite and DTE with first order rate constants obtained in the presence of 0.2 M perchloric acid at 25 °C.

The nitrosation of DTT and DTE can be thought of as two first order reactions occurring simultaneously leading to an increase in absorbance at 333 nm. A suggested reaction scheme for the nitrosation of the two thiol groups is shown in scheme 3.2. The rate of reaction was measured by following the formation of the nitrosated thiol groups. Therefore the double exponential model represents the absorbance with respect to time where A_1 and A_2 are pre-exponential factors, k_1 and k_2 are the first order rate constants for the two reactions, t is time and c is a constant. (see equation 3.2)
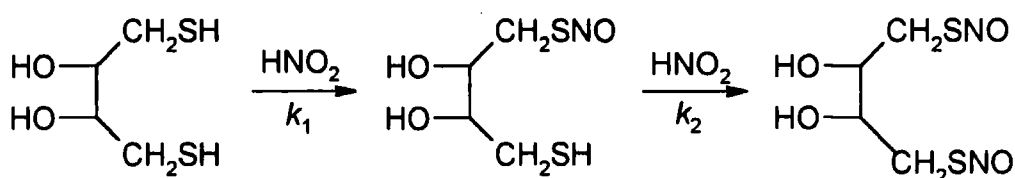
Scheme 3.2 Proposed series of reactions for the nitrosation of DTT and DTE.

$$\text{Absorbance} = A_1\exp^{(-k_1 t)} + A_2\exp^{(-k_2 t)} + c$$

Equation 3.2 The equation for the double exponential model.

When k_1 and k_2 in the double exponential model are roughly the same the change in absorbance with respect to time fits the first order model. This is a reasonable assumption for DTT and DTE because the environments of the two thiol groups are very similar.

When the experiment was repeated using DMPS first order rate constants could not be obtained from the reaction profiles. However they were found to fit the double exponential model shown in equation 3.2 and the results obtained are in table 3.6.

[DMPS] / M	[NaNO$_2$] / M	k_1 / s^{-1}	k_2 / s^{-1}
0.0005	0.005	5.7	1.93
0.0005	0.006	7.1	2.53
0.0005	0.007	8.6	2.94
0.0005	0.008	10.1	3.52
0.0005	0.009	11.8	4.02
0.0005	0.010	13.4	4.52

$k'_3 = 7\ 730 \pm 125\ dm^6\ mol^{-2}\ s^{-1}$.

$k''_3 = 2\ 570 \pm 50\ dm^6\ mol^{-2}\ s^{-1}$.

Table 3.6 Concentration of sodium nitrite and DMPS with first order rate constants obtained in the presence of 0.2 M perchloric acid at 25°C.

Two third order rate constants from rate = $k'_3[H^+][DMPS][HNO_2]$ and rate = $k''_3[H^+][DMPS][HNO_2]$, were obtained corresponding to the rate constant for nitrosation of the two individual thiol groups. This is because the selectivity of the two thiol groups in DMPS are significantly different so the nitrosation reactions occur at two different rates.

3.3 Thermal Decomposition of S-Nitroso Dithiols

Some of the S-nitroso dithiols that were generated *in situ* in the laboratory rapidly decomposed. Reaction profiles for the thermal / photolytic pathway were recorded and fitted a first order model.

3.3.1 Thermal Decomposition of Mono-S-nitroso DTT and DTE

Reaction solutions containing 1×10^{-3} M mononitrosated dithiol, 9×10^{-3} M dithiol, 1×10^{-4} M EDTA and 0.01 M perchloric acid were prepared. Dithiol was present due to the fact mononitrosation reactions were performed with thiol in ten fold excess. The decomposition of mono-S-nitroso DTT and DTE in acidic solution was measured by following absorbance at 340 nm over fourteen hours. The values for the rate constants assuming a first order process are shown in table 3.7 and must be considered as estimates because the entire reaction was not followed to completion.

S-Nitrosothiol	k_{obs} / s^{-1}
Mono-S-nitroso DTT	$1.5 \times 10^{-6} \pm 0.5 \times 10^{-6}$ s^{-1}
Mono-S-nitroso DTE	$4.4 \times 10^{-6} \pm 0.9 \times 10^{-6}$ s^{-1}

Table 3.7 Rate constants for mono-S-nitroso DTT and DTE decomposition at 25 °C.

The rate constants obtained are comparable to those found for tertiary S-nitrosothiols in section 2.3.3. The presence of thiol means that a component of these rate constants could be a thiol induced decomposition.

3.3.2 Thermal Decomposition of Di-S-nitroso DTT and DTE

Reaction solutions containing 5×10^{-4} M dinitrosated dithiol, 1×10^{-4} M EDTA and either 0.2 M perchloric acid or 0.15 M phosphate buffer (pH 7.4) were prepared. The absorbance at 333 nm was followed over time and reaction profiles fitted the first order model giving the rate constants shown in table 3.8. The rate constants obtained in acidic solution and with buffer were the same.

S-Nitrosothiol	0.2 M H^+ : k_{obs} / s^{-1}	pH 7.4 : k_{obs} / s^{-1}
Di-S-nitroso DTT	1.6×10^{-3}	1.6×10^{-3}
Di-S-nitroso DTE	1.4×10^{-3}	1.4×10^{-3}

Table 3.8 Rate constants obtained for the thermal reaction of di-S-nitroso DTT and DTE in acidic solution and pH 7.4 at 25 °C.

3.3.3 Thermal Decomposition of Di-S-nitroso DMPS

Reaction solutions containing 5×10^{-4} M di-S-nitroso DMPS, 1×10^{-4} M EDTA and either 0.2 M perchloric acid or 0.15 M phosphate buffer (pH 7.4) were prepared. Absorbance at 338 nm was followed over time and again first order rate constants could be calculated from the reaction traces. (see table 3.9) The change in rate constant with pH was very small.

Reaction Conditions	k_{obs} / s^{-1}
0.2 M H^+	4.7×10^{-5}
pH 7.4	3.9×10^{-5}

Table 3.9 Rate constants obtained for the thermal reaction of di-S-nitroso DMPS in acidic solution and pH 7.4 at 25 °C.

3.3.4 Thermal Reaction Product Analysis

One of the expected products of the photochemical / thermal decomposition of S-nitrosothiols is NO.[10] In aerobic conditions NO is believed to oxidise quantitatively to give nitrite ions in aqueous solution.[11,12] The concentration of nitrite ions in solution can be determined accurately using the Griess Test. (procedure explained in section 2.3.2)

Solutions containing 5×10^{-4} M dinitrosated DTT, DTE and DMPS with 1×10^{-4} M EDTA and 0.15 M phosphate buffer (pH 7.4) were made up. When the S-nitrosothiols had fully decomposed the nitrite ion concentration was measured, and the yields calculated assuming

two molecules of NO and disulfide were the products of the reaction are shown in table 3.10.

S-Nitrosothiol	Nitrite Yield
Di-S-nitroso DTT	97 %
Di-S-nitroso DTE	100 %
Di-S-nitroso DMPS	81 %

Table 3.10 Nitrite yields for the decomposition of di-S-nitroso DTT, DTE and DMPS.

The product analysis was repeated for reactions in acidic conditions and reduced levels of nitrite ions were found. The nitrite yields calculated for di-S-nitroso DTT, DTE and DMPS were 67 %, 68 % and 19 % respectively. It has been found that the rate equation for the oxidation of NO to nitrite is unaffected in the pH region 1 - 13.[12]

The decomposition of di-S-nitroso DTT under anaerobic conditions has been followed and the principal gas product was found to be NO (> 95 %) using mass spectrometry techniques.[8] An explanation could be that the oxidised product of NO at low concentrations can decompose in aqueous solution via a different pathway in acidic solution.

3.3.5 Possible Thermal Reaction Intermediates

Di-S-nitrosated DTT and DTE molecules were more sensitive to thermal decomposition compared to the mono-S-nitrosated derivatives. The introduction of a second S-nitroso group in the molecule leads to a more rapid decomposition via the thermal pathway. This implies that there is a weakening of a sulfur nitrogen bond in the S-nitrosothiol.

An interaction between the two S-nitroso groups is proposed in figure 3.4 leading to the weakening of a sulfur nitrogen bond. Electron density is drawn to the nitrogen atom reducing the sulfur atoms ability to bond with the nitrogen atom.
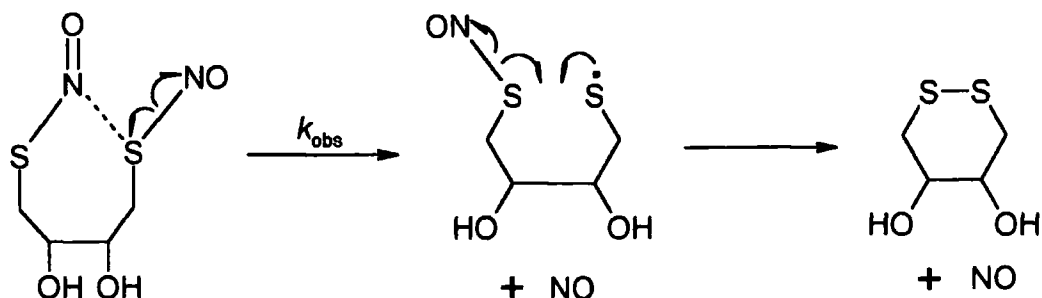
Figure 3.4 Proposed mechanism for di-S-nitrosated DTT and DTE thermal decomposition. (the dotted line represents an atom-atom interaction)

Di-S-nitroso DTT and DTE decompose via the thermal pathway faster than di-S-nitroso DMPS does and using the proposed intermediates in figures 3.4 this can be explained. DTT and DTE could initially form a seven membered ring. Assuming DMPS decomposed via the same process a sterically less favourable five membered ring would have to form.

3.4 The Reaction of Dithiols with S-Nitrosothiols

A possible explanation for the presence of a S-nitrosated dithiol in the body could be a transnitrosation reaction occurring between the dithiol and an S-nitrosothiol. Transnitrosation rate constants were measured for the reaction of the dithiols with low molecular weight S-nitrosothiols. The rate equation for the forward reaction of a transnitrosation reaction between thiol and an S-nitrosothiol has been established.[13] (see equation 3.3)

Rate = k_2[RSNO][RS'H]

Equation 3.3 The rate equation for a transnitrosation reaction.

3.4.1 The Reaction of DMPS with S-Nitrosothiols

It was found that the addition of DMPS to a GSNO solution lead to a rapid reduction of absorbance at 340 nm. This is because mono-S-nitroso DMPS decomposes rapidly at pH 7.4. (see section 3.5.2) When DMPS in large excess was reacted with GSNO reactions were

followed by recording absorbance at 340nm and the reaction profiles fitted a first order model. The rate constants obtained are shown in table 3.11. A plot of observed rate constant against DMPS concentration was linear (see figure 3.5) with a gradient corresponding to the second order rate constant for transnitrosation and a near zero intercept.

[GSNO] / M	[DMPS] / M	k_{obs} / s^{-1}
5×10^{-4}	0.005	0.128
5×10^{-4}	0.006	0.161
5×10^{-4}	0.007	0.185
5×10^{-4}	0.008	0.208
5×10^{-4}	0.009	0.244
5×10^{-4}	0.010	0.270

$k_2 = 28 \pm 1$ dm^3 mol^{-1} s^{-1}.

Table 3.11 Concentration of GSNO and DMPS with first order rate constants obtained in the presence of 0.15 M phosphate buffer (pH 7.4) at 25 °C.
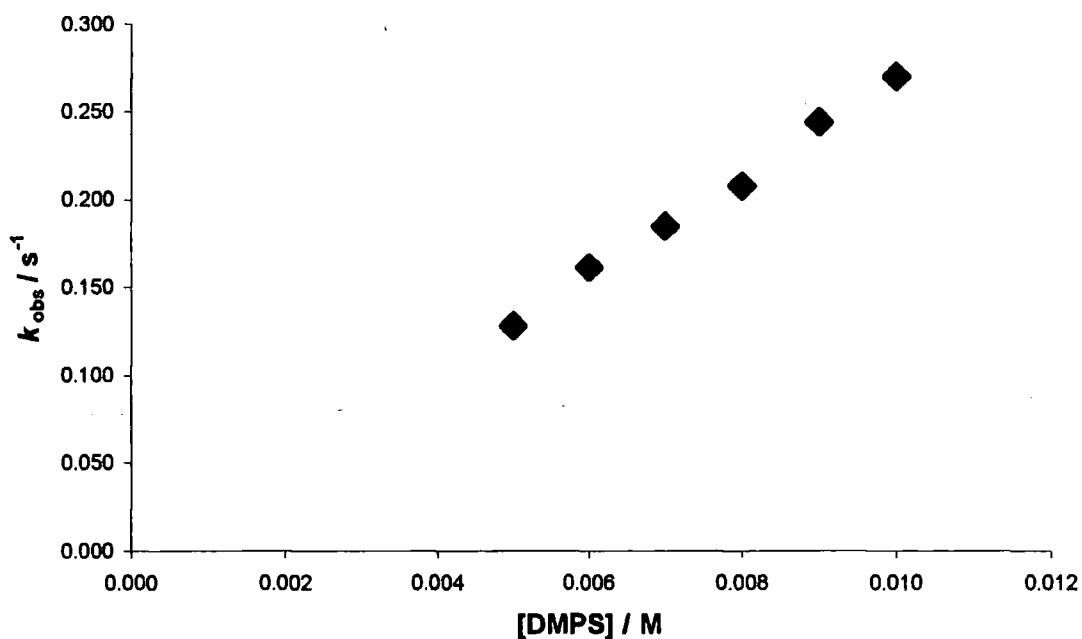
Figure 3.5 Observed first order rate constants plotted against DMPS concentration from table 3.11.

The experiment was repeated using the metal ion chelator EDTA to determine whether the reaction was metal ion dependent. The rate constants obtained are shown in table 3.12. Theoretically, like ascorbic acid, DMPS could decompose GSNO by reducing trace copper ions or by a direct reaction.[14]

[GSNO] / M	[DMPS] / M	k_{obs} / s^{-1}
5×10^{-4}	0.006	0.134
5×10^{-4}	0.007	0.167
5×10^{-4}	0.008	0.209
5×10^{-4}	0.009	0.234
5×10^{-4}	0.010	0.263

$k_2 = 33 \pm 2$ dm^3 mol^{-1} s^{-1}.

Table 3.12 Concentration of GSNO and DMPS with first order rate constants obtained in the presence of 0.15 M phosphate buffer (pH 7.4) and 1×10^{-4} M EDTA at 25 °C.

The kinetic data obtained for the reaction of DMPS with GSNO did not change significantly when EDTA was present. This result is probably due to the fact that DMPS can complex copper ions. DMPS has been used to treat Wilsons disease[15], a condition that occurs when there is a build up of copper in the liver. It has also been used to remove other metal ions from the body.

The experiment was repeated with several other S-nitrosothiols and second order rate constants were obtained. No significant intercepts were found due to the reaction being effectively irreversible due to the lifetime of the mononitrosated DMPS at pH 7.4 and DMPS being present in large excess over the S-nitrosothiols.

DMPS was reacted with a range of S-nitrosothiols and the second order rate constants obtained are shown in table 3.13. The rate constants obtained are mostly very similar with the two smallest S-nitrosothiols, S-nitrosocysteine and S-nitroso-1-amino-2-methyl-2-propane thiol having the highest reactivity.

S-Nitrosothiol	k_2 / dm^3 mol^{-1} s^{-1}
GSNO	28 ± 1
S-Nitrosocysteine	128 ± 4
SNAC	6.4 ± 0.2
SNOCAP	2.1 ± 0.1
SNAP	6.3 ± 0.2
S-Nitrosohomocysteine	11.5 ± 0.5
S-Nitroso-1-amino-2-methyl-2-propane thiol	193 ± 11

Table 3.13 Second order rate constants determined for the transnitrosation reactions of several S-nitrosothiols with DMPS in the presence of 0.15 M phosphate buffer (pH 7.4) at 25 °C.

3.4.2 Effect of pH on the Reaction of DMPS with GSNO

It has been found that in transnitrosation reactions the thiol reacts with S-nitrosothiols via the thiolate anion.[13] The dependence on pH of the second order rate constant was investigated to determine the reactivity of DMPS and its mono and dianions.

pH Range	Buffer System
5.8 – 8.0	Potassium dihydrogenphosphate / NaOH
8.1 – 9.0	Tris(hydroxymethyl)aminomethane / HCl
9.1 – 11.0	Sodium bicarbonate / NaOH
11.1 – 12.0	Dipotassium hydrogenphosphate / NaOH

Table 3.14 Buffer systems used in the pH study.

An excess of DMPS was reacted with 2.5×10^{-4} M GSNO at different buffers pH values (see table 3.14), and the second order rate constants obtained are shown in table 3.15. When the reactions were complete the pH of the solutions was measured. The full pH curve could not be obtained because at high hydroxide ion concentration a competing reaction occurred

leading to the formation of an unstable yellow species that absorbed at 340 nm. This has been attributed to the formation of the sulfenic acid of GSH.[16]

pH	k_2 / dm^3 mol^{-1} s^{-1}
6.45	2.4 ± 0.2
6.95	8.5 ± 0.3
7.36	25 ± 1
7.85	59 ± 3
8.53	98 ± 3
8.97	134 ± 4
9.26	195 ± 11
9.70	185 ± 6
10.17	189 ± 8
10.57	225 ± 11
10.92	274 ± 14
11.50	363 ± 24

Table 3.15 Second order rate constants obtained for the reaction of DMPS with GSNO in the presence of 0.075 M buffer solutions at 25 °C.

The mathematical equation for the second order rate constant dependence on pH has been derived and is shown in equation 3.4. $k_{H,DM}$, k_{HDM^-} and $k_{DM^{2-}}$ are the rate constants for reaction via DMPS, DMPS monoanion and DMPS dianion respectively, K_1 and K_2 are the acid dissociation constants of DMPS thiol groups and k_2 is the second order rate constant for the reaction with GSNO at a given pH.

$$k_2 = \left(\frac{\left(k_{H_2DM}[H^+]^2 + k_{HDM^-} \cdot K_1[H^+] + k_{DM^{2-}} \cdot K_1 K_2\right)}{\left(K_1 K_2 + K_1[H^+] + [H^+]^2\right)} \right)$$

Equation 3.4 The equation for the dependence of k_2 upon pH.

The data in table 3.15 were fitted to equation 3.4 using Scientist[17] and a good fit was obtained. The experimental data plotted with the fit from Scientist is shown in figure 3.6. The following constants were obtained,

$k_{H_2DM} = 6 \pm 10 \ dm^3 \ mol^{-1} \ s^{-1}$.

$k_{HDM^-} = 187 \pm 14 \ dm^3 \ mol^{-1} \ s^{-1}$.

$k_{DM^{2-}} = 490 \pm 99 \ dm^3 \ mol^{-1} \ s^{-1}$.

$pK_1 = 8.41 \pm 0.18$.

$pK_2 = 11.35 \pm 0.32$.
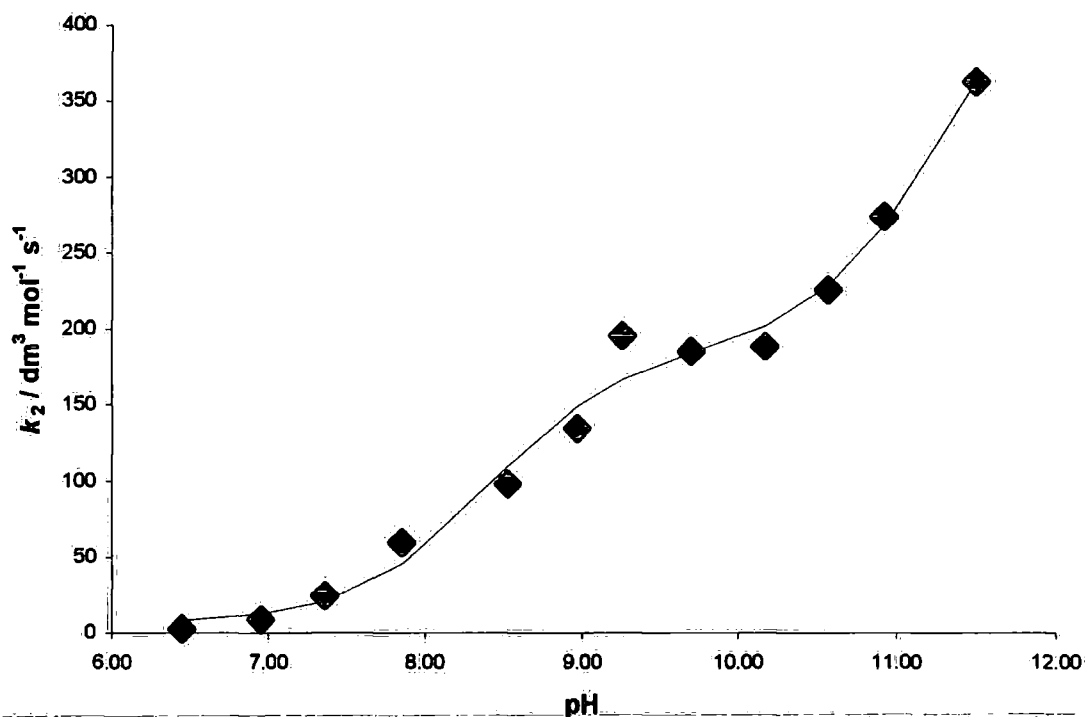
Figure 3.6 Experimental data obtained for the second order rate constant dependence on pH (♦) and the best fit line obtained using Scientist (the solid line).

The pK_a values for the thiol groups in the DMPS molecule have been determined as 11.62 ± 0.01 and 8.525 ± 0.004.[18] The values obtained from the pH study are in good agreement with them. An interesting feature of the results obtained is the fact that DMPS itself (i.e. the

thiol form), as well as the thiolate forms appears to react with the GSNO molecule as well. Fixing the rate constant value for DMPS to zero meant that the fit line deviated from the experimental data between pH six and eight.

The possibility of a reaction between the sulfonate group on DMPS and GSNO was considered. Propane-1-sulfonate was reacted with GSNO in the presence of 0.15 M phosphate buffer (pH 7.4) for fourteen hours. No reaction was observed suggesting the sulfonate group on DMPS does not contribute to the reaction with GSNO.

3.4.3 The Reaction of DTT and DTE with GSNO

The mononitrosated DTT and DTE are relatively stable in solution compared to the mononitrosated DMPS so decomposition of the mononitroso products was not observed over the time of the reaction. The extinction co-efficient at 340 nm for GSNO has been detemined as 895 ± 7.[19] When DTT and DTE were reacted with GSNO an increase in absorbance was observed and reaction profiles fitted the first order model. (see tables 3.16 and 3.17) The reactions were performed with 1×10^{-4} M EDTA to eliminate any contribution from copper ions.

[GSNO] / M	[DTT] / M	k_{obs} / s^{-1}
5×10^{-4}	0.006	0.407
5×10^{-4}	0.007	0.468
5×10^{-4}	0.008	0.533
5×10^{-4}	0.009	0.612
5×10^{-4}	0.010	0.674

$k_2 = 68 \pm 2$ dm^3 mol^{-1} s^{-1}.

Table 3.16 Concentration of GSNO and DTT with first order rate constants obtained in the presence of 0.15 M phosphate buffer (pH 7.4) at 25 °C.

[GSNO] / M	[DTE] / M	k_{obs} / s^{-1}
5×10^{-4}	0.005	0.175
5×10^{-4}	0.006	0.226
5×10^{-4}	0.007	0.269
5×10^{-4}	0.008	0.283
5×10^{-4}	0.009	0.327
5×10^{-4}	0.010	0.366

$k_2 = 36 \pm 2$ dm^3 mol^{-1} s^{-1}.

Table 3.17 Concentration of GSNO and DTE with first order rate constants obtained in the presence of 0.075 M phosphate buffer (pH 7.4) at 25 °C.

The rate constants are very similar to the ones obtained for the reaction of GSNO with DMPS.

3.4.4 Product Analysis of the DMPS Reaction with GSNO

It was found that in an equimolar solution of DMPS and GSNO at pH 7.4 the GSNO did not fully decompose. Reaction solutions were made up with 2.5×10^{-3} M GSNO and different stoichiometric ratios of DMPS in the presence of 0.15 M phosphate buffer (pH 7.4). Figure 3.7 shows the effect of changing [DMPS] : [GSNO] upon the final absorbance at 340 nm.

The experiment clearly showed that the reaction stoichiometry for the decomposition of GSNO with DMPS was 2 : 1 [DMPS] : [GSNO]. Reaction solutions containing DMPS in at least two fold excess were made up to determine the products of the reaction.
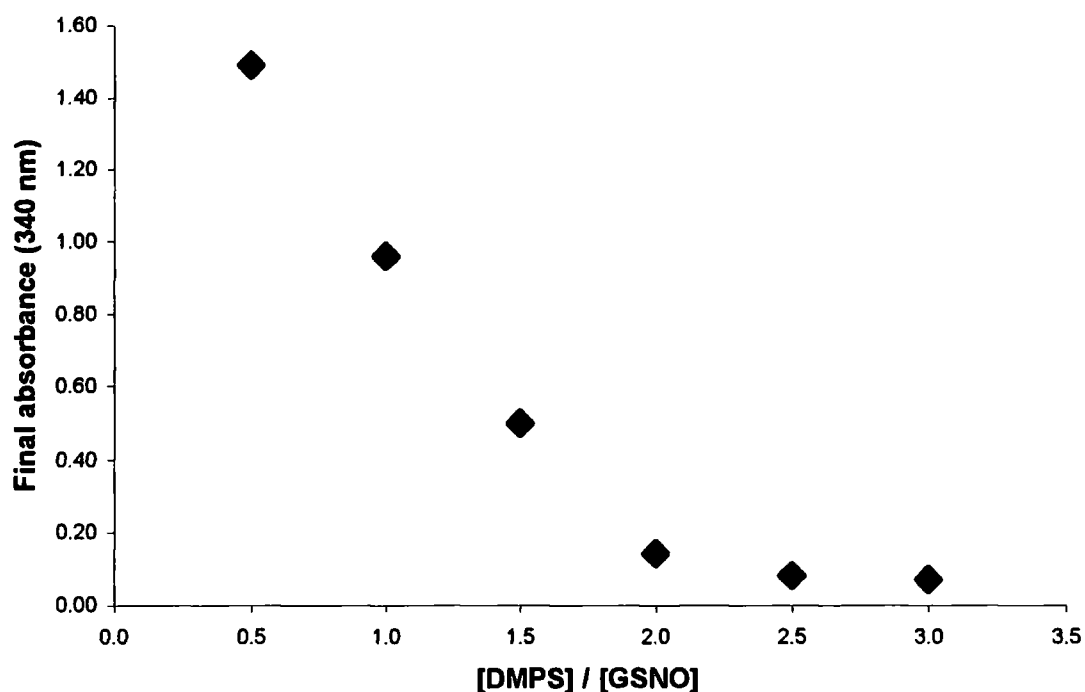
Figure 3.7 Final absorbance of the reaction solutions plotted against [DMPS] / [GSNO].

One of the major products of the reaction was found to be ammonia. The concentration of ammonia was determined using the standard diagnostic kit available at Aldrich. The development of the test is attributed to H. C. van Anken and M. E. Schiphorst.[20] A reaction solution containing 5×10^{-4} M GSNO, 5×10^{-3} M DMPS and 0.15 M phosphate buffer (pH 7.4) was made up. When the S-nitrosothiol had fully decomposed ammonia was found in 94 % yield.

The nitrite concentration of two reaction solutions was analysed using the Griess Test. (described in section 2.3.2) The test was carried out after the S-nitrosothiol had fully decomposed and the results are shown in table 3.18.

[GSNO] / M	[DMPS] / M	Nitrite Yield
5×10^{-4}	1×10^{-3}	5.9 %
5×10^{-4}	5×10^{-3}	0.3 %

Table 3.18 Concentration of GSNO and DMPS in the presence of 0.15 M phosphate buffer (pH 7.4) and percentage yield of nitrite ions.

The concentration of NO generated during the DMPS induced decomposition of GSNO was measured using an NO electrode. The calibration is described in section 6.1.3 and a typical result is shown in table 3.19 and figure 3.8. A value of $1.51 \times 10^{-3} \pm 0.02 \times 10^{-3}$ A dm^3 mol^{-1} was found for the current dependence on NO concentration.

[NO] / M	Current / A
1×10^{-6}	1.649×10^{-9}
2×10^{-6}	3.275×10^{-9}
3×10^{-6}	4.700×10^{-9}
4×10^{-6}	6.272×10^{-9}
5×10^{-6}	7.722×10^{-9}

Table 3.19 Current measured with NO concentration during NO electrode calibration.
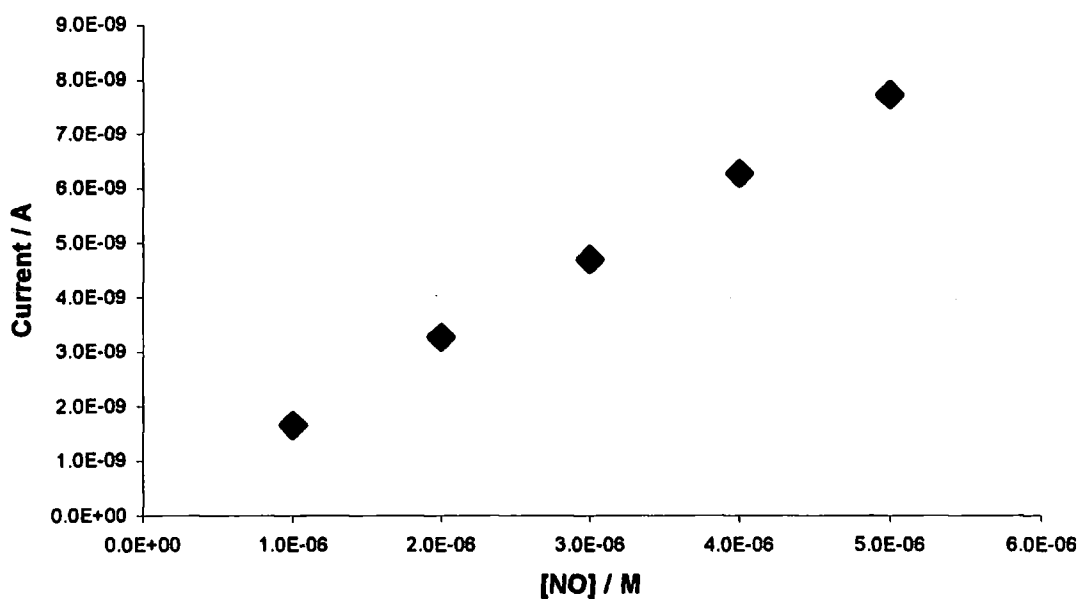
Figure 3.8 Graph of NO concentrations against current from values in table 3.19.

A reaction solution containing 5×10^{-3} M DMPS, 5×10^{-4} M GSNO and 0.15 M phosphate buffer (pH 7.4) was made up. When the reaction was followed using stopped flow spectrophotometry it went to completion in one minute. The NO electrode monitored NO concentration at 25 °C for several minutes. The maximum concentration of NO found was 3.7×10^{-7} mol dm^{-3}. (i.e. 0.1 %) A calibration was performed over the NO concentration range studied.

The second part of the product analysis was to look at the sulfur containing product. It has been found that GSH, GSSG and GSNO can be separated using HPLC.[14] The HPLC was carried out using an ODS 2 column and the conditions were 0.7 ml min^{-1} flow rate, 10 μL injection loop, with detection at 200 nm. The eluent used was 90 % 300 mM phosphate buffer (pH 2.7) and 10 % methanol.

To allow for the differing response factors of GSH and GSSG the HPLC machine was calibrated. A solution containing each compound at 1×10^{-3} M was used to determine the retention time and relative peak area of the compounds. (see table 3.20) Calculating the ratio of peak areas gave a method of determining the percentage of each compound present in a mixture. GSNO could be detected, and eluted at eight minutes.

Compound	Retention times / min	Peak area / arbitrary units	Relative Absorbance
GSH	4.5	45158976	1
GSSG	5.2	51767700	1.15

Table 3.20 Retention times and peak area for GSH and GSSG. The retention times could change on a daily basis but the order they came off the column did not.

A reaction solution containing 1×10^{-3} M GSNO, 2×10^{-3} M DMPS and 0.15 M phosphate buffer (pH 7.4) was mixed together. After thirty minutes a sample from the solution was put through the column.

It was assumed that all the GSNO had reacted to form GSH or GSSG because no other product was detected. Using the ratio of response factors the percentage of sulfur centres

from GSNO found as GSH or GSSG could be calculated. The result of the experiment was 76 % sulfur centres found as GSSG, 24 % sulfur centres found as GSH.

A solution containing 1×10^{-3} M DMPS was put through the column. DMPS was found to have a retention time of 11.8 minutes but the absorbance was very weak compared to GSH, GSSG and GSNO so it would not interfere with the experiment.

3.5 Decomposition of *S*-Nitroso Dithiols with Excess Parent Dithiol Present

The kinetics for the reaction of S-nitrosothiols with their parent thiols at high concentration have been studied.[21] Products of this reaction were found to be ammonia and disulfide. The decomposition of di-*S*-nitroso DTT and DTE in the presence of excess parent dithiol were studied at pH 7.4 in the presence of EDTA.[21] The rate constants (k_2 in equation 3.5) for the direct reaction were found to be 0.273 dm^3 mol^{-1} s^{-1} for DTT and 0.135 dm^3 mol^{-1} s^{-1} for DTE. k_1 represents the contribution from the thermal / photochemical decomposition.

Rate = k_2[RSNO][RSH] + k_1[RSNO]

Equation 3.5 Rate equation established for the high thiol reaction.

A similar rate equation has been described for the decomposition of mononitrosated dithiols.[8] The nitroso group of the mononitrosated dithiol can be attacked by the thiol group within the molecule or by a thiol group from another dithiol molecule. As expected the reactions were first order for the intramolecular process and second order for the intermolecular reaction.

3.5.1 Decomposition of Mono-*S*-nitroso DTT and DTE with Excess Thiol

The decomposition of mono-*S*-nitroso DTT and DTE was followed by decrease in absorbance at 333 nm. The parent thiol was present in excess and reaction profiles fitted the first order model. Rate constants obtained are shown in tables 3.21 and 3.22. A plot of first order rate constant against thiol concentration gave k_2 from the gradient (intermolecular

88

pathway) and k_1 from the intercept (intramolecular pathway). The experimental data for DTT are plotted in figure 3.9.

[RSNO] / M	[DTT] / M	k_{obs} / s^{-1}
5×10^{-4}	0.005	0.0029
5×10^{-4}	0.006	0.0032
5×10^{-4}	0.007	0.0035
5×10^{-4}	0.008	0.0039
5×10^{-4}	0.009	0.0043
5×10^{-4}	0.010	0.0046

$k_2 = 0.35 \pm 0.01$ dm^3 mol^{-1} s^{-1}.
$k_1 = 1.12\times10^{-3} \pm 0.08\times10^{-3}$ s^{-1}.

Table 3.21 Concentration of mono-S-nitroso DTT and DTT with first order rate constants obtained in the presence of 1×10^{-4} M EDTA and 0.15 M phosphate buffer (pH 7.4) at 25 °C.
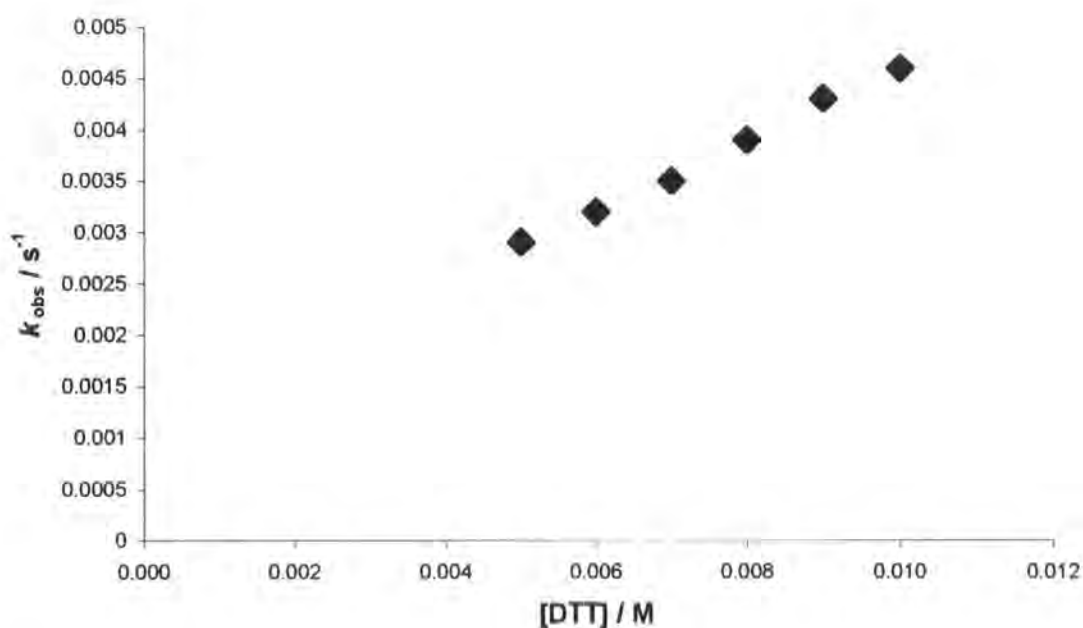
Figure 3.9 First order rate constants for mono-S-nitroso DTT decomposition plotted against DTT concentration from table 3.21.

[RSNO] / M	[DTE] / M	k_{obs} / s^{-1}
5x10^{-4}	0.005	0.0015
5x10^{-4}	0.006	0.0018
5x10^{-4}	0.007	0.0019
5x10^{-4}	0.008	0.0021
5x10^{-4}	0.009	0.0023
5x10^{-4}	0.010	0.0026

$k_2 = 0.21 \pm 0.01$ dm^3 mol^{-1} s^{-1}.

$k_1 = 5x10^{-4} \pm 1x10^{-4}$ s^{-1}.

Table 3.22 Concentration of mono-S-nitroso DTE and DTE with first order rate constants obtained in the presence of 1x10^{-4} M EDTA and 0.15 M phosphate buffer (pH 7.4) at 25 °C.

3.5.2 Decomposition of Mono-S-nitroso DMPS with Excess DMPS

The mononitrosated DMPS was found to decompose rapidly at pH 7.4 so the decomposition was initially studied in acidic solutions. A slower rate of reaction allowed the dependence on DMPS concentration to be studied. The absorbance at 336 nm was measured over time and the reaction profiles fitted the first order model. Rate constants obtained are shown in table 3.23.

[RSNO] / M	[DMPS] / M	k_{obs} / s^{-1}
1×10^{-3}	0.010	4.85×10^{-4}
1×10^{-3}	0.012	5.06×10^{-4}
1×10^{-3}	0.014	5.26×10^{-4}
1×10^{-3}	0.016	5.39×10^{-4}
1×10^{-3}	0.018	5.61×10^{-4}
1×10^{-3}	0.020	5.81×10^{-4}

$k_2 = 9.4 \times 10^{-3} \pm 0.3 \times 10^{-3} \ dm^3 \ mol^{-1} \ s^{-1}$.

$k_1 = 3.92 \times 10^{-4} \pm 0.04 \times 10^{-4} \ s^{-1}$.

Table 3.23 Concentration of mono-S-nitroso DMPS, DMPS and first order rate constants obtained in the presence of 0.01 M perchloric acid and 1×10^{-4} M EDTA at 25 °C.

The pH of the reaction solution with the lowest DMPS concentration was found to be 1.75. Increasing the concentration of DMPS did not change this value significantly. This backed up the result obtained when the transnitrosation was studied which indicated the fully protonated DMPS molecule could react with an S-nitrosothiol.

A reaction solution containing 1×10^{-3} M mono-S-nitroso DMPS, 1×10^{-2} M DMPS, 1×10^{-4} M EDTA and 0.15 M phosphate buffer (pH 7.4) was made up. The decomposition using only one DMPS concentration could be studied due the S-nitroso compounds instability and is shown in figure 3.10.
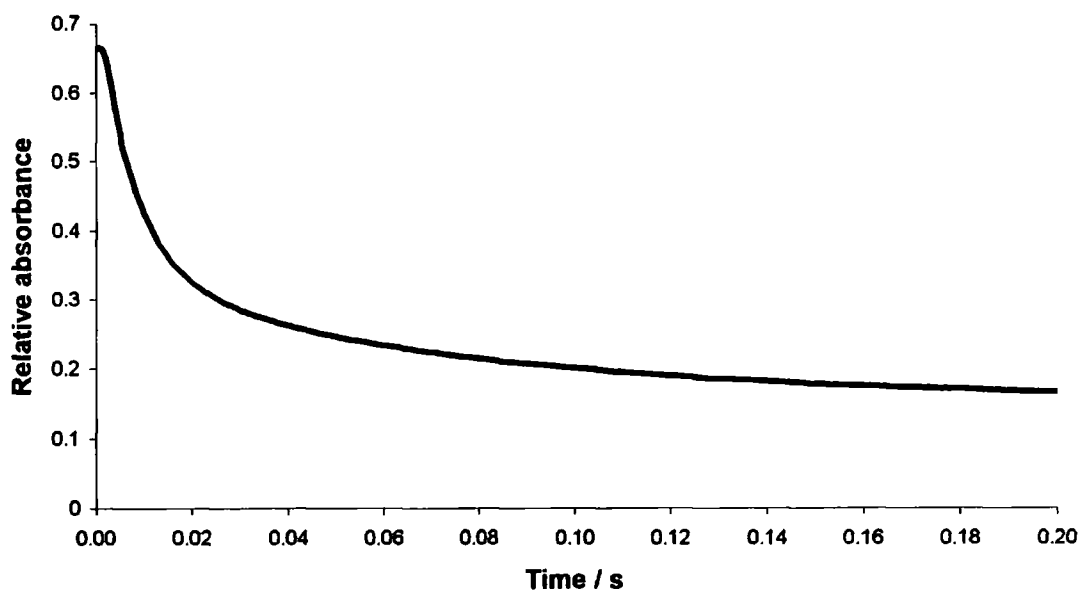
Figure 3.10 Decomposition of absorbance at 336 nm due to mono-S-nitroso DMPS at pH 7.4.

The decomposition profile fitted the double exponential model described in equation 3.2 indicating that a fast and slower reaction was occurring. Two first order rate constants were obtained, $118.6 \pm 1.2 \text{ s}^{-1}$ and $13.5 \pm 0.3 \text{ s}^{-1}$. An explanation for this could be that the two different mono-S-nitrosated forms of DMPS decompose at different rates at pH 7.4. When all the thiol is protonated this effect does not occur probably because the rates of decomposition become very similar.

The mono-S-nitroso DMPS decomposes much faster than expected compared to the two other dithiols at pH 7.4. The rate constant for a transnitrosation reaction is normally greater than the value obtained for the high thiol reaction. For example the rate constant for DTT reacting with GSNO is $68 \pm 2 \text{ dm}^3 \text{ mol}^{-1} \text{ s}^{-1}$ (see table 3.16) and the rate constant for mono-S-nitroso DTT reacting with the parent thiol is $0.35 \pm 0.01 \text{ dm}^3 \text{ mol}^{-1} \text{ s}^{-1}$ (see table 2.21). The faster than expected decomposition could be due to a very favourable internal nucleophilic attack.

3.5.3 Product Analysis of the Mono-S-nitroso DMPS Decomposition

When GSNO was reacted with DMPS one of the major products of the reaction was found to be ammonia. (see section 3.4.4) It is reasonable to suggest that the reaction goes via an initial transnitrosation and mono-S-nitroso DMPS forms. Therefore if an intermediate from the reaction is being studied it should decompose to form ammonia also.

Two reaction solutions were made up containing $5x10^{-4}$ M mono-S-nitroso DMPS, $4.5x10^{-3}$ M DMPS and either 0.15 M phosphate buffer (pH 7.4) or 0.01 M perchloric acid. When the S-nitrosothiol in both solutions had fully decomposed the concentration of ammonia was measured and a yield was calculated. (see table 3.24)

Reaction Conditions	Ammonia Yield
pH 7.4	99 %
0.01 M H^+	59 %

Table 3.24 Percentage yield of ammonia obtained in acidic conditions and pH 7.4.

The concentration of nitrite ions in both solutions was examined using the Griess test, but no significant levels were found.

3.5.4 An Explanation for Ammonia Formation

Using the experimental data obtained in this chapter a possible mechanistic scheme for the formation of ammonia has been put forward. Another mechanism has been proposed for the formation of ammonia from S-nitrosothiols.[22] However in general, ammonia is not the product of a transnitrosation reaction and the unexpected outcome of the reaction was investigated for this special case.

The proposed mechanism by which ammonia is formed from the reaction of GSNO with DMPS (see scheme 3.3) can be broken down into three different steps. Firstly there is an initial transnitrosation reaction that forms the mononitrosated DMPS molecule.

Hydroxylamine is then formed via a series of reactions involving NO^- with thiol and finally hydroxylamine reacts with thiol to give ammonia.

1st Step : transnitrosation,

$$GS-NO + (\text{DMPS, dithiol-}SO_3^-) \xrightarrow{k_{obs}} (\text{ON}-S\text{-thiol-}SO_3^-, SH) + GSH$$
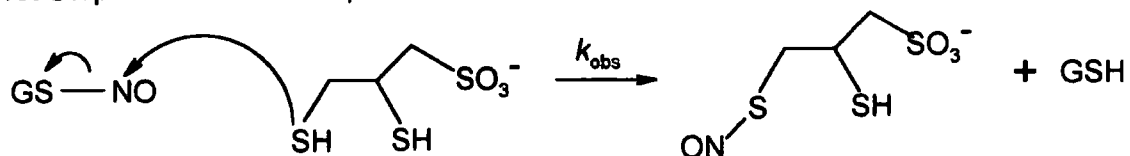
2nd Sequence of Steps : hydroxylamine formation,

$$(\text{cyclic ON-S, SH, }SO_3^-) \xrightarrow{-H^+} (\text{S}-S, SO_3^-) + NO^-$$

$$O=N^- + (\text{dithiol-}SO_3^-, SH, SH) \xrightarrow{H^+} (\text{HONH-S, SH, }SO_3^-)$$

$$(\text{cyclic HONH-S, SH, }SO_3^-) \longrightarrow (\text{S}-S, SO_3^-) + NH_2OH$$
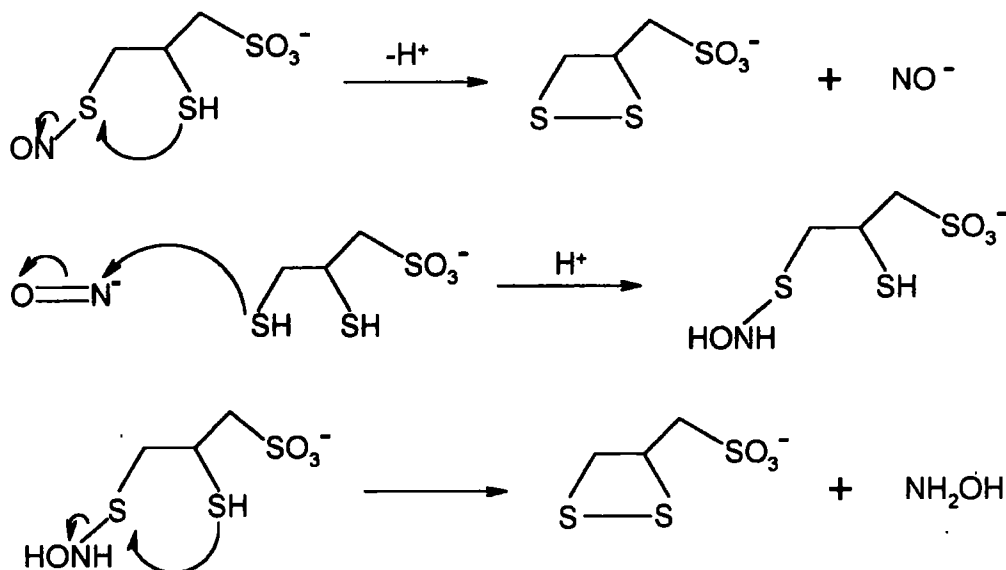
3rd Sequence of Steps : ammonia formation,

$$RSH + NH_2OH \longrightarrow RSNH_2 + H_2O$$

$$RSNH_2 + H_2O \longrightarrow RSOH + NH_3$$

$$2RSOH \longrightarrow RSSR + H_2O + 1/2 O_2$$

Overall chemical equation,

$$2GSNO + 4DMPS \longrightarrow GSSG + 2NH_3 + H_2O + 1/2 O_2$$
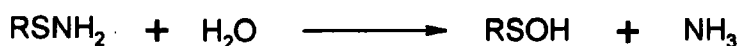
Scheme 3.3 Proposed mechanism for ammonia formation from DMPS reacting with GSNO.

Two studies have proposed the internal nucleophilic attack by a thiol group as a possible decomposition pathway for a mono-S-nitrosodithiol.[8,23] Hydroxylamine has been identified as one product of the reaction, but only in very low yield.[23]

The product analysis of the reaction between GSNO and DMPS found evidence that the [DMPS] : [GSNO] reaction stoichiometry was 2 : 1. (see figure 3.7) The overall chemical equation shown in scheme 3.3 agrees with the reaction stoichiometry found for the reaction of GSNO with DMPS. The product analysis for the reaction can be explained using these steps.

It has been found that HNO is reduced by two equivalents of thiol to yield disulfide and hydroxylamine.[24] HNO is a highly unstable species that has only been observed in aqueous solution using pulse radiolysis.[25] Therefore for the proposed mechanism to be viable, the reaction of thiol with HNO has to be faster than competing reactions at pH 7.4.

It was found that in acidic conditions the yield of ammonia from mono-S-nitroso DMPS was reduced compared with pH 7.4. (see table 3.24) The pK_a of HNO has been measured to be 4.7.[25] In aqueous solution HNO dimerises to give N_2O and water. The second order rate constant for this process at pH 7 and 25 °C has been calculated as $2x10^9 - 7x10^9$ dm^3 mol^{-1} s^{-1}.[26] The change in reaction products could be due to the effect low pH solutions have on the effectiveness of thiol to act as a nucleophile. (see table 3.15) As more thiol becomes protonated the rate of reaction via the thiolate anions decreases. This could make the reaction of HNO via dimerisation more favourable.

When NO concentrations were measured during a reaction only very small concentrations were detected indicating that nitrite was not formed from the oxidation of NO. Another possibility is the oxidation of hydroxylamine to nitrite ions, which could compete with the reaction of hydroxylamine with the thiol. This would explain why the nitrite yield increases when the thiol concentration is decreased. (see table 3.18) The HPLC analysis of the stoichiometric reaction of DMPS with GSNO indicated GSH was present. This could be due to a high amount of nitrite generated because hydroxylamine had been oxidised.

The sulfenic acid of GSH has been suggested as an intermediate leading to GSSG formation.[27] A series of reactions have been studied showing a possible pathway to disulfide formation from a sulfenic acid.[27] (see scheme 3.4) Sulfenic acids are known to dimerise to form thiosulfinates and the thiosulfinates can undergo disproportionation to form disulfides and the corresponding thiosulfonate. Only the disulfide GSSG was found in the reaction solutions so it is assumed that the thiosulfonate decomposed to the disulfide also. In some cases the yield of disulfide from the disproportionation of a thiosulfinate has been found to be as high as 83 % with no thiosulfonate found.

$$2RSOH \longrightarrow RSOSR + H_2O$$
$$2RSOSR \longrightarrow RSSR + RSO_2SR$$
$$RSO_2SR \longrightarrow RSSR + O_2$$

Overall,

$$2RSOH \longrightarrow RSSR + H_2O + 1/2O_2$$
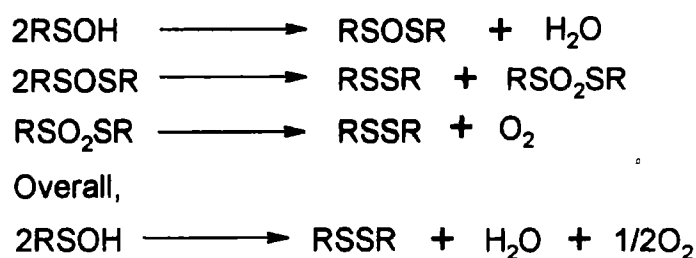
Scheme 3.4 Proposed reactions leading to RSSR formation from a sulfenic acid.

An alternative reaction proposed for the formation of GSSG from the sulfenic acid of GSH is shown in scheme 3.5.[28] The sulfenic acid reacts with GSH to form the disulfide and water. However this would not explain the reaction stoichiometry found in this study because two thiol groups would be required in the last step of the reaction that leads to ammonia formation.

$$GSH + GSOH \longrightarrow GSSG + H_2O$$

Scheme 3.5 Reaction of the sulfenic acid of GSH with GSH to form GSSG.

The HPLC analysis of the stoichiometric reaction between GSNO and DMPS found only GSH and GSSG as products of the reaction. This suggests that GSH only takes part in the last step of the reaction, leading to ammonia formation. If this were not the case then the major products would be mixed disulfides.

If the reaction of NO⁻ with DMPS were substantially more favourable than with GSH then this would lead to a situation where GSH could be solely responsible for the formation of ammonia from hydroxylamine.

3.6 Copper Ion Induced S-Nitroso Dithiol Decomposition

In general the decomposition of a number of simple S-nitrosothiols at pH 7.4 is a reaction catalysed by copper(+2) ions that are present as impurities or specifically added. The rate equation for the copper ion decomposition has been determined.[29] (see equation 3.6) k_2 is the rate constant for copper decomposition and k_1 is the rate constant for decomposition by other first order pathways, for example the thermal reaction. It has also been found that copper bound to proteins can be made available for this process to occur.[30]

Rate = $k_2[Cu^{2+}][RSNO] + k_1[RSNO]$

Equation 3.6 Rate equation for the copper catalysed decomposition of S-nitrosothiols.

3.6.1 Effect of Copper Ions on Di-S-nitroso DTT, DTE and DMPS Decomposition

The decomposition of di-S-nitroso DTT and DTE was followed by the decrease in absorbance at 336 nm. There was very little dependence of the measured rate constants on $[Cu^{2+}]$. When the decomposition of di-S-nitroso DMPS was followed using the same range of copper(+2) concentrations the absorbance at 338 nm was measured and there was a significant dependence as shown in table 3.25.

[RSNO] / M	$[Cu^{2+}]$ / M	k_{obs} / s^{-1}
5×10^{-4}	1×10^{-5}	0.00117
5×10^{-4}	2×10^{-5}	0.00171
5×10^{-4}	3×10^{-5}	0.00217
5×10^{-4}	4×10^{-5}	0.00272
5×10^{-4}	5×10^{-5}	0.00295

$k_2 = 45.7 \pm 3.2$ dm^3 mol^{-1} s^{-1}.

Table 3.25 Concentration of di-S-nitroso DMPS and copper ions with first order rate constants obtained in the presence of 0.15 M phosphate buffer (pH 7.4) at 25 °C.

The di-S-nitroso DMPS reaction profiles deviated from the first order model before the reaction went to completion. For example figure 3.11 shows the reaction profile for the reaction using 2×10^{-5} M copper(+2). The data points recorded for the first 1 500 s of each reaction solution fitted the first order model and this was how the rate constants were calculated. This suggests that the disulfide formed in the reaction could complex copper ions like GSNO[31] and this would lead to a deviation from first order kinetics.
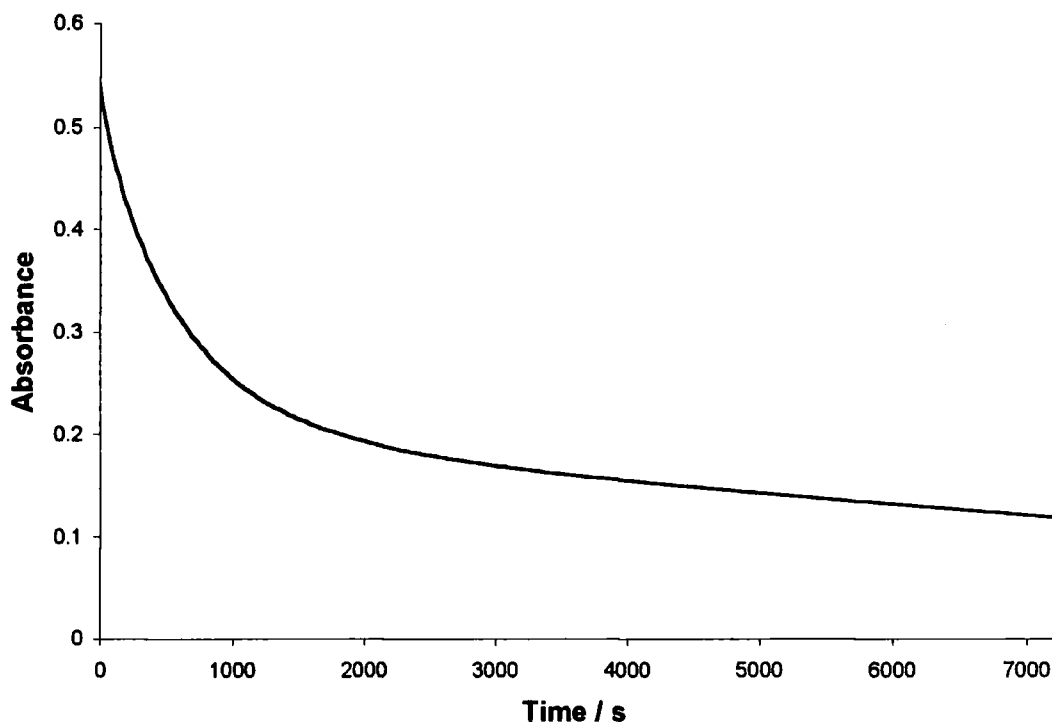
Figure 3.11 The reaction profile used to obtain a rate constant for the decomposition of di-S-nitroso DMPS in the presence of 2×10^{-5} M copper(+2).

The presence of copper ions only had an effect on the decomposition of di-S-nitroso DMPS. This could be due to the presence of the sulfonate group on the DMPS molecule giving copper ions a favourable co-ordination site. Another factor could be the relatively fast thermal decompositions of di-S-nitroso DTT and DTE, which would make a much slower decomposition pathway insignificant.

3.6.2 Effect of Copper Ions on Mono-S-nitroso DTT and DTE Decomposition

The decomposition of the mono-S-nitroso dithiols was followed at 333 nm and first order rate constants were obtained using the copper concentration range shown in table 3.25. No significant change in rate of decomposition was found. This could be because of the large rate of decomposition via other reaction pathways.

The experiment was not done using mono-S-nitroso DMPS because DMPS is a known copper chelator.

3.7 Discussion

Several reaction pathways were investigated involving nitrosated dithiols and interesting results were obtained concerning the thermal and high thiol reaction. Di-S-nitroso dithiols have been found to decompose rapidly via the thermal / photolytic pathway. Decomposition of mononitrosated dithiols at high thiol concentration was found to occur via an intermolecular and intramolecular process. The mononitrosated vicinal thiol was found to decompose most rapidly at pH 7.4 yielding ammonia.

The addition of a second S-nitroso group to a DTT or DTE molecule increased the rate of reaction via the thermal / photolytic pathway. This suggested that there was an interaction between the two S-nitroso groups leading to a sulfur nitrogen bond becoming weakened in the molecule.

The thermal rate of reaction for dinitrosated DTT and DTE is faster than for the vicinal dithiol DMPS. This could be because there are more chemical bonds between the thiol groups that make the cyclic intermediates proposed sterically more favourable.

Increasing the number of bonds between the thiol groups lead to an increase in the rate of decomposition via the thermal reaction. However the mononitrosated vicinal dithiol DMPS was found to decompose more rapidly at pH 7.4 than DTT or DTE.

The rapid decomposition of mononitrosated DMPS at pH 7.4 could have been due to a rapid internal nucleophilic attack by thiol. A reaction involving another molecule of DMPS would have probably been a much slower reaction.

Using the kinetic data for the mononitrosated DTT and DTE decomposition at pH 7.4 (see tables 3.21 and 3.22) and the mononitrosated DMPS decomposition in acidic solution (see table 3.23), the percentage of decomposition via the internal nucleophilic pathway could be calculated for a particular reaction solution. (see table 3.26) The data used were for the reaction solution that contained the lowest concentration of dithiol (dithiol in ten fold excess to the mononitrosated dithiol). The mononitrosated DMPS was found to decompose the most via the internal pathway.

Dithiol	k_1 / s^{-1}	k_{obs} / s^{-1}	$(k_1/k_{obs}) \times 100$
DTT	1.1×10^{-3}	2.9×10^{-3}	38 %
DTE	0.5×10^{-3}	1.5×10^{-3}	33 %
DMPS	3.92×10^{-4}	4.85×10^{-4}	81 %

Table 3.26 Calculation of percentage decomposition via the internal pathway for mononitrosated DTT, DTE and DMPS reaction solutions.

One of the products of the mononitrosated DMPS decompostion at pH 7.4 was found to be ammonia. It has been concluded that this occurs via the formation of NO^-, which is a likely product of an internal nucleophilic attack.

Decomposition pathways of S-nitrosated dithiols have been studied and some rate constants obtained were very different compared with other low molecular weight S-nitrosothiols. The position of the two thiols in a molecule was found to affect the rate of reaction.

3.8 References

1) W. L. Gross, M. I. Bak, J. S. Ingwall, M. A. Arstall, T. W. Smith, J. Balligand and R. A. Kelly, *Proc. Natl. Acad. Sci. USA*, 1996, **93**, 5604.

2) R. Gopalakrishna, Z. H. Chen and U. Gundimeda, *J. Biol. Chem.*, 1993, **268**, 27180.

3) R. J. Duhe, M. D. Nielsen, A. H. Dittman, E. C. Villacres, E. Choi and D. R. Storm, *J. Biol. Chem.*, 1994, **269**, 7290.

4) R. A. Garcia, L. L. Hirschberger and M. H. Stipanuk, *Anal. Biochem.*, 1988, **170**, 432.

5) G. L. Newton, J. A. Aguilera, R. C. Fahey, J. F. Ward, A. E. Radkowsky and E. M. Kosower, *Anal. Chem.*, 1992, **201**, 30.

6) R. P. Diaugustine, R. Henry, C. H. Sewall, C. A. Suarez-Quian and M. P. Walker, *Growth Factors*, 1999, **17**, 37.

7) M. Scigelova, P. S. Green, A. E. Giannakopulos, A. Rodger, D. H. G. Crout and P. J. Derrick, *Eur. J. Mass Spectrom.*, 2001, **7**, 29.

8) M. Le, H. Zhang and G. E. Means, *Bioorg. Med. Chem. Lett.*, 1997, **7**, 1393.

9) P. A. Morris and D. L. H. Williams, *J. Chem. Soc., Perkin Trans. 2*, 1988, 513.

10) D. J. Sexton, A. Muruganandam, D. J. McKenney and B. Mutus, *Photochem. Photobiol.*, 1994, **59**, 463.

11) D. A. Wink, J. F. Darbyshire, R. W. Nims, J. E. Saavedra and P. C. Ford, *Chem. Res. Toxicol.*, 1993, **6**, 23.

12) H. H. Awad and D. M. Stanbury, *Int. J. Chem. Kinet.*, 1993, **25**, 375.

13) D. J. Barnett, J. McAninly and D. L. H. Williams, *J. Chem. Soc., Perkin Trans. 2*, 1994, 1131.

14) A. J. Holmes and D. L. H. Williams, *J. Chem. Soc., Perkin Trans. 2*, 2000, 1639.

15) H. V. Aposhian, R. M. Maiorino, D. Gonzalez-Ramirez, M. Zuniga-Charles, Z. Xu, K. M. Hurlbut, P. Junco-Munoz, R. C. Dart and M. M. Aposhian, *Toxicology*, 1995, **97**, 23.

16) P. J. Coupe, Ph.D. thesis, University of Durham, 2001, 163.

17) Scientist package, version 2.02, Micromath Scientific Software, Salt Lake City, UT, USA. www.micromath.com

18) A. Avdeef and A. R. Chemotti, Jr., *J. Chem. Soc., Dalton Trans.*, 1991, 1189.

19) D. J. Barnett, Ph.D. thesis, University of Durham, 1994, 77.

20) H. C. van Anken and M. E. Schiphorst, *Clinica Chimica Acta*, 1974, **56**, 151.

21) A. P. Dicks, E. Li, A. P. Munro, H. R. Swift and D. L. H. Williams, *Can. J. Chem.*, 1998, **76**, 789.

22) S. P. Singh, J. S. Wishnok, M. Keshive, W. M. Deen and S. R. Tannenbaum, *Proc. Natl. Acad. Sci. USA*, 1996, **93**, 14428.

23) D. R. Arnelle and J. S. Stamler, *Arch. Biochem. Biophys.*, 1995, **318**, 279.

24) M. P. Doyle, S. N. Mahapatro, R. D. Broene and J. K. Guy, *J. Am. Chem. Soc.*, 1988, **110**, 593.

25) M. Grätzel, S. Taniguchi and A. Henglein, *Ber. Bunsenges. Phys. Chem.*, 1970, **74**, 1003.

26) D. A. Bazylinski and T. C. Hollocher, *Inorg. Chem.*, 1985, **24**, 4285.

27) F. A. Davies, L. A. Jenkins and R. L. Billmers, *J. Org. Chem.*, 1986, **51**, 1033.

28) J. R. Prohaska, *Biochim. Biophys. Acta*, 1980, **611**, 87.

29) S. C. Askew, D. J. Barnett, J. McAninly and D. L. H. Williams, *J. Chem. Soc., Perkin Trans. 2*, 1995, 741.

30) A. P. Dicks and D. L. H. Williams, *Chem. Biol.*, 1996, **3**, 655.

31) D. R. Noble and D. L. H. Williams, *Nitric Oxide: Biol. Chem.*, 2000, **4**, 392.

Chapter 4

Reactions of *S*-Nitrosothiols with an Iron(+2) Dithiol Complex

Chapter 4: Reactions of S-Nitrosothiols with an Iron(+2) Dithiol Complex

4.1 Introduction

S-Nitrosothiols are biologically active compounds that can induce vasodilation[1] and inhibit platelet aggregation.[2] It is commonly thought that this occurs because of S-nitrosothiol decomposition to NO. S-Nitrosothiols decompose at physiological pH (pH 7.4) via a copper(+2) catalysed reaction[3] which is shown in scheme 4.1. A much slower metal ion independent thermal / photochemical reaction can also occur giving the same products.[4]

$$RS^- \ + \ Cu^{2+} \ \longrightarrow \ 1/2RSSR \ + \ Cu^+$$

$$Cu^+ \ + \ RSNO \ \longrightarrow \ NO \ + \ Cu^{2+} \ + \ RS^-$$
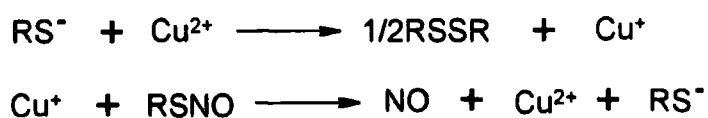
Scheme 4.1 Proposed reactions for the copper catalysed decomposition of S-nitrosothiols.

Studies have found that the copper(+1) chelator bathocuproine sulfonate reduced the biological activity of GSNO and S-nitrosocysteine.[5,6] The ability of the S-nitrosothiols to induce inhibition of platelet aggregation was also reduced significantly. It has also been found that when neocuproine, another copper(+1) chelator is present, vasodilation induced by S-nitrosothiols is hindered.[7,8] These experiments suggest that the biological activity observed is in part copper(+1) dependent.

A study has shown that copper bound to proteins and peptides can be made available for the catalytic decomposition of S-nitrosothiols.[9] However it has not been determined whether the copper is required by the S-nitrosothiol for the biological process to occur. Evidence has also been put forward which suggests that the biological activity of S-nitrosothiols does not require decomposition of the S-nitrosothiol to NO.

Attempts have been made to correlate the biological activity of S-nitrosothiols with their stability in aqueous solution. One study compared the stability of S-nitrosothiols by following decrease in absorbance at 330 nm, then used much lower concentrations to measure the biological activity.[10] Another study looked at the stability of S-nitrosothiols and their ability to cause vasodilation at the same concentrations.[11] In both cases no

correlation could be found between the stability and the biological activity of the *S*-nitrosothiols. One major problem with these studies is that many factors affect the lifetime of *S*-nitrosothiols in aqueous solution, which is discussed in chapter one (eg. thiol and disulfide concentration and the presence of ascorbic acid). Possible decomposition pathways of the *S*-nitrosothiols in the biological experiments were not discussed.

The bronchodilating effects of GSNO and other *S*-nitrosothiols have been studied using a guinea pig lung.[12] When two NO scavengers were present to remove all free NO from the buffer solutions the biological activity of the *S*-nitrosothiols was not hindered. Another study used the NO trap haemoglobin to compare levels of NO present when NO and *S*-nitrosocysteine were used to cause vasodilation.[13] An EPR signal was observed when NO was used but not with *S*-nitrosocysteine. These studies implied that the biological activity was due to the intact *S*-nitrosothiol molecule.

A study looked at many compounds that caused vasodilation including NO itself and found that they all required the presence of thiol.[1] Therefore it was concluded that an *S*-nitrosothiol could be an intermediate in the biological process.

Vasodilation and inhibition of platelet aggregation is believed to occur when NO binds to an iron centre in the protein guanylate cyclase[14] and this is shown in figure 4.1. The strong trans effect of the NO ligand causes the histidine group to become detached and this leads to a build up of guanosine 3',5'-cyclic monophosphate, which brings about smooth muscle relaxation.[15]
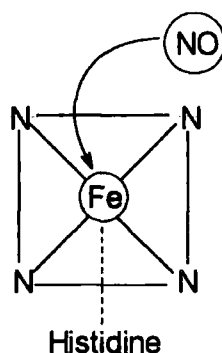
Figure 4.1 Simplified view of NO binding to a haem group in guanylate cyclase.

Experimental data obtained by a research group at the University of St. Andrews lead by Dr. A. R. Butler suggested that S-nitrosothiols could transfer NO directly to an iron(+2) dithiol complex. The results have been reviewed and further work completed to gain a mechanistic understanding of the reaction. This chapter examines the possibility that S-nitrosothiols can react directly with iron complexes.

4.2 Physical Properties of the Iron(+2) Dithiol Complex

The iron(+2) complex with 2,3-dimercapto-1-propanesulfonic acid (DMPS) has been developed for the trapping of NO in flue gases[16] and the proposed structure is shown in figure 4.2. It was found to absorb NO more effectively when oxygen was present compared with the more oxygen sensitive iron(+2) EDTA complex.

$$\left[{}^-O_3S \diagdown \diagup S \diagdown \diagup S \diagdown \diagup SO_3^- \quad Fe^{2+} \right]^{4-}$$
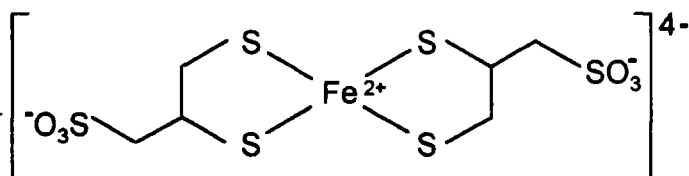
Figure 4.2 The suggested iron(+2) complex with DMPS.

This complex has been used as a very simple model for the active site of guanylate cyclase for two reasons. Guanylate cyclase and the complex both have iron centres that have a high affinity for NO. There is also similar co-ordination around the iron centre, the iron centres are both in the centre of a plane defined by four atoms, with guanylate cyclase they are nitrogen, with this model they are sulfur.

4.2.1 Measurement of the Iron(+2) DMPS Equilibrium Constant

It was found that the formation of the iron complex (which is red in colour) required the presence of base or phosphate buffer (pH 7.4). This suggested that the deprotonated DMPS molecule reacted with the iron(+2). The use of phosphate buffer (pH 7.4) was required anyway because reactions were to be performed at physiological pH. The presence of the red complex could be determined visually or quantitatively by the absorbance at 509 nm.

Initial attempts to determine an equilibrium constant failed due to the fact that increasing DMPS concentration never appeared to take the complexation to completion. The introduction of the reducing agent sulfite brought about coherent results. (see table 4.1 and figure 4.3) This suggested that the problem was the oxidation of iron(+2) leading to instability of the complex being studied. Using ascorbic acid as a reducing agent instead of sulfite gave the same results.

[DMPS] / M	Absorbance at 509 nm
0.0×10^{-3}	0.000
0.2×10^{-3}	0.147
0.4×10^{-3}	0.351
0.6×10^{-3}	0.587
0.8×10^{-3}	0.688
1.0×10^{-3}	0.753
1.2×10^{-3}	0.785
1.4×10^{-3}	0.809
1.6×10^{-3}	0.823
1.8×10^{-3}	0.813
2.0×10^{-3}	0.812
2.2×10^{-3}	0.831
2.4×10^{-3}	0.802

Table 4.1 Absorbance at 509 nm measured with 2×10^{-4} M $FeSO_4$, 2×10^{-3} M Na_2SO_3 and 0.15 M phosphate buffer (pH 7.4) present with varying DMPS concentrations.

The proposed chemical equilibrium between reactants and the iron complex is shown in scheme 4.2, and from this the equation for the equilibrium constant was derived. (see equation 4.1)

$$Fe^{2+} + 2DMPS \underset{}{\overset{K}{\rightleftharpoons}} \{Fe(II)(DMPS)_2\}^{4-}$$

Scheme 4.2 Chemical equilibrium for the formation of the iron complex.

$$K = \frac{[\{Fe(II)(DMPS)_2\}^{4-}]}{[Fe(II)][DMPS]^2}$$

Equation 4.1 Expression for the equilibrium constant of iron(+2) DMPS complex formation.

The experimental data in table 4.1 were fitted to equation 4.1 using Scientist[17] and a good fit was obtained. (see figure 4.3) When analysing data in Scientist it was found that the model was not valid when the iron(+2) concentration was equal to the DMPS concentration, therefore the DMPS concentration was entered as 1.999×10^{-4} M. The model uses two assumptions:

i) The 1 : 1 iron(+2) : DMPS complex is present in very small concentrations.

ii) All other species have an insignificant absorbance at 509 nm, therefore at zero DMPS concentration the absorbance was set at zero.
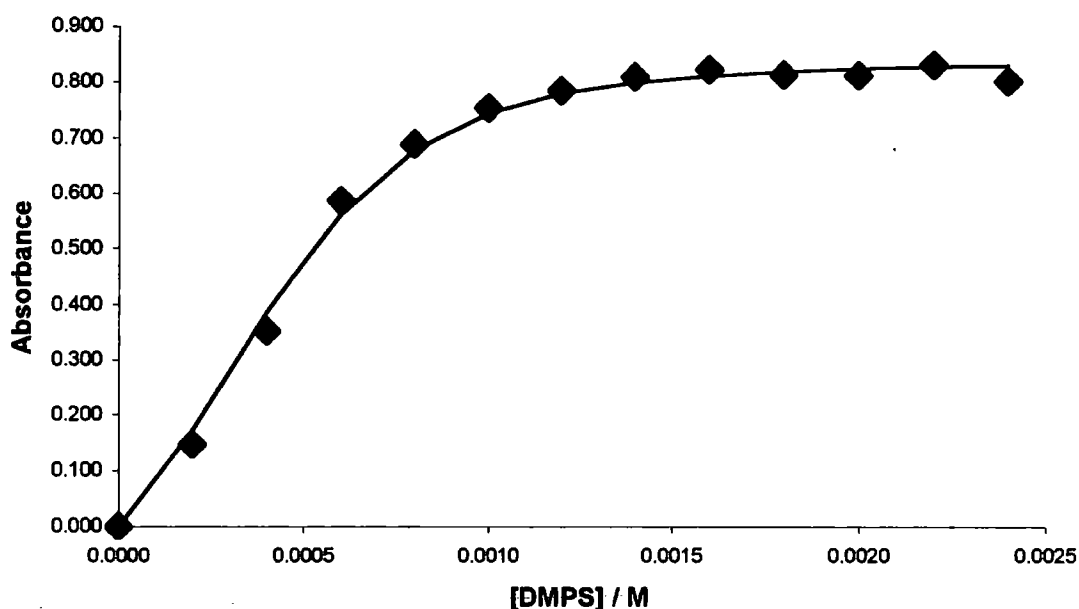
Figure 4.3 Experimental data (♦) from table 4.1 plotted against the fit obtained in Scientist (the solid line).

The model gave an equilibrium constant, $K = 1.8 \times 10^7 \pm 0.2 \times 10^7$ dm^6 mol^{-2} and an extinction coefficient at 509 nm, $\varepsilon_{509nm} = 4\,205 \pm 44$ dm^3 mol^{-1} cm^{-1}.

4.2.2 Determination of the Iron Complex UV / Vis Spectroscopic Parameters

The reaction conditions and amount of DMPS required for complete complexation of iron(+2) had been found. (see figure 4.3) Absorbance maxima for the iron complex were found and extinction coefficients calculated using the Beer-Lambert law. The method is described more fully in section 2.2.1.

A solution containing 2×10^{-4} M $FeSO_4$, 2×10^{-3} M Na_2SO_3 and 1.6×10^{-3} M DMPS in the presence of 0.15 M phosphate buffer (pH 7.4) was prepared and diluted down to several concentrations. The UV / Vis spectra at different complex concentrations are shown in figure 4.4, and the measured absorbance values in table 4.2.
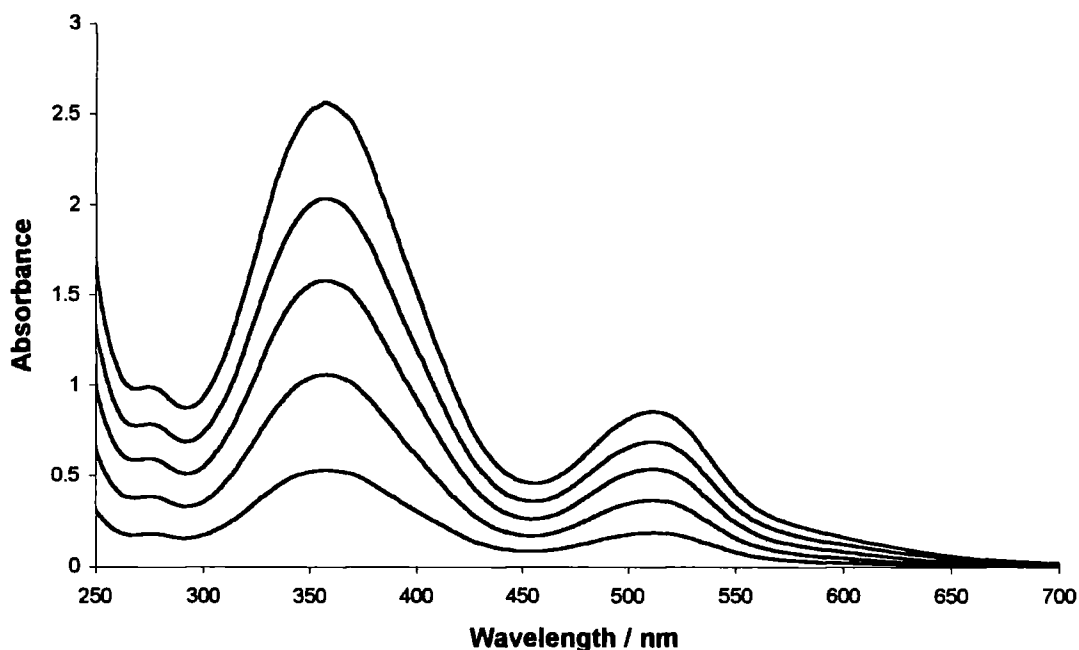
Figure 4.4 UV / Vis spectra of $\{Fe(II)(DMPS)_2\}^{4-}$ at 2.0×10^{-4}, 1.6×10^{-4}, 1.2×10^{-4}, 0.8×10^{-4} and 0.4×10^{-4} M.

[{Fe(II)(DMPS)$_2$}$^{4-}$] / M	Abs. (276 nm)	Abs. (358 nm)	Abs. (509 nm)
0.4x10^{-4}	0.183	0.531	0.183
0.8x10^{-4}	0.382	1.058	0.361
1.2x10^{-4}	0.593	1.577	0.537
1.6x10^{-4}	0.787	2.029	0.688
2.0x10^{-4}	0.990	2.562	0.854

Table 4.2 Measured absorbance at 276, 358 and 509 nm for different iron complex concentrations.

$\varepsilon_{276nm} = 5\ 050 \pm 30$ dm^3 mol^{-1} cm^{-1}.

$\varepsilon_{358nm} = 12\ 580 \pm 180$ dm^3 mol^{-1} cm^{-1}.

$\varepsilon_{509nm} = 4\ 170 \pm 70$ dm^3 mol^{-1} cm^{-1}.

The extinction coefficient found for the absorbance at 509 nm was the same as that obtained by Scientist (within the error) when modelling the equilibrium curve in figure 4.3.

4.3 UV / Vis Spectra of Various Iron Nitrosyl Complexes

One characteristic feature of iron nitrosyl complexes is they can have several overall oxidation states.[18] The oxidation state can change the colour of the complex, therefore the UV / Vis spectrum can change also.

When making the iron nitrosyl complexes, NO was blown through the solutions using nitrogen as a carrier gas. It has been found that small amounts of oxygen present in the nitrogen can cause oxidation of a iron nitrosyl complex.[19] The addition of the reducing agent sulfite stopped this occurring.

4.3.1 The Reaction of Nitric Oxide with the Iron Complex

UV / Vis spectra of the iron nitrosyl complexes were required to determine what product if any was forming when S-nitrosothiols were reacted with the iron complex. The iron(+2)

and DMPS concentration were present in the same ratio as used in kinetic runs to get comparable spectra. NO was generated by adding solid sodium nitrite to a solution of 0.1 M ascorbic acid. (see scheme 4.3) Nitrogen was bubbled through all solutions for fifteen minutes and any solution transfer was done under a nitrogen atmosphere to minimise oxygen levels.
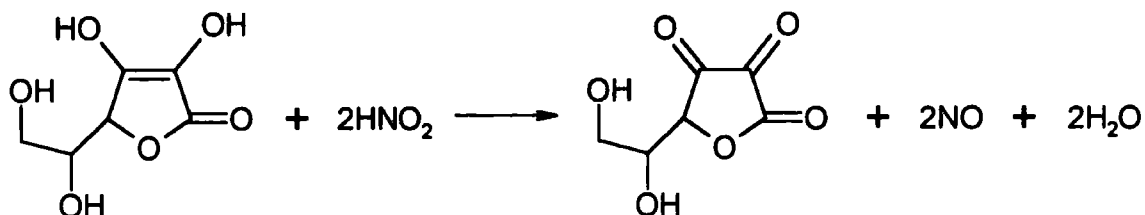
Scheme 4.3 Chemical equation for the formation of NO and dehydroascorbic acid from ascorbic acid and nitrous acid.

A solution containing 2×10^{-4} M $FeSO_4$, 4×10^{-4} M DMPS and 0.15 M phosphate buffer (pH 7.4) was reacted with NO. NO was bubbled through the iron complex solution for fifteen minutes using nitrogen in anaerobic conditions. The concentration of the solution was then halved using water and the UV / Vis spectrum of the solution is shown in figure 4.5.
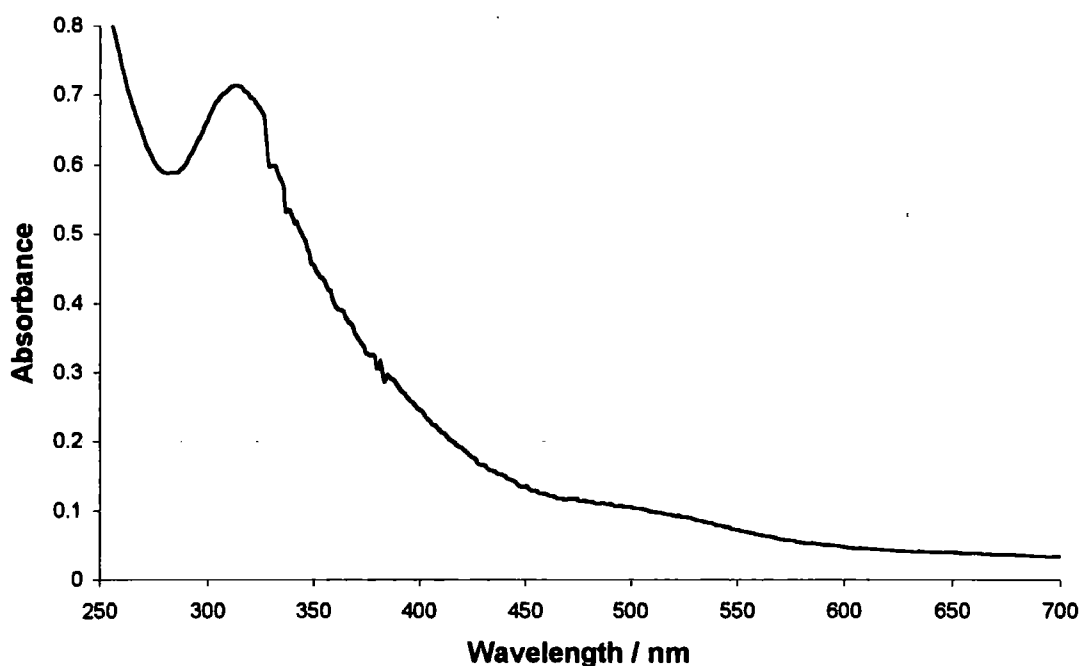
Figure 4.5 A UV / Vis spectrum of 1×10^{-4} M $FeSO_4$ and 2×10^{-4} M DMPS in the presence of 0.075 M phosphate buffer (pH 7.4) reacted with NO in anaerobic conditions.

111

The UV / Vis spectrum of the resulting yellow / orange coloured solution in figure 4.5 had a characteristic absorbance peak at 313 nm. The experiment was then repeated using a ten fold excess of sulfite over iron(+2) to determine whether an oxidation occurred.

NO was bubbled through the reaction solution until a colour change from red to orange was observed. Nitrogen was then immediately blown through the solution for fifteen minutes to stop formation of the dinitrosyl iron complex. (see section 4.3.2) The UV / Vis spectrum of the reaction solution (see figure 4.6) showed peaks at 338 and 507 nm.
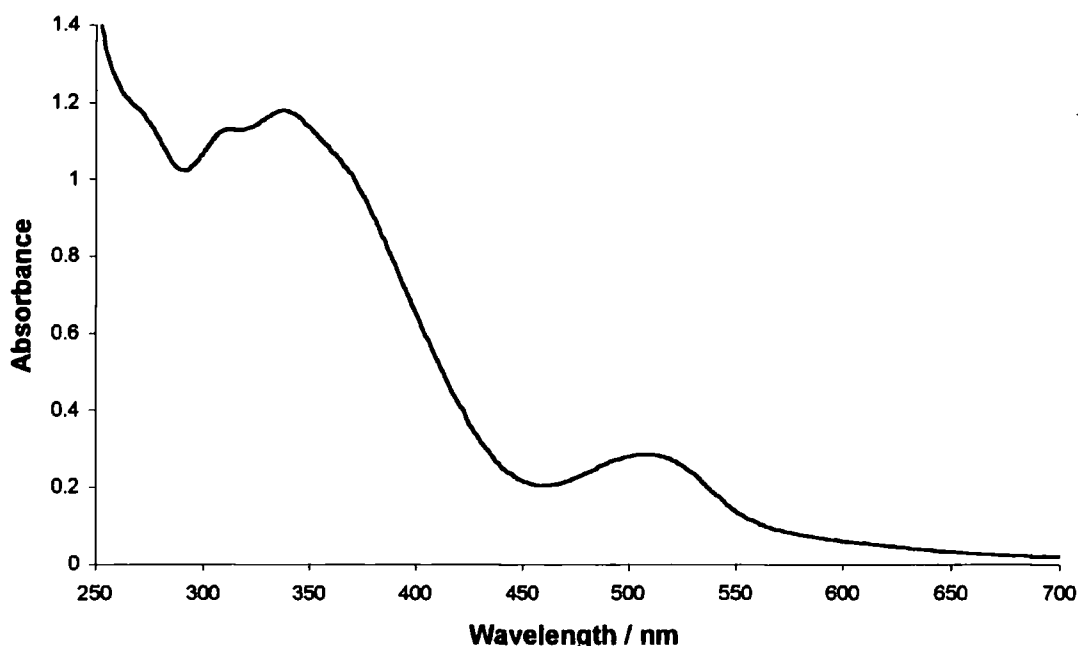
Figure 4.6 A UV / Vis spectrum of 2×10^{-4} M FeSO$_4$, 4×10^{-4} M DMPS and 2×10^{-3} M Na$_2$SO$_3$ in the presence of 0.15 M phosphate buffer (pH 7.4) reacted with NO in anaerobic conditions followed by removal of excess NO by a nitrogen flow.

4.3.2 Evidence of the Formation of a Dinitrosyl Complex

Evidence has been obtained using infra red spectroscopy that the iron complex at high NO concentrations forms a dinitrosyl iron complex.[16] This was likely to form under experimental conditions in this study because of the large amounts of NO generated. This was to overcome NO loss during the reaction because of leaks and oxidation.

When making the mono nitrosyl iron complex in the presence of sulfite it was found that a peak slowly formed over time after NO was bubbled through the solution for a minute. A peak can be seen just beginning to form at 309 nm in figure 4.6. It was found that bubbling nitrogen through the solution immediately after NO stopped the peak increasing in size. An explanation for the apparent slower chemical reaction could be the formation of the dinitrosyl iron complex.

NO was blown through an iron complex solution containing sulfite for fifteen minutes. A UV / Vis spectrum was taken of the reaction solution which is shown in figure 4.7. Two peaks were found, one at 309 nm with a shoulder at 330 nm and one at 507 nm.
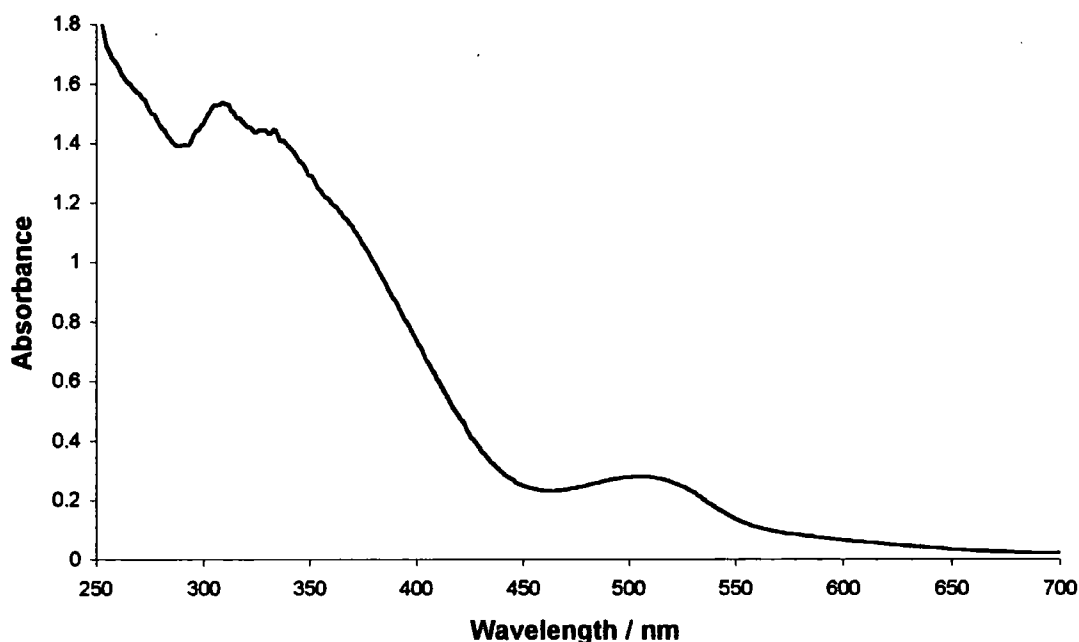
Figure 4.7 A UV / Vis spectrum of 2×10^{-4} M $FeSO_4$, 4×10^{-4} M DMPS and 2×10^{-3} M Na_2SO_3 in the presence of 0.15 M phosphate buffer (pH 7.4) reacted with NO in anaerobic conditions.

Considering the spectral data obtained, and taking into account prior reports, the series of reactions shown in scheme 4.4 are proposed for the reactions of NO with the iron(+2) DMPS complex.

{Fe(III)(DMPS)$_2$NO}$^{3-}$ — Absorbance maximum, 313 nm.

NO / O$_2$

{Fe(II)(DMPS)$_2$}$^{4-}$

Absorbance maxima, 276, 358, 509 nm.

NO / Na$_2$SO$_3$

{Fe(II)(DMPS)$_2$NO}$^{4-}$ — Absorbance maxima, 338, 507 nm.

excess NO

{Fe(II)(DMPS)$_2$(NO)$_2$}$^{4-}$ — Absorbance maxima, 309, 507 nm.
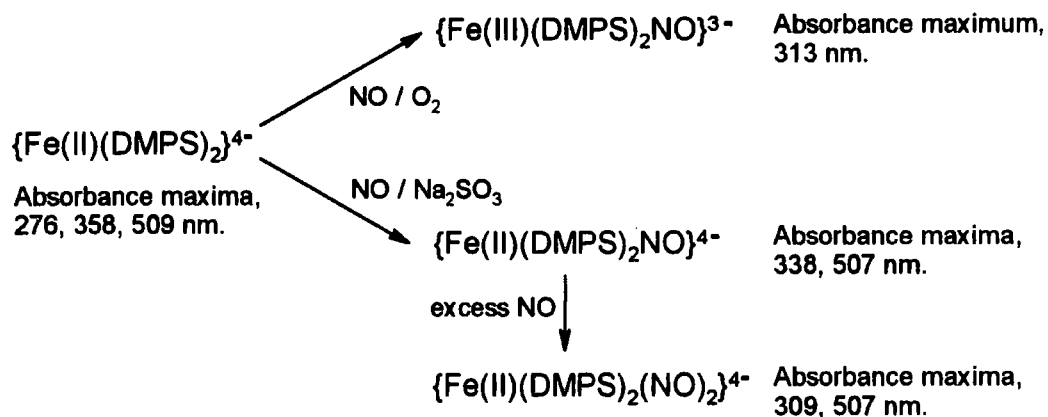
Scheme 4.4 Proposed reactions of NO with the iron complex.

4.4 Evidence of a Direct Reaction Between the Iron Complex and S-Nitrosothiols

Initial work on these reactions used a method to generate the iron(+2) complex under aerobic conditions.[20] The DMPS was dissolved in 24 mM phosphate buffer (pH 7.4) then poured over solid iron(+2) sulfate. Concentrated phosphate buffer was then added to give a final concentration of 0.15 M. All of the buffer could not be added initially due to the low solubility of iron(+2) in phosphate solutions.

The [DMPS] : [iron(+2)] reaction ratio used was 2 : 1 for two reasons. At a 1 : 1 ratio the iron phosphate precipitated out of solution and secondly increasing the DMPS concentration was not sensible because DMPS reacts with S-nitrosothiols. (see chapter 3) Initial work used a stock solution of the complex where the final iron concentration was 1×10^{-3} M. It was found that decreasing the concentration made the complex present more air sensitive.

In this chapter the concentration of the iron complex solution, sometimes called the total iron concentration is the total concentration of iron ions in the solution. DMPS was reacted with iron(+2) in a 2 : 1 stoichiometric ratio to form the complex and its concentration can be calculated using the equilibrium constant for its formation.

4.4.1 Kinetics of the Reaction Between the Iron Complex and S-Nitrosothiols

A solution containing the iron complex was made up using the method described previously. GSNO like the other S-nitrosothiols used was generated *in situ* by reacting equimolar quantities of thiol with sodium nitrite in the presence of 0.02 M perchloric acid. Concentrated phosphate buffer (pH 7.4) was then added so that the buffer concentration was 0.15 M. This concentration was used in the kinetic experiment.

It was found that the addition of GSNO to a solution of the iron complex caused the disappearance of the red colour in the solution. This reaction was followed by measuring the decrease in absorbance at 509 nm over time. GSNO was reacted with the iron complex in sufficient excess so that if a reaction occurred and could be followed, it would probably be under pseudo first order conditions.
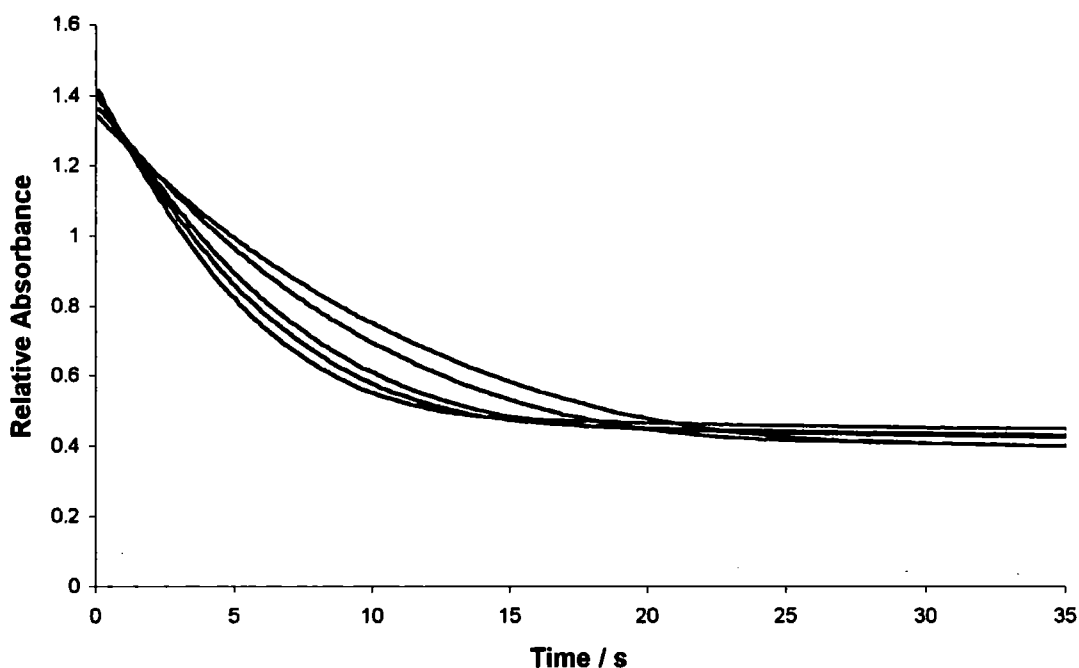
Figure 4.8 Decomposition at 509 nm of the iron complex solution at 5×10^{-4} M with a) 0.5×10^{-2} M, b) 0.6×10^{-2} M, c) 0.8×10^{-2} M, d) 0.9×10^{-2} M and e) 1.0×10^{-2} M GSNO in the presence of 0.15 M phosphate buffer (pH 7.4) at 25 °C.

The reaction profiles that are shown in figure 4.8 have large final absorbance values. This could have been because of iron phosphate interactions.

The absorbance change is larger than expected for all first order reaction profiles obtained in this chapter. All spectral data of nitrosyl iron complexes in section 4.3 showed significant absorbance at 509 nm. It is thought that a nitrosyl iron complex was formed during the reactions but was unstable in aerobic conditions and rapidly decomposed so it did not affect reaction kinetics.

First order rate constants were determined from the reaction profiles and these are shown in table 4.3. When the first order rate constants were plotted against GSNO concentration a straight line was obtained which is shown in figure 4.9. A second order rate constant was calculated from the gradient of the graph and no significant intercept was found. These kinetic data show that the reaction is first order with respect to both GSNO and the iron complex. The rate equation for the reaction is shown in equation 4.2.

[GSNO] / M	Total [iron] / M	k_{obs} / s^{-1}
0.5×10^{-2}	5×10^{-4}	0.099
0.6×10^{-2}	5×10^{-4}	0.127
0.8×10^{-2}	5×10^{-4}	0.173
0.9×10^{-2}	5×10^{-4}	0.201
1.0×10^{-2}	5×10^{-4}	0.220

$k_2 = 24 \pm 1$ dm^3 mol^{-1} s^{-1}.

Table 4.3 Total iron and GSNO concentrations in the reaction solutions with pseudo first order rate constants obtained in the presence of 0.15 M phosphate buffer (pH 7.4) at 25 °C.
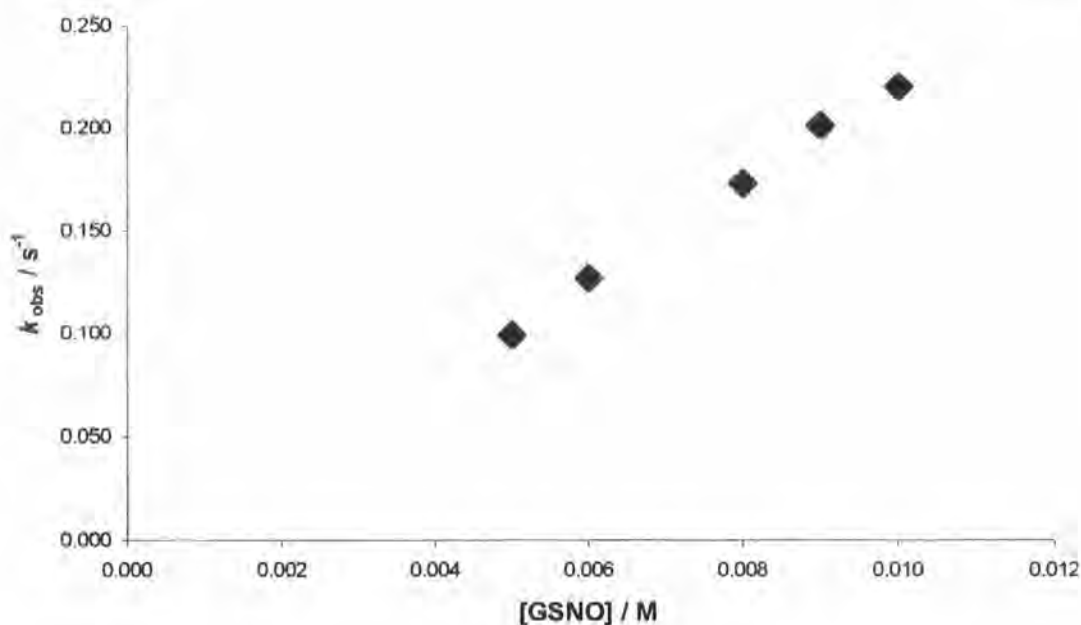
Figure 4.9 Pseudo first order rate constants plotted against GSNO concentration.

Rate = k_2[GSNO][Iron Complex]

Equation 4.2 Rate equation for the reaction of GSNO with the iron complex.

S-Nitroso-N-acetylcysteine (SNAC) and S-nitrosocaptopril (SNOCAP) were reacted with the iron complex without EDTA like GSNO because of their relative stability in solution at pH 7.4 (no apparent reaction with small quantities of copper ions present). Second order rate constants could be obtained for these S-nitrosothiols as well. (see table 4.4 and 4.5)

[SNAC] / M	Total [iron] / M	k_{obs} / s^{-1}
0.5×10^{-2}	5×10^{-4}	0.0325 ± 0.0003
0.6×10^{-2}	5×10^{-4}	0.0341 ± 0.0002
0.7×10^{-2}	5×10^{-4}	0.0430 ± 0.0003
0.8×10^{-2}	5×10^{-4}	0.0472 ± 0.0003
0.9×10^{-2}	5×10^{-4}	0.0565 ± 0.0004

$k_2 = 6.1 \pm 0.7$ dm^3 mol^{-1} s^{-1}.

Table 4.4 Total iron and SNAC concentrations in the reaction solutions with pseudo first order rate constants obtained in the presence of 0.15 M phosphate buffer (pH 7.4) at 25 °C.

[SNOCAP] / M	Total [iron] / M	k_{obs} / s^{-1}
0.6×10^{-2}	5×10^{-4}	0.047
0.7×10^{-2}	5×10^{-4}	0.056
0.8×10^{-2}	5×10^{-4}	0.061
0.9×10^{-2}	5×10^{-4}	0.069
1.0×10^{-2}	5×10^{-4}	0.078

$k_2 = 7.5 \pm 0.4$ dm^3 mol^{-1} s^{-1}.

Table 4.5 Total iron and SNOCAP concentrations in the reaction solutions with pseudo first order rate constants obtained in the presence of 0.15 M phosphate buffer (pH 7.4) at 25 °C.

4.4.2 Kinetic Studies Carried Out in the Presence of EDTA

Some S-nitrosothiols can decompose rapidly at pH 7.4 due to copper(+2) ions that are present in all water.[21] Therefore the metal ion chelator EDTA had to be present in some kinetic experiments to prevent copper induced decomposition of the S-nitrosothiol solutions.

The effect of EDTA present on the stability of the iron complex was examined. It was found that EDTA could cause a slow decomposition of the iron complex. EDTA was used to stop the copper decomposition of the S-nitrosothiols occurring in stock solutions. Iron complex concentration was followed by recording absorbance at 509 nm over time. The stability of the iron complex in the presence of EDTA was analysed using two iron complex solution concentrations. (see figure 4.10)
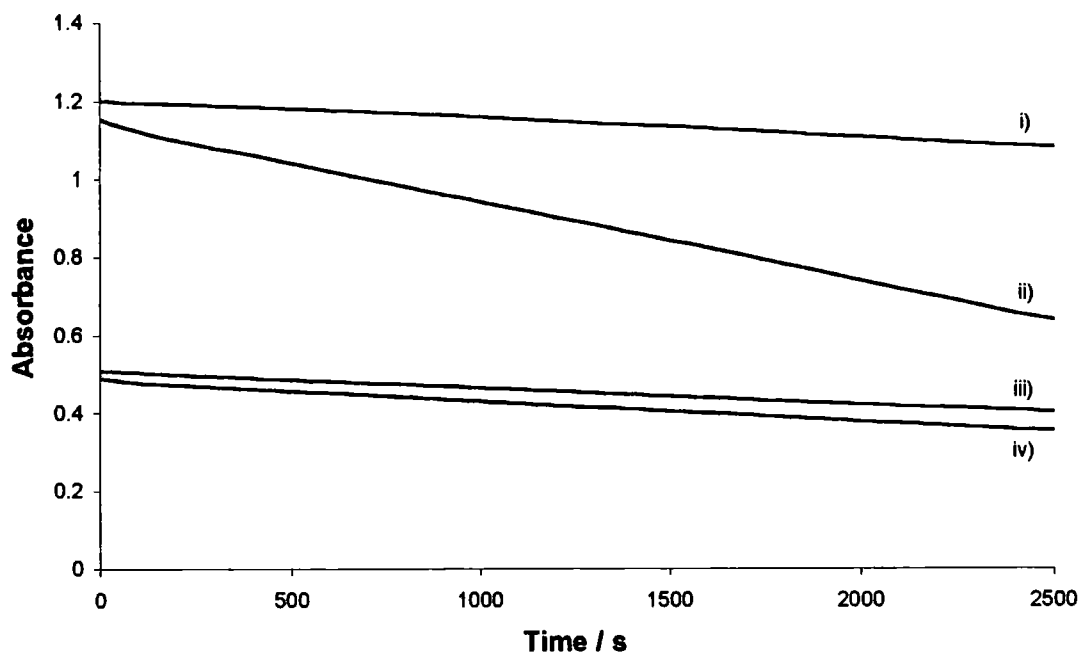
Figure 4.10 Decomposition at 509 nm of the iron complex solution at 5×10^{-4} M with i) no EDTA, ii) 1×10^{-4} M EDTA and at 2×10^{-4} M with iii) no EDTA, iv) 1×10^{-4} M EDTA all in the presence of 0.15 M phosphate buffer (pH 7.4) at 25 °C.

Lowering the iron complex solution concentration to 2×10^{-4} M nearly stopped the EDTA promoted decomposition of the iron complex. The stock solution of the iron complex was more air sensitive at this lower concentration but stable enough to use in kinetic experiments. Second order rate constants obtained for the reactions of two S-nitrosothiols (S-nitrosocysteine and S-nitrosohomocysteine) with the iron complex in the presence of EDTA are shown in table 4.6 and 4.7.

[S-nitrosocysteine] / M	Total [iron] / M	k_{obs} / s^{-1}
2.0×10^{-3}	2×10^{-4}	0.107 ± 0.001
2.4×10^{-3}	2×10^{-4}	0.127 ± 0.001
2.8×10^{-3}	2×10^{-4}	0.149 ± 0.001
3.2×10^{-3}	2×10^{-4}	0.179 ± 0.001
3.6×10^{-3}	2×10^{-4}	0.213 ± 0.001
4.0×10^{-3}	2×10^{-4}	0.248 ± 0.001

$k_2 = 71 \pm 4$ dm^3 mol^{-1} s^{-1}.

Table 4.6 Total iron and S-nitrosocysteine concentrations in the reaction solutions with pseudo first order rate constants obtained in the presence of 0.15 M phosphate buffer (pH 7.4) and 1×10^{-4} M EDTA at 25 °C.

[S-nitrosohomocysteine] / M	Total [iron] / M	k_{obs} / s^{-1}
2.0×10^{-3}	2×10^{-4}	0.030
2.4×10^{-3}	2×10^{-4}	0.034
2.8×10^{-3}	2×10^{-4}	0.039
3.2×10^{-3}	2×10^{-4}	0.046
3.6×10^{-3}	2×10^{-4}	0.057
4.0×10^{-3}	2×10^{-4}	0.059

$k_2 = 16 \pm 1$ dm^3 mol^{-1} s^{-1}.

Table 4.7 Total iron and S-nitrosohomocysteine concentrations in the reaction solutions with pseudo first order rate constants obtained in the presence of 0.15 M phosphate buffer (pH 7.4) and 1×10^{-4} M EDTA at 25 °C.

4.4.3 The Reaction of Tertiary S-Nitrosothiols with the Iron Complex

The reaction of S-nitrosopenicillamine with the iron complex was attempted but it was found that the reaction profiles were not reproducible. The rate of decomposition of the iron

complex kept increasing when runs were repeated using the same *S*-nitrosothiol concentration. Use of an NO electrode revealed the *S*-nitrosothiol solutions contained significant quantities of NO. It is believed that the NO was being generated via the thermal / photolytic decomposition pathway.

The decompositions involving *S*-nitroso-1-amino-2-methyl-2-propane thiol were followed using a stopped flow spectrometer. Reactions involving SNAP were much slower and could be followed using a conventional UV / Vis spectrometer. The reaction of SNAP and *S*-nitroso-1-amino-2-methyl-2-propane thiol with the iron complex in the presence of 1×10^{-4} M EDTA gave reproducible reaction profiles. However the decompositions obtained did not fit a first order model. This suggested that something different was occurring in the system being studied.

4.5 Product Analysis of the Reaction of Iron Complex with *S*-Nitrosothiol

Experimental evidence was found that the *S*-nitrosothiols reacted with the iron complex. Nitrosyl iron complex formation could be determined using the UV / Vis absorbance maxima measured in section 4.3.

4.5.1 UV / Vis Analysis of the Reaction with GSNO

GSNO was reacted with an iron complex solution in a 1 : 1 reaction. The reaction was performed in anaerobic conditions since the nitrosyl iron complexes are unstable in aerobic solutions. A UV / Vis spectrum was taken of the reaction solution after fifteen minutes and is shown in figure 4.11.
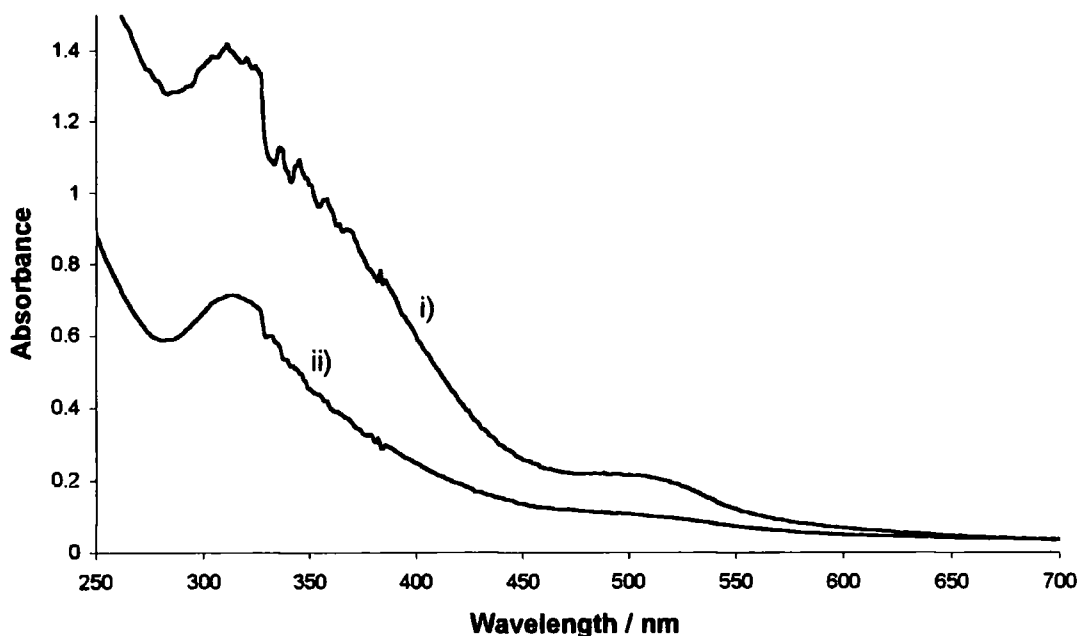
Figure 4.11 i) The UV / Vis spectrum of 2×10^{-4} M GSNO reacted with an equimolar iron complex solution in the presence of 0.15 M phosphate buffer (pH 7.4). ii) The UV / Vis spectrum shown in figure 4.5, believed to be of $\{Fe(III)(DMPS)_2NO\}^{3-}$.

The UV / Vis spectra are very similar, both showing a peak at 313 nm. A similar spectrum was obtained when S-nitrosocysteine was reacted with an iron complex solution in the presence of 1×10^{-4} M EDTA and 0.15 M phosphate buffer (pH 7.4).

The 1 : 1 reaction solution UV / Vis spectrum was recorded at double the concentration so that the peak at 313 nm would be clear. This could have been due to it being a reaction solution rather than a prepared sample so other products make the peak less clear.

4.5.2 UV / Vis Analysis of the Reaction with S-Nitroso-1-amino-2-methyl-2-propane Thiol

In order to determine what happened with tertiary S-nitrosothiols, S-nitroso-1-amino-2-methyl-2-propane thiol was reacted with the iron complex in a similar 1 : 1 reaction to GSNO. The UV / Vis spectrum of the anaerobic reaction solution was taken after fifteen minutes and is shown in figure 4.12.
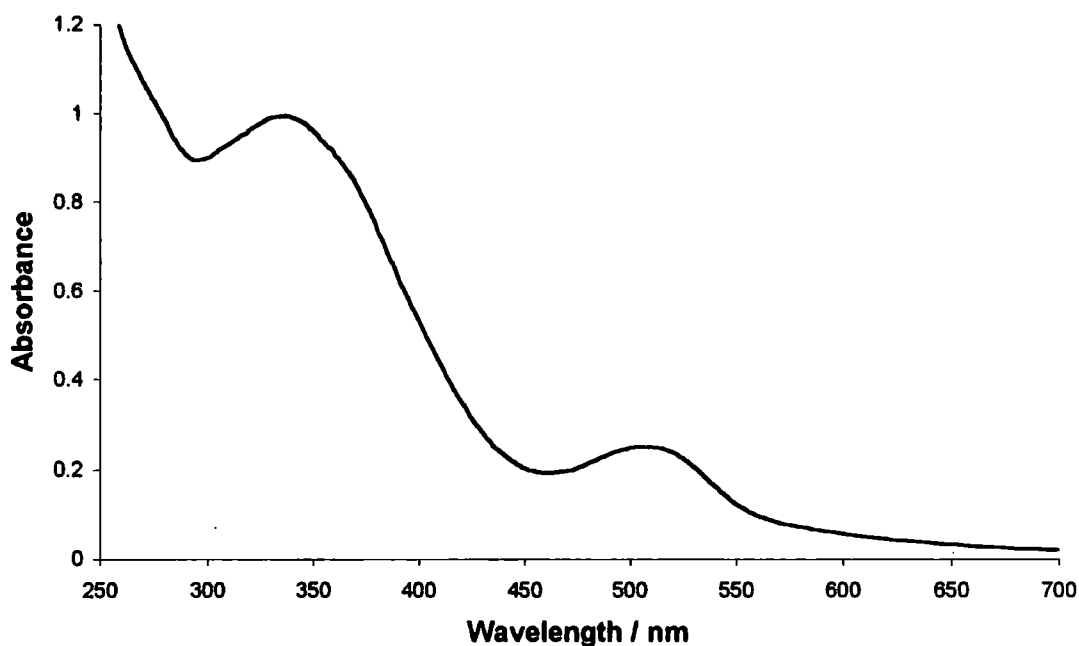
Figure 4.12 The UV / Vis spectrum of $2x10^{-4}$ M S-nitroso-1-amino-2-methyl-2-propane thiol reacted with an equimolar iron complex solution in the presence of 0.15 M phosphate buffer (pH 7.4) and $1x10^{-4}$ M EDTA.

The solution turned from red to orange and absorbance maxima were found at 338 and 507 nm, the same as figure 4.6. This suggests that NO had been transferred to the iron complex.

4.5.3 HPLC Analysis of the Reaction with GSNO

Evidence for iron nitrosyl complex formation was seen in section 4.5.1. The second part of the product analysis was to look at the thiol containing product. It has been found that glutathione (GSH), its disulfide (GSSG) and GSNO can be separated and observed using HPLC techniques.[22] The HPLC machine setup and calibration was performed as described in section 3.4.4.

A 1 : 1 GSNO : iron complex reaction solution with 0.15 M phosphate buffer (pH 7.4) in anaerobic conditions was mixed together. The concentration used was $1x10^{-3}$ M to give sufficient concentrations at the HPLC detector. Samples from the solution were analysed at various times using HPLC. (see table 4.8)

123

It was assumed that all the GSNO had reacted to form GSH or GSSG because no other product was detected. Using the ratio of absorbance the percentage of sulfur centres from GSNO found as GSH and GSSG could be calculated. (see table 4.8)

Time After Mixing / s	% GSH	% GSSG
900	57.4	42.6
1740	47.8	52.2
2640	45.7	54.3
4080	37.3	62.7
4980	35.2	64.8

Table 4.8 Percentage sulfur centres detected as GSH and GSSG at different time intervals for the 1 : 1 reaction of GSNO with an iron complex solution using HPLC techniques.

It was found that over time GSH was converted to GSSG. The reaction could occur faster than expected because of the incomplete complexation of iron by DMPS. The free iron was likely to be present as iron(+3) because of the instability of iron(+2) in neutral conditions. The iron-catalysed oxidation of cysteine between pH 7 and pH 9 has been studied.[23] The rate equation for the reaction when the iron(+3) concentration was greater than 5×10^{-6} M was determined. (see equation 4.3)

$$\text{Rate} = k_2[\text{Fe}^{3+}][\text{RS}^-]$$

Equation 4.3 Rate equation for the iron(+3) catalysed oxidation of cysteine by oxygen.

The percentage yield of GSH calculated for the reaction of GSNO with the iron complex solution must take into account two factors. GSH would be oxidised to GSSG and free iron(+3) present was likely to catalyse the reaction. The other factor was that the product distribution of GSH and GSSG was from two reactions, the reaction of GSNO with the iron complex and GSNO with uncomplexed DMPS. (see scheme 4.5)

$$\text{"Fe"} + 2\text{DMPS} \xrightleftharpoons{\quad K \quad} \{\text{Fe(II)(DMPS)}_2\}^{4-}$$

$$\downarrow + \text{GSNO} \qquad\qquad \downarrow + \text{GSNO}$$

$$\boxed{\text{Overall Reaction Products}}$$
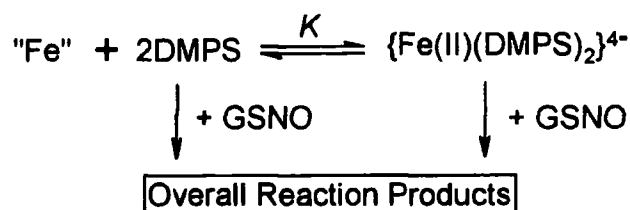
Scheme 4.5 The possible reactions occurring involving GSNO when the *S*-nitrosothiol was reacted with an iron complex solution.

Using the equilibrium constant calculated in section 4.2.1 the concentration of iron complex and free DMPS in the reaction solution could be calculated. Experimental work in chapter 3 has shown that DMPS reacts with *S*-nitrosothiols in a 2 : 1 stoichiometric ratio. The reaction is first order with respect to both DMPS and GSNO, with a second order rate constant similar to the one obtained for the direct reaction of GSNO with the iron complex.

The thiol-containing product of the reaction between GSNO and DMPS has been quantified using HPLC. (see chapter 3) Twenty four percent of sulfur centres were found as GSH. It has been assumed that the iron complex equilibrium is maintained during the reaction with GSNO. No evidence of a change in the equilibrium was found in the product analysis because UV / Vis spectra were compared successfully. The data in table 4.9 show the concentrations of iron complex and free DMPS in the reaction solution. The expected percentage sulfur centres from GSNO converted to GSH when reacted with an iron complex solution was therefore 83.2 %.

Component	Concentration / M	Expected % GSH from the Reaction
$\{\text{Fe(II)(DMPS)}_2\}^{4-}$	7.79×10^{-4}	100
DMPS	4.42×10^{-4}	24

Table 4.9 Concentration of iron complex and free DMPS in the reaction solution with expected percentage of sulfur centres present as GSH product from each reaction.

The amount of GSH generated before it was oxidised by iron(+3) was calculated using equation 4.3. If the iron(+3) concentration was roughly constant, the decomposition of GSH would be first order. This is a valid assumption because oxygen would be present to

regenerate iron(+3) from iron(+2) due to leaks in apparatus and when samples were removed from the solution. The percentage sulfur centres found as GSH measured over time in table 4.8 were fitted to a first order model using the computer package Scientist.[17] (see figure 4.13)
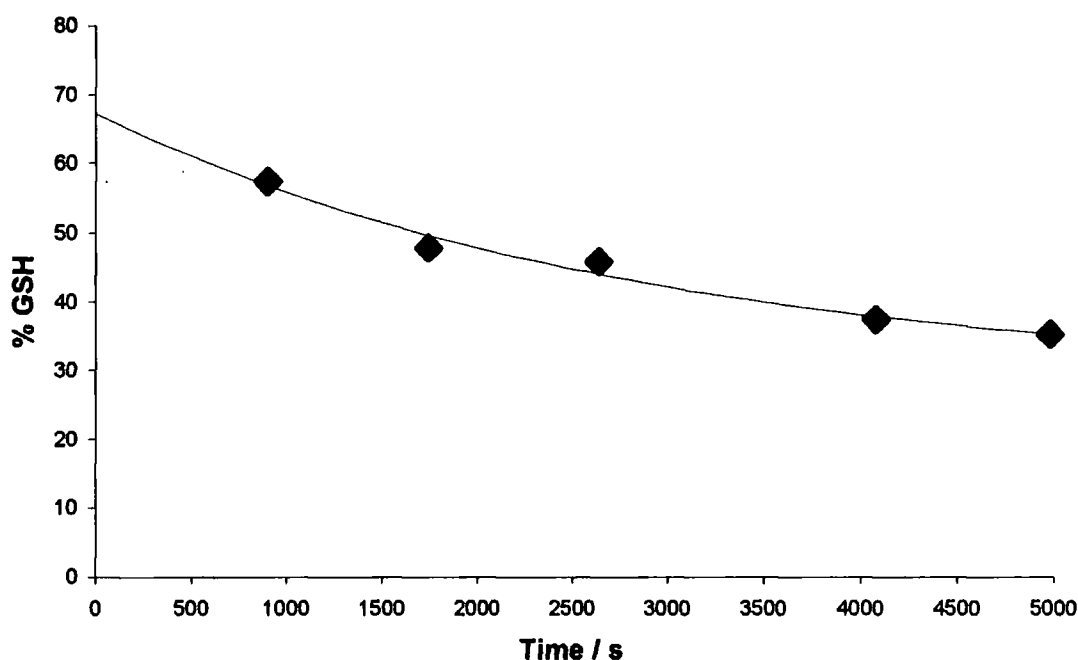
Figure 4.13 Data plotted from table 4.8 (♦) and the first order model fit from Scientist (the solid line).

The percentage sulfur centres found as GSH at time = 0 s was calculated as 67.2 %. That is 81 % of the expected amount of GSH formed from the reaction of GSNO with an iron complex solution using data in table 4.9. The NO^+ transfer was found to be a rapid reaction therefore at high reactant concentrations the reaction was expected to go to completion in a very short period of time.

The disulfide of N-acetylpenicillamine (NAP) was prepared and characterised by the method described in section 6.2.3. However it was found that NAP and its disulfide were not easily detectable using HPLC techniques and had very large retention times.

4.6 Discussion

4.6.1 Kinetic Parameters Determined for Primary S-Nitrosothiols

When primary S-nitrosothiols were reacted in excess with the iron (+2) complex of DMPS a first order decomposition of the complex was observed. Plots of pseudo first order rate constant against S-nitrosothiol concentration were found to be linear. The rate equation shown in equation 4.4 was determined and this suggests that the S-nitrosothiol reacts directly with the iron complex.

$$Rate = k_2[RSNO][Iron \; Complex]$$

Equation 4.4 Rate equation for the reaction of primary S-nitrosothiols with the iron complex.

There are only small differences in the second order rate constants obtained for the primary S-nitrosothiols studied. (see table 4.10) However the simplest S-nitrosothiol studied structurally, S-nitrosocysteine gave the largest rate constant.

S-Nitrosothiol	$k_2 / dm^3 \; mol^{-1} \; s^{-1}$
GSNO	24 ± 1
SNAC	6.1 ± 0.7
SNOCAP	7.5 ± 0.4
S-Nitrosocysteine	71 ± 4
S-Nitrosohomocysteine	16 ± 1

Table 4.10 Second order rate constants determined for primary S-nitrosothiols reacting with the iron complex.

4.6.2 Explanation of the Reaction Profiles Obtained for Tertiary S-Nitrosothiols

The reaction profiles obtained when reacting tertiary S-nitrosothiols with the iron complex did not fit the first order model. However the product analysis suggested that the complex $\{Fe(II)(DMPS)_2NO\}^{4-}$ formed. The nitrosyl iron complex has an absorbance maximum at 507 nm so the disappearance in absorbance at 509 nm was probably due to the decomposition of the complex by oxidation.

The transfer of NO is unlikely to be because of a copper catalysed decomposition of the S-nitrosothiol because no free copper ions would have been present. This is because DMPS and EDTA are metal ion chelators that can form complexes with copper.

A reaction mechanism has not been proposed for this process because no kinetic data were obtained. The transfer of NO from an S-nitrosothiol to an iron complex is discussed further in chapter 5.

4.6.3 The Role of the Sulfonate Group and Ammonia Formation

One mechanistic possibility for the reactions observed was the reaction of the S-nitrosothiol with the sulfonate functional group of DMPS leading to the formation of the nitrosyl iron complex. To analyse this possibility, propane-1-sulfonate was reacted in excess with GSNO at pH 7.4 in the presence of 1.25×10^{-3} M EDTA at 25 °C. The reaction was followed by absorbance at 340 nm. No significant change in absorbance was observed over fourteen hours indicating that there was no reaction between the sulfonate group and GSNO. The reactions observed with the complex were therefore not reactions involving the sulfonate group of the DMPS ligand.

It has been found that when DMPS reacts with S-nitrosothiols ammonia and nitrite are formed. (see chapter 3) When ammonia and nitrite were reacted with the iron complex at pH 7.4 no change in the UV / Vis spectrum of the iron complex was observed. Amounts of ammonia could not be determined in the reaction solutions containing the iron complex because the ammonia test does not work when iron ions are present.

4.6.4 Proposed Chemical Equations and Mechanism

The results of the experiments described in this chapter suggest that the reactions shown in scheme 4.6 can occur.

Primary RSNOs,

$$\{Fe(II)(DMPS)_2\}^{4-} \ + \ RSNO \ \xrightarrow{\ \text{NO}^+ \ \text{transfer}\ } \ \{Fe(III)(DMPS)_2NO\}^{3-} \ + \ RS^-$$

Tertiary RSNOs,

$$\{Fe(II)(DMPS)_2\}^{4-} \ + \ RSNO \ \xrightarrow{\ \text{NO transfer}\ } \ \{Fe(II)(DMPS)_2NO\}^{4-} \ + \ 1/2RSSR$$
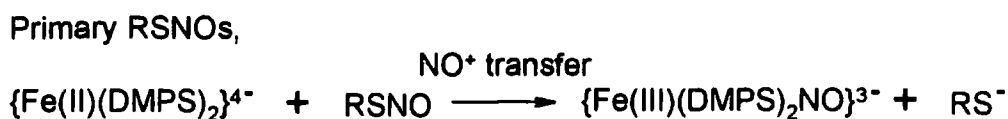
Scheme 4.6 Proposed chemical equations for the reaction of primary and tertiary S-nitrosothiols with the iron complex.

It is known that compounds can undergo oxidative addition reactions with transition metal complexes.[24] If primary S-nitrosothiols initially formed an addition product at the iron centre of the complex then a rearrangement involving the NO ligand could take place. (see scheme 4.7)
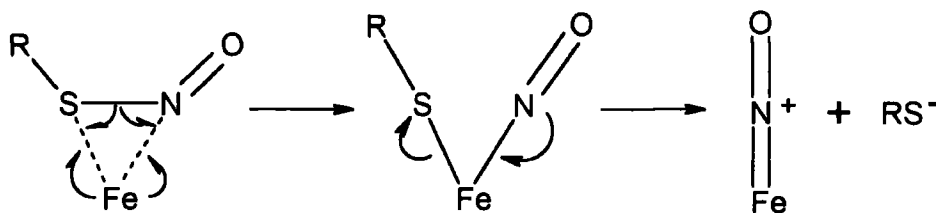
Scheme 4.7 Proposed mechanism for the reaction of primary S-nitrosothiols with the iron complex.

This study has shown that S-nitrosothiols can form nitrosyl iron complexes via a direct reaction with an iron complex. It appears that NO^+ or NO can be the group transferred depending on the nature of the S-nitrosothiol. This could be due to the preferred conformations of primary and tertiary S-nitrosothiols that are shown in figure 4.14.[25] Primary S-nitrosothiols favour a cis conformation that could make bond insertion easier compared to tertiary S-nitrosothiols.
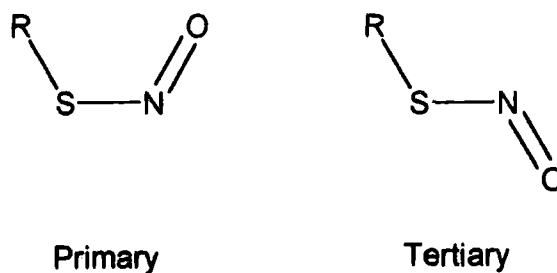
Primary   Tertiary

Figure 4.14 Preferred structural conformation of primary and tertiary S-nitrosothiols.

It has been shown that S-nitrosothiols can form nitrosyl iron complexes by a direct reaction with an iron complex. The NO^+ transfer mechanism has a big advantage over NO transfer because it could not lead to the formation of a highly reactive and damaging thiyl radical.

4.7 References

1) L. J. Ignarro, H. Lippton, J. C. Edwards, W. H. Baricos, A. L. Hyman, P. J. Kadowitz and C. A. Gruetter, *J. Pharmacol. Exp. Ther.*, 1981, **218**, 739.

2) B. T. Mellion, L. J. Ignarro, C. B. Myers, E. H. Ohlstein, B. A. Ballott, A. L. Hyman and P. J. Kadowitz, *Mol. Pharmacol.*, 1983, **23**, 653.

3) D. L. H. Williams, *J. Chem. Soc., Chem. Commun.*, 1996, 1085.

4) D. J. Sexton, A. Muruganandam, D. J. McKenney and B. Mutus, *Photochem. Photobiol.*, 1994, **59**, 463.

5) M. P. Gordge, D. J. Meyer, J. Hothersall, G. H. Neild, N. N. Payne and A. Noronha-Dutra, *Br. J. Pharmacol.*, 1995, **114**, 1083.

6) M. P. Gordge, J. S. Hothersall, G. H. Neild and A. A. Noronha Dutra, *Br. J. Pharmacol.*, 1996, **119**, 533.

7) H. H. Al-Sa'doni, I. L. Megson, S. Bisland, A. R. Butler and F. W. Flitney, *Br. J. Pharmacol.*, 1997, **121**, 1047.

8) J. G. De Man, T. G. Moreels, B. Y. De Winter, A. G. Herman and P. A. Pelckmans, *Eur. J. Pharmacol.*, 1999, **381**, 151.

9) A. P. Dicks and D. L. H. Williams, *Chem. Biol.*, 1996, **3**, 655.

10) W. R. Mathews and S. W. Kerr, *J. Pharmacol. Exp. Ther.*, 1993, **267**, 1529.

11) E. A. Kowaluk and H. Fung, *J. Pharmacol. Exp. Ther.*, 1990, **255**, 1256.

12) G. Bannenberg, J. Xue, L. Engman, I. Cotgreave, P. Moldéus and Å. Ryrfeldt, *J. Pharmacol. Exp. Ther.*, 1995, **3**, 1238.

13) G. M. Rubanyi, A. Johns, D. Wilcox, F. N. Bates and D. Harrison, *Journal of Cardiovascular Pharmacology*, 1991, **17**(Suppl. 3), S41.

14) A. J. Hobbs, *TiPS*, 1997, **18**, 484.

15) P. D. Senter and F. Eckstein, *J. Biol. Chem.*, 1983, **258**, 6741.

16) E. K. Pham and S. Chang, *Nature*, 1994, **369**, 139.

17) Scientist, version 2.02, Micromath Scientific Software, Salt Lake City, UT, USA. www.micromath.com

18) J. A. McCleverty, *Prog. Inorg. Chem.*, 1968, **10**, 176.

19) J. A. McCleverty, N. M. Atherton, J. Locke, E. J. Wharton and C. Winscom, *J. Am. Chem. Soc.*, 1967, **89**, 6082.

20) S. Ekins-Daukes, Final Year Project, St. Andrews University, 1999, 15.

21) S. C. Askew, D. J. Barnett, J. McAninly and D. L. H. Williams, *J. Chem. Soc., Perkin Trans. 2*, 1995, 741.

22) A. J. Holmes and D. L. H. Williams, *J. Chem. Soc., Perkin Trans. 2*, 2000, 1639.

23) L. Ehrenberg, M. Harms-Ringdahl, I. Fedorcsák and F. Granath, *Acta. Chem. Scand.*, 1989, **43**, 177.

24) R. Henderson, 'The Mechanism of Reactions at Transition Metal Sites', Oxford University Press, Oxford, 1993.

25) M. D. Bartberger, K. N. Houk, S. C. Powell, J. D. Mannion, K. Y. Lo, J. S. Stamler and E. J. Toone, *J. Am. Chem. Soc.*, 2000, **122**, 5889.

Chapter 5

Reactions of an *S*-Nitrosothiol with Iron

Dithiocarbamate Complexes

Chapter 5: Reactions of an *S*-Nitrosothiol with Iron Dithiocarbamate Complexes

5.1 Introduction

The chemistry of dithiocarbamate complexes studied up to 1977 has been reviewed thoroughly.[1,2] The structure of the dithiocarbamate functional group is shown in figure 5.1.

Figure 5.1 Structure and resonance forms of the dithiocarbamate functional group.

It has been found that the solid state structure of the iron(+2) diethyldithiocarbamate (DETC) complex {Fe(II)(DETC)$_2$}, contains a five co-ordinate square pyramidal arrangement of sulfur atoms around the metal centre.[3] The complex was believed to form dimers in a similar way to {Cu(II)(DETC)$_2$}. The crystal structure of the nitrosyl iron(+2) DETC complex has been determined and is shown in figure 5.2.[4]
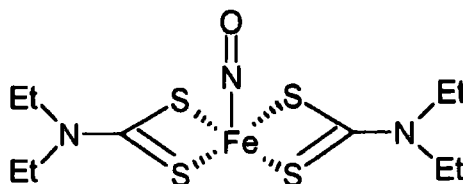
Figure 5.2 Structure of the nitrosyl iron(+2) DETC complex.

The iron(+2) complexes containing the ligands DETC and *N*-methyl-D-glucamine dithiocarbamate (MGD) have been used to detect NO in biological systems.[5] NO reacts with the complexes to form iron nitrosyl complexes, which can then be detected using ESR spectroscopy.

Iron(+2) dithiocarbamate complexes are now considered a test for the detection of NO. Many studies published in the literature have used the complexes to determine that NO is present in biological systems.[6-13]

It has been found that *S*-nitrosothiols can react with an iron(+2) dithiol complex to form iron nitrosyl complexes. (see chapter 4) If this occurs with iron(+2) dithiocarbamate complexes the test for NO in aqueous solution could be compromised because the test might be unable to discriminate between the reactions of NO and *S*-nitrosothiols. This chapter looks into the possibility that *S*-nitrosoglutathione (GSNO) reacts with iron MGD complexes.

5.2 Preparation of the Iron MGD Complexes

The low solubility of the iron(+2) DETC complex in aqueous solution has meant that other iron(+2) dithiocarbamate complexes have been developed for use in experimental work. The iron(+2) MGD complex is one that has been used to overcome the solubility problem. (see figure 5.3) MGD was prepared and characterised as described in section 6.2.3.
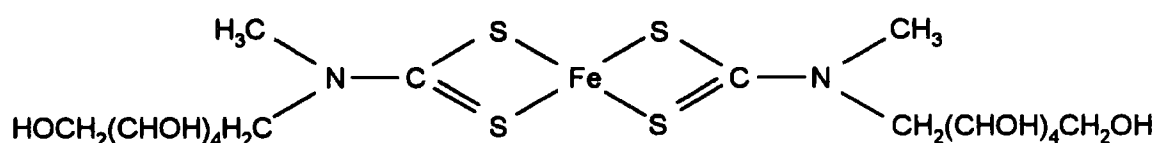
Figure 5.3 Proposed structure of the iron(+2) MGD complex.

5.2.1 UV / Vis Spectroscopic Parameters of MGD

The dithiocarbamate ligand was found to have a characteristic absorbance maximum at 354 nm in the UV / Vis region. MGD was dissolved in water then diluted and UV / Vis spectra were taken of the resulting solutions. The absorbance values measured at 354 nm are shown in table 5.1.

[MGD] / M	Absorbance (354 nm)
0.005	0.23
0.010	0.49
0.015	0.77
0.020	1.00
0.025	1.26

Table 5.1 Concentration of MGD and absorbance values measured at 354 nm.

Using the Beer-Lambert law the extinction co-efficient $\varepsilon_{354nm} = 51.4 \pm 0.8$ dm^3 mol^{-1} cm^{-1} was calculated by the method described in section 2.2.1.

5.2.2 Preparation of the Iron(+3) MGD Complex and its Nitrosyl Complex

The amount of dithiocarbamate required to complex fully the iron(+3) was calculated by varying the concentration of MGD in the presence of 1×10^{-4} M FeCl$_3$ and measuring the absorbance at 340 nm. (see table 5.2) The graph of absorbance at 340 nm plotted against [MGD] / [Fe^{3+}] is shown in figure 5.4.

[MGD] / M	Absorbance (340 nm)
1×10^{-4}	0.24
2×10^{-4}	0.71
3×10^{-4}	0.90
4×10^{-4}	0.89
5×10^{-4}	0.85
6×10^{-4}	0.84

Table 5.2 Absorbance at 340 nm measured for solutions containing 1×10^{-4} M FeCl$_3$ with varying concentrations of MGD.
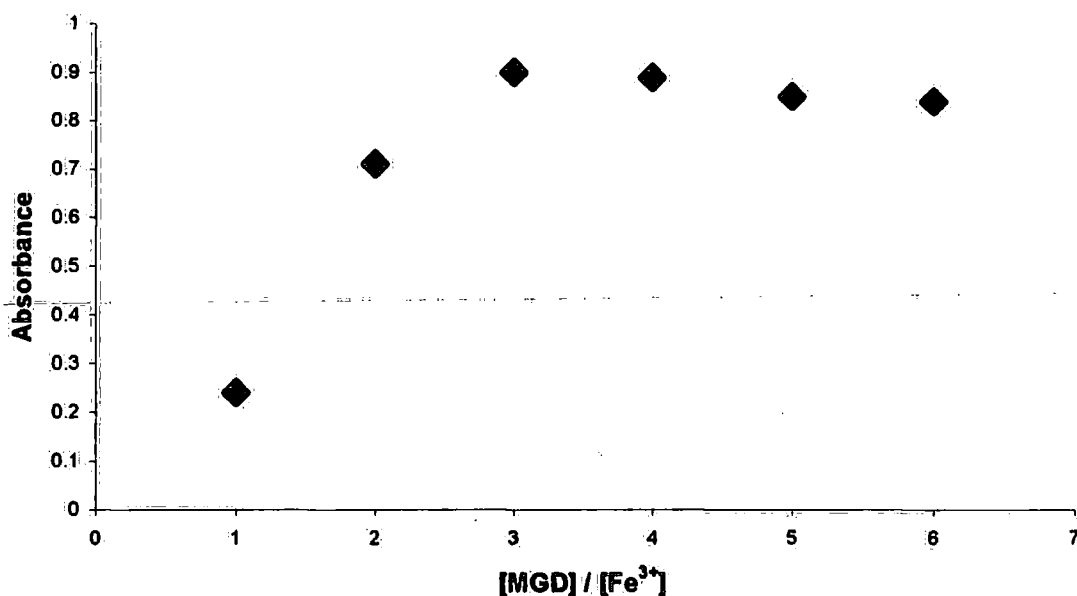
Figure 5.4 Absorbance at 340 nm plotted against [MGD] / [Fe^{3+}] from values in table 5.2.

At the lower MGD concentrations an absorbance maximum at 440 nm was observed which disappeared when there was full complexation of the iron(+3). This suggested that there were intermediate complexes between free iron(+3) and the fully complexed product. Full complexation occurred when MGD was in a three fold excess to $FeCl_3$. This is not surprising because the iron complex is believed to be $\{Fe(III)(MGD)_3\}$[1] and the equilibrium constant is expected to be large.

The solutions were made up and used immediately because the brown coloured complex was found to decompose slowly. As MGD concentration was increased the rate of iron complex decomposition increased also.

One reason the complex decomposed could be because of the formation of the iron(+3) hydroxide complex. Iron is known to rust forming the hydrated complex $\{Fe(III)(OH)_3\}$ or $\{Fe(O)(OH)\}$.[16] The pK_a of MGD has been measured as 9.56[17] so it would make the solution alkaline because of the protonation of the dithiocarbamate group.

A solution containing 1×10^{-4} M $FeCl_3$ and 3×10^{-4} M MGD was made up and a UV / Vis spectrum of the resulting solution is shown in figure 5.5. Absorbance maxima were found at 340 nm and 520 nm with a shoulder at 385 nm. The absorbance values were recorded for one solution only due to the instability of the complex, and are shown in table 5.3.
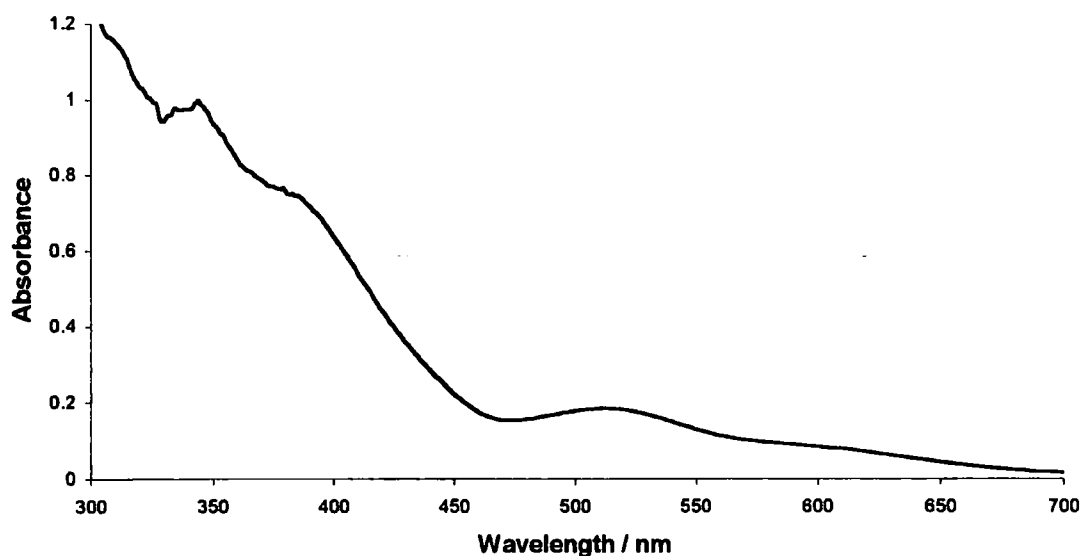
Figure 5.5 UV / Vis spectrum of a solution containing 1×10^{-4} M $FeCl_3$ and 3×10^{-4} M MGD.

Wavelength / nm	Absorbance	Extinction Co-efficient
340	0.98	$\varepsilon_{340nm} = 9\,800$ dm^3 mol^{-1} cm^{-1}
385	0.75	$\varepsilon_{383nm} = 7\,500$ dm^3 mol^{-1} cm^{-1}
520	0.18	$\varepsilon_{511nm} = 1\,800$ dm^3 mol^{-1} cm^{-1}

Table 5.3 Approximate extinction co-efficients for {Fe(III)(MGD)$_3$}.

The absorbance value at 340 nm correlates fairly well with the one obtained in table 5.2 but the extinction co-efficients are significantly different to the ones in the literature.[18] They are $\varepsilon_{340nm} = 20\,000$ M^{-1}, $\varepsilon_{385nm} = 15\,000$ M^{-1} and $\varepsilon_{520nm} = 3\,000$ M^{-1}. Measurements in the study were taken in anaerobic conditions suggesting that significant decomposition of the iron complex may have occurred in the presence of oxygen. However the units stated are not correct so it is unclear what the values represent.

The chemistry of the iron complexes with GSNO was to be studied at pH 7.4 because biological experiments are performed at physiological pH. Therefore the effect of buffer on {Fe(III)(MGD)$_3$} was analysed.

Iron(+3) dithiocarbamate solutions were made up containing 1×10^{-4} M FeCl$_3$, 5×10^{-4} M MGD and either 0.15 M phosphate buffer (pH 7.4) or 0.025 M TRIS buffer (pH 7.4). The amount of complexation in solution was determined by the presence of absorbance maxima in UV / Vis spectra. Phosphate buffer (pH 7.4) was found to decompose the iron complex but TRIS buffer did not. This could be due to the formation of iron(+3) phosphate complexes.

It has been found that NO reacts with the iron(+3) MGD complex in the presence of 0.1 M TRIS buffer (pH 7.4) to give a iron nitrosyl complex in 95 % yield.[17] The reaction shown in scheme 5.2 has been proposed.[19] One sulfur atom bonded to iron(+3) in the octahedral complex is believed to become detached and replaced by NO.

{Fe(III)(MGD)$_3$} + NO ⟶ {Fe(III)(MGD)$_3$(NO)}
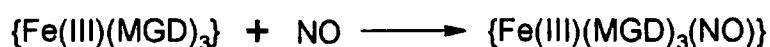
Scheme 5.1 Proposed chemical equation for the reaction of {Fe(III)(MGD)$_3$} with NO.

A solution containing 4×10^{-4} M $FeCl_3$ and 2×10^{-3} M MGD was made up and NO was bubbled through the reaction solution under anaerobic conditions for fifteen minutes. This was to ensure the NO did not oxidise prior to any reaction with the iron complex. The colour of the solution changed from brown to yellow. NO was generated by adding solid sodium nitrite to a 0.1 M solution of ascorbic acid, the NO was then bubbled through the solution of the iron complex on a stream of nitrogen.

When NO had been reacted with $\{Fe(III)(MGD)_3\}$, the solution was diluted down four fold and a UV / Vis spectrum was taken of the solution. This was compared to a UV / Vis spectrum of the solution at the same concentration before the addition of NO. (see figure 5.6)
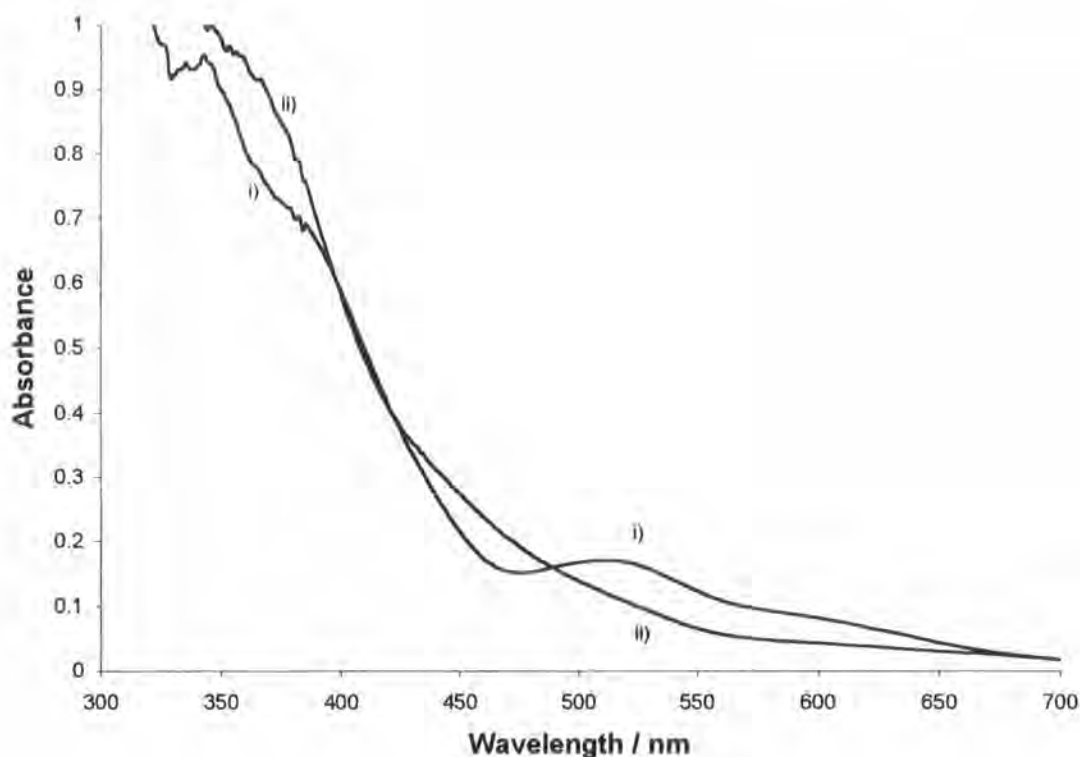
Figure 5.6 UV / Vis spectra of a $\{Fe(III)(MGD)_3\}$ solution i) before and ii) after the addition of NO.

The iron nitrosyl complex had no distinct absorbance maxima but there was a colour change and the UV / Vis spectrum of the solution changed also when NO was added to the $\{Fe(III)(MGD)_3\}$ solution.

138

5.2.3 Preparation of the Iron(+2) MGD Complex and its Nitrosyl Complex

The iron(+2) dithiocarbamate complexes are very oxygen sensitive so had to be prepared under anaerobic conditions. The iron(+2) MGD complex was prepared as described in the literature.[5] The MGD was reacted with $FeSO_4$ in a 5 : 1 stoichiometric ratio under anaerobic conditions. MGD was dissolved in buffer and the resulting deoxygenated solution was poured over solid $FeSO_4$ under a nitrogen atmosphere.

It was found that when 0.15 M phosphate buffer (pH 7.4) was present in a solution containing 4×10^{-4} M $FeSO_4$ and 2×10^{-3} M MGD a white turbid solution formed, which could have been due to iron phosphate interactions. Reducing the buffer concentration to 0.024 M stopped this reaction and a brown coloured complex formed.

A solution containing 4×10^{-4} M $FeSO_4$, 2×10^{-3} M MGD and 0.024 M phosphate buffer (pH 7.4) was reacted with NO as described in section 5.2.2. It has been found that this method can be used to prepare nitrosyl iron(+2) dithiocarbamate complexes.[20] The solution was diluted four fold and a UV / Vis spectrum was taken of the resulting green solution. This was compared to a spectrum of the solution at the same concentration before NO was added. (see figure 5.7)
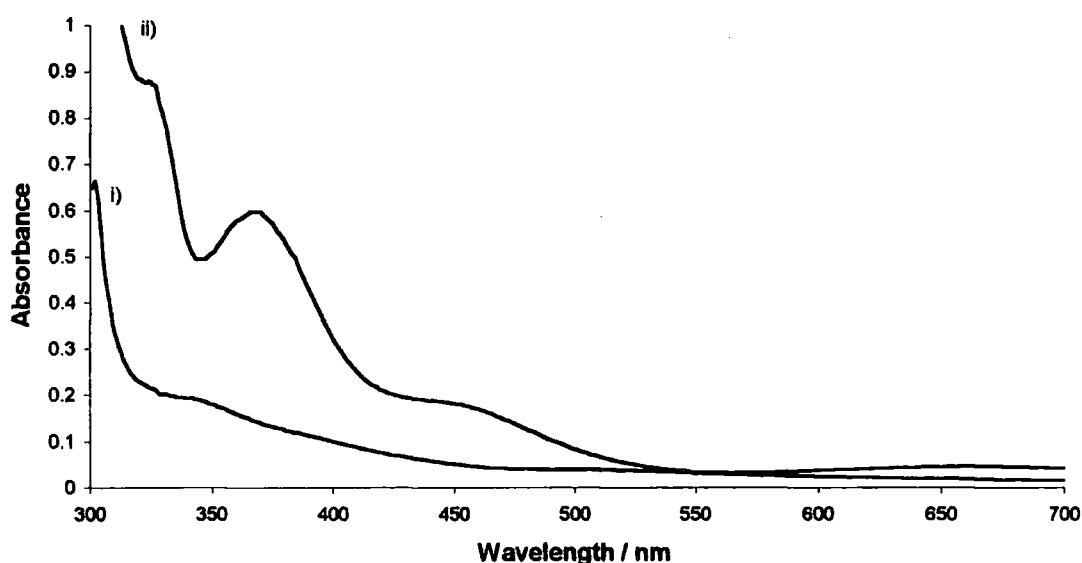
Figure 5.7 UV / Vis spectra of a 1×10^{-4} M {Fe(II)(MGD)$_2$} solution in the presence of 0.024 M phosphate buffer (pH 7.4) i) before and ii) after the addition of NO.

The nitrosyl iron(+2) MGD complex was found to have absorbance maxima at 368 nm and 660 nm with shoulders at 314 nm and 450nm. The absorbance was measured at these points in the spectrum and the extinction co-efficients calculated are shown in table 5.4.

Wavelength / nm	Absorbance	Extinction Co-efficient
314	0.98	$\varepsilon_{314nm} = 9\ 800\ dm^3\ mol^{-1}\ cm^{-1}$
368	0.60	$\varepsilon_{368nm} = 6\ 000\ dm^3\ mol^{-1}\ cm^{-1}$
450	0.18	$\varepsilon_{450nm} = 1\ 800\ dm^3\ mol^{-1}\ cm^{-1}$
660	0.05	$\varepsilon_{660nm} = 500\ dm^3\ mol^{-1}\ cm^{-1}$

Table 5.4 Calculation of extinction co-efficients for {Fe(II)(MGD)$_2$(NO)}.

Extinction co-efficients for {Fe(II)(MGD)$_2$(NO)} have been published and were found to be $\varepsilon_{314nm} = 18\ 000\ M^{-1}$, $\varepsilon_{368nm} = 12\ 500\ M^{-1}$ and $\varepsilon_{450nm} = 5\ 600\ M^{-1}$.[18] Again the values are very different to the ones found in this study.

When solid ascorbic acid was added to a nitrosyl iron(+3) MGD solution, a UV / Vis spectrum was obtained very similar to the one for the iron nitrosyl complex shown in figure 5.7. The iron MGD complexes are believed to react with NO via the pathways shown in scheme 5.2.

$$\{Fe(II)(MGD)_2\}\ +\ NO \longrightarrow \{Fe(II)(MGD)_2(NO)\}$$

$$\uparrow\ \text{Ascorbic Acid} - MGD$$

$$\{Fe(III)(MGD)_3\}\ +\ NO \longrightarrow \{Fe(III)(MGD)_3(NO)\}$$
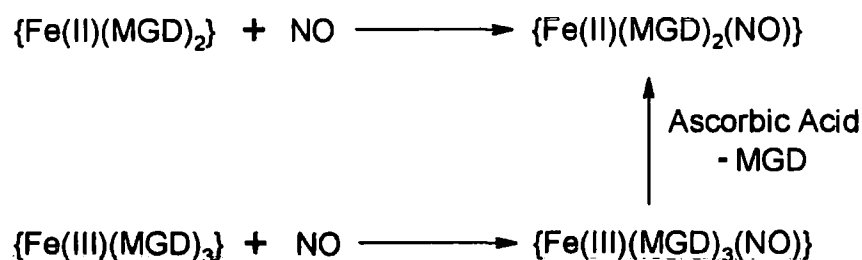
Scheme 5.2 Proposed reactions of NO with the iron MGD complexes.

5.3 The Reaction of GSNO with the Iron(+2) MGD Complex

The UV / Vis spectra of the iron MGD complexes and the iron nitrosyl complexes were obtained to establish which wavelengths could be used to study any reaction between the complexes and GSNO.

GSNO was generated *in situ* for these experiments from the reaction of glutathione (GSH) with an equimolar quantity of sodium nitrite in the presence of 0.02 M perchloric acid. GSNO was generated at a high concentration then diluted down to ensure effective buffering in the presence of 0.024 M phosphate buffer (pH 7.4).

5.3.1 UV / Vis Analysis of the GSNO Reaction with the Iron(+2) Complex

Two anaerobic solutions were prepared in 0.024 M phosphate buffer, one containing 4×10^{-4} M $FeSO_4$ and 2×10^{-3} M MGD, and the other 4×10^{-4} M GSNO. Equal volumes of these solutions were mixed under a nitrogen atmosphere and a UV / Vis spectrum obtained after fifteen minutes. (see figure 5.8)
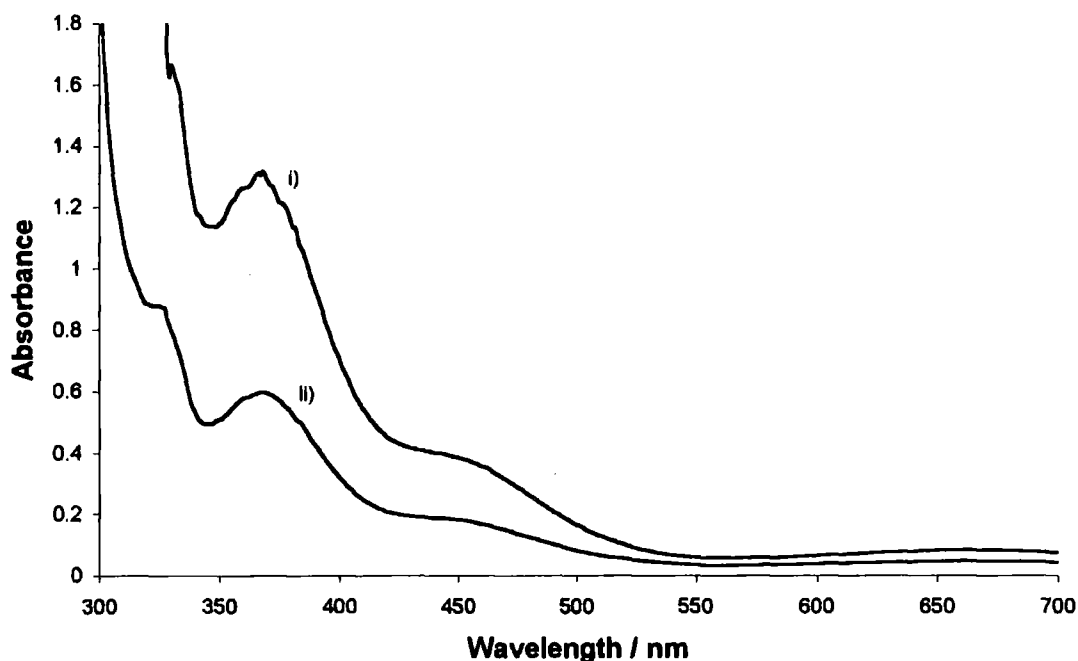
Figure 5.8 UV / Vis spectrum of i) a 2×10^{-4} M 1 : 1 GSNO : $\{Fe(II)(MGD)_2\}$ reaction solution and ii) 1×10^{-4} M $\{Fe(II)(MGD)_2NO\}$ shown in figure 5.7.

The UV / Vis spectra shown in figure 5.8 are very similar suggesting that GSNO does react with the iron(+2) complex to form a iron nitrosyl complex. Anaerobic conditions were maintained during the experiment because the iron nitrosyl complex was found to decompose in the presence of oxygen. Kinetic data could not be obtained because of the instability of the $\{Fe(II)(MGD)_2\}$ complex in the stopped flow spectrophotometer.

5.3.2 HPLC Analysis of the GSNO Reaction with the Iron(+2) MGD Complex

Evidence that GSNO transferred NO to the iron(+2) complex was obtained in the previous section. This section reports work carried out to identify the sulfur-containing product of the reaction. HPLC can be used to analyse solutions containing GSNO, GSH and glutathione disulfide (GSSG).[21] The method used was the same as that described in section 3.4.4.

The reaction was carried out in anaerobic conditions because of the instability of {Fe(II)(MGD)$_2$} and the iron nitrosyl complex product. A reaction solution containing 1×10^{-3} M GSNO, 1×10^{-3} M {Fe(II)(MGD)$_2$} and 0.024 M phosphate buffer (pH 7.4) was prepared. The higher concentration of reactants was used in order to obtain adequate response in HPLC analyses.

A sample from the reaction solution was analysed five minutes after mixing took place. No GSNO was detected in the solution showing that the reaction had gone to completion. A large peak corresponding to GSSG and a very small peak due to GSH were observed. There was a much broader peak that eluted at eleven minutes which could have been the iron nitrosyl complex.

When a sample solution containing 1×10^{-3} M MGD was analysed, no absorbing species were eluted. This could be because MGD does not absorb significantly at 200 nm, or the compound did not come off the column.

The HPLC data showed that in the reaction GSNO decomposed to its disulfide. A small quantity of GSH was present probably due to the reversibility of nitrosation of the thiol.[22]

5.4 Nitrosation of MGD and DETC

The reaction of nitrous acid with the dithiocarbamate functional group is known and is shown in scheme 5.3.[23] The nitrosation of the dithiocarbamate functional group was studied because the S-nitroso compound was a likely intermediate if MGD reacted with GSNO (the study of the reaction is in section 5.5).

Scheme 5.3 Chemical equation for the reaction of nitrous acid with the dithiocarbamate functional group.

5.4.1 Product Analysis Using Diethyldithiocarbamate

When diethyldithiocarbamate was reacted with nitrous acid the solution went turbid suggesting that the product of the reaction was less soluble than the reactants. A 20 ml solution containing 0.2 M diethyldithiocarbamate, 0.2 M sodium nitrite and 0.1 M perchloric acid was made up. Initially no reaction was observed, which was attributed to protonation of the dithiocarbamate functional group neutralising the acidity of the solution. 0.4 M perchloric acid was added drop wise until the solution went turbid.

Solid was removed from the turbid solution after it was allowed to settle for two days. The product was analysed and evidence was found that the solid obtained was tetraethylthiuram disulfide. The structure of the product is shown in figure 5.9.
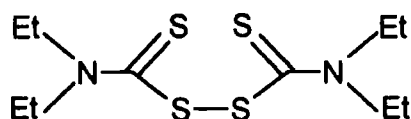
Figure 5.9 Structure of tetraethylthiuram disulfide.

Melting Point – solid obtained melted over the range 62 – 65 °C and the literature value is 70 °C.[24] The slightly lower than expected melting point could have been due to impurities because the solid was not purified.

Mass spectroscopy – positive electrospray ionisation was used to look at 1) sodium diethyldithiocarbamate and 2) the solid obtained from the reaction.

1) $(M+Na)^+$, $C_5H_{10}S_2NNa_2$, require m/z = 194, found m/z = 194. 2) $(M+Na)^+$, $C_{10}H_{20}S_4N_2Na$, require m/z = 319, found m/z = 319.

Elemental analysis for $C_{10}H_{20}S_4N_2$, expected C: 40.51, H: 6.80, N: 9.45, found C: 40.28, H: 6.77, N: 9.34.

There is a study in the literature that describes the decomposition of diethyldithiocarbamate in acidic conditions.[25] The reaction was followed by the formation of carbon disulfide via the reaction shown in scheme 5.4.

Scheme 5.4 Proposed chemical reaction for the decomposition of DETC in acidic conditions.

A UV / Vis spectrum was taken of a solution containing 2×10^{-2} M DETC and 0.2 M perchloric acid. An absorbance maximum at 349 nm was observed corresponding to the dithiocarbamate functional group. The solution was analysed using UV / Vis spectroscopy and three days later it was found that the position of the absorbance maximum was the same and the absorbance was 98 % of the original value. Any decomposition reaction appears to be very slow under the experimental conditions used in this series of experiments.

Only ten percent of the expected mass of the tetraethylthiuram disulfide was found as solid in the solution. This is probably because much of the product remained in solution.

5.4.2 Measurement of NO Produced During Reactions

When solid MGD was added to a solution containing 1.25×10^{-2} M $NaNO_2$ and 0.1 M perchloric acid a short lived yellow coloured species was observed and a gas was given off. An NO electrode was put in the solution and was quickly saturated by the high levels of NO present. NO concentrations were measured to try and show quantitative NO production using an NO electrode.

The NO electrode was calibrated as described in section 3.4.4. A solution containing 1×10^{-2} M MGD and 0.1 M perchloric acid was made up. Sodium nitrite was added to the solution

so that the final concentration of nitrous acid was 1×10^{-6} M. A quantitative amount of NO was expected but only 25 % of the expected amount was detected. The experiment was repeated with DETC but an even lower yield of NO was found.

There are several possible explanations for the fact that NO was not found quantitatively. The nitrosation reaction could have been too slow at the low nitrous acid concentrations leading to insignificant levels of NO building up in solution. Another explanation could be that the MGD complexed the trace iron ions in solution and were able to trap out the NO. There is also the possibility that S-nitrosated dithiocarbamates do not decompose to form NO with a large excess of dithiocarbamate present.

5.4.3 Product Analysis Using Ellmans Reagent

Concentrations of thiol in aqueous solution can be measured using the Ellmans test.[26] The reaction scheme for the test is shown in scheme 5.5.
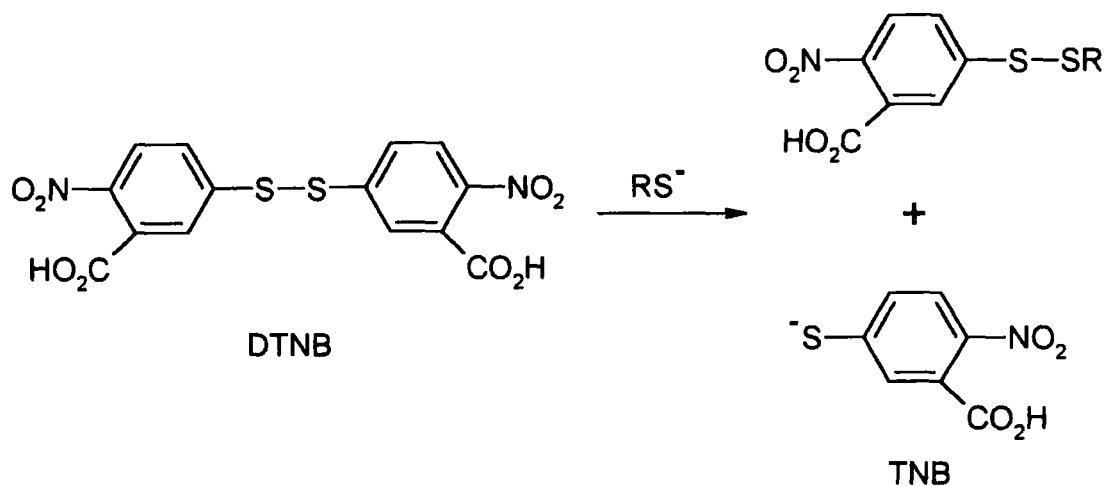
Scheme 5.5 The reaction scheme for the Ellmans test.

Reaction solutions containing 5×10^{-4} M 5,5'-dithiobis(2-nitrobenzoic acid) (DTNB) and varying amounts of GSH were made up in the presence of 0.15 M phosphate buffer (pH 7.4). Fifteen minutes after mixing at room temperature UV / Vis spectra of the solutions were taken and the absorbance at 412 nm was measured. (see table 5.5) The absorbance was due to the thiolate anion of 2-nitro-5-thiobenzoic acid (TNB).

145

[GSH] / M	[DTNB] / M	Absorbance (412 nm)
1×10^{-5}	5×10^{-4}	0.15
2×10^{-5}	5×10^{-4}	0.32
3×10^{-5}	5×10^{-4}	0.44
4×10^{-5}	5×10^{-4}	0.57
5×10^{-5}	5×10^{-4}	0.70

Table 5.5 Concentration of DTNB and GSH in the presence of 0.15 M phosphate buffer (pH 7.4) with the absorbance measured at 412 nm fifteen minutes after mixing.

The extinction co-efficient calculated was $\varepsilon_{412nm} = 13\ 500 \pm 470\ dm^3\ mol^{-1}\ cm^{-1}$. This is close to the literature value, which is $\varepsilon_{412nm} = 13\ 600\ dm^3\ mol^{-1}\ cm^{-1}$.

GSH was replaced by MGD in the Ellmans test and reaction solutions were made up as shown in table 5.6. The absorbance at 412 nm was recorded after keeping the solutions at 25 °C for two hours because of the slower reaction.

[MGD] / M	[DTNB] / M	Absorbance (412 nm)
1×10^{-5}	5×10^{-4}	0.09
2×10^{-5}	5×10^{-4}	0.16
3×10^{-5}	5×10^{-4}	0.24
4×10^{-5}	5×10^{-4}	0.31
5×10^{-5}	5×10^{-4}	0.38

Table 5.6 Concentration of MGD and DTNB in the presence of 0.15 M phosphate buffer (pH 7.4) with absorbance obtained at 412 nm two hours after mixing.

A plot of absorbance against MGD concentration using data in table 5.6 gave a straight line with a near zero intercept. The value for the extinction co-efficient was calculated as ε_{412nm} $= 7\ 300 \pm 100\ dm^3\ mol^{-1}\ cm^{-1}$. This suggested that the reaction had not gone to completion. When absorbance at 412 nm was measured over two hours for the reaction solutions the absorbance was still increasing.

A solution containing 5×10^{-3} M MGD, an equal amount of sodium nitrite and 0.02 M perchloric acid was made up. The solution was then tested for MGD using the Ellmans test and after two hours there was no increase in absorbance at 412 nm. Using the data obtained in this study the reactions that are believed to occur are shown in scheme 5.6.
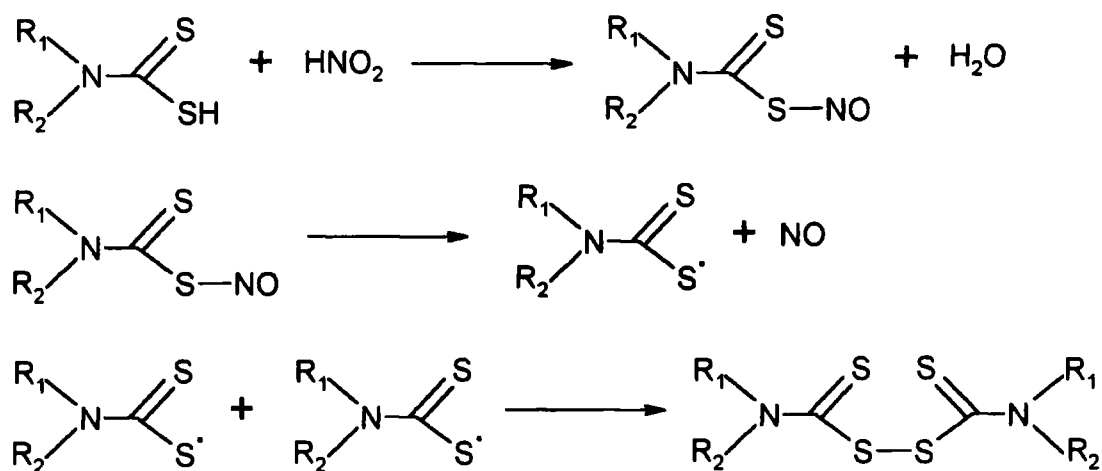
Scheme 5.6 Proposed reaction scheme for the nitrosation of a dithiocarbamate.

The reaction kinetics could not be determined because of the similarity in absorbance maxima and extinction co-efficients of the reactants.

5.5 The Reaction of MGD with GSNO

The reaction of MGD with GSNO was studied to see if it could lead to the formation of an iron nitrosyl complex. MGD was used rather than DETC because when DETC was reacted with GSNO the solution went turbid, preventing study of the reaction kinetics using UV / Vis techniques.

The reaction of GSNO with DETC has been studied and the products were found to be nitrite, nitrate, disulfuram (tetraethylthiuram disulfide), GSSG, and the DETC GSH mixed disulfide.[27]

5.5.1 Kinetic Data for the Reaction of MGD with GSNO

GSNO was reacted with MGD in excess at different concentrations in the presence of 0.15 M phosphate buffer (pH 7.4). The decrease in absorbance at 545 nm was followed over time and first order rate constants were obtained from the reaction profiles. (see table 5.7)

[MGD] / M	[GSNO] / M	k_{obs} / s^{-1}
0.020	2×10^{-3}	0.00107
0.024	2×10^{-3}	0.00126
0.028	2×10^{-3}	0.00147
0.032	2×10^{-3}	0.00166
0.036	2×10^{-3}	0.00174
0.040	2×10^{-3}	0.00195

Table 5.7 Concentration of MGD and GSNO in the presence of 0.15 M phosphate buffer (pH 7.4) with first order rate constants obtained at 25°C.

A plot of observed rate constant against MGD concentration was linear with a near zero intercept and is shown in figure 5.10. The gradient of the graph gave the second rate constant $k_2 = 0.043 \pm 0.002$ dm^3 mol^{-1} s^{-1} and the rate equation is shown in equation 5.1.

Rate = k_2[MGD][GSNO]

Equation 5.1 Rate equation for the reaction between GSNO and MGD.
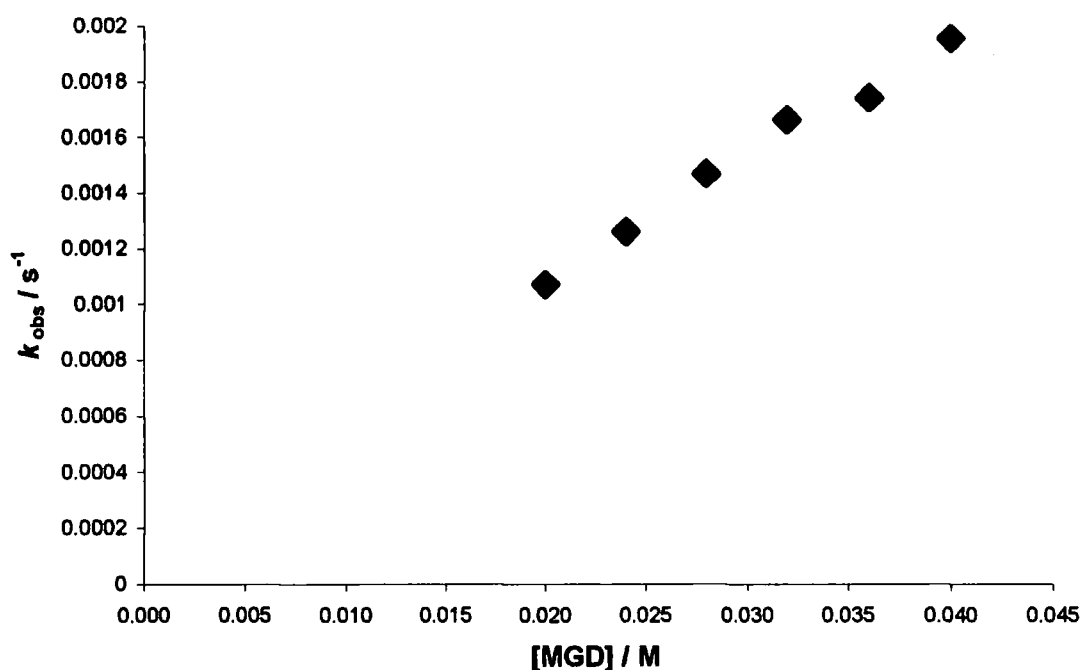
Figure 5.10 First order rate constants plotted against MGD concentration from table 5.7.

The experiment was repeated in the presence of EDTA and first order rate constants were again obtained from the reaction profiles. (see table 5.8)

[MGD] / M	[GSNO] / M	k_{obs} / s^{-1}
0.020	2×10^{-3}	0.00149
0.024	2×10^{-3}	0.00173
0.028	2×10^{-3}	0.00201
0.032	2×10^{-3}	0.00215
0.036	2×10^{-3}	0.00236
0.040	2×10^{-3}	0.00273

Table 5.8 Concentration of MGD and GSNO in the presence of 0.15 M phosphate buffer (pH 7.4) and 1×10^{-4} M EDTA with first order rate constants obtained at 25 °C.

The second order rate constant obtained in the presence of the metal ion chelator EDTA was $k_2 = 0.059 \pm 0.003$ dm^3 mol^{-1} s^{-1}. This value is similar to the one obtained from data in

149

table 5.7 but suggested that the presence of EDTA slightly increased the rate of reaction between MGD and GSNO.

5.5.2 UV / Vis Spectral Properties of Copper MGD Complexes

Copper(+2) ions can catalyse the decomposition of S-nitrosothiols at pH 7.4 leading to the formation of NO and disulfide.[28] The presence of the reducing agent ascorbic acid at low concentration can decompose GSNO at concentrations where it is normally considered stable.[21] Release by ascorbic acid of copper(+2) ions bound to GSSG, and reduction to copper(+1), enables the decomposition of GSNO to occur. MGD was reacted with copper ions to study the interactions between the two species.

Copper ions were reacted with MGD at different concentrations and UV / Vis spectra were taken of the resulting solutions. (see table 5.9) The UV / Vis spectra of the solutions are shown in figure 5.11.

Solution No.	[MGD] / M	[Cu^{2+}] / M
1	0.5×10^{-4}	1×10^{-4}
2	1.0×10^{-4}	1×10^{-4}
3	1.5×10^{-4}	1×10^{-4}
4	2.0×10^{-4}	1×10^{-4}
5	2.5×10^{-4}	1×10^{-4}
6	3.0×10^{-4}	1×10^{-4}
7	3.5×10^{-4}	1×10^{-4}
8	4.0×10^{-4}	1×10^{-4}

Table 5.9 Concentrations of MGD and CuSO$_4$ in solutions made up for UV / Vis spectroscopic analysis.
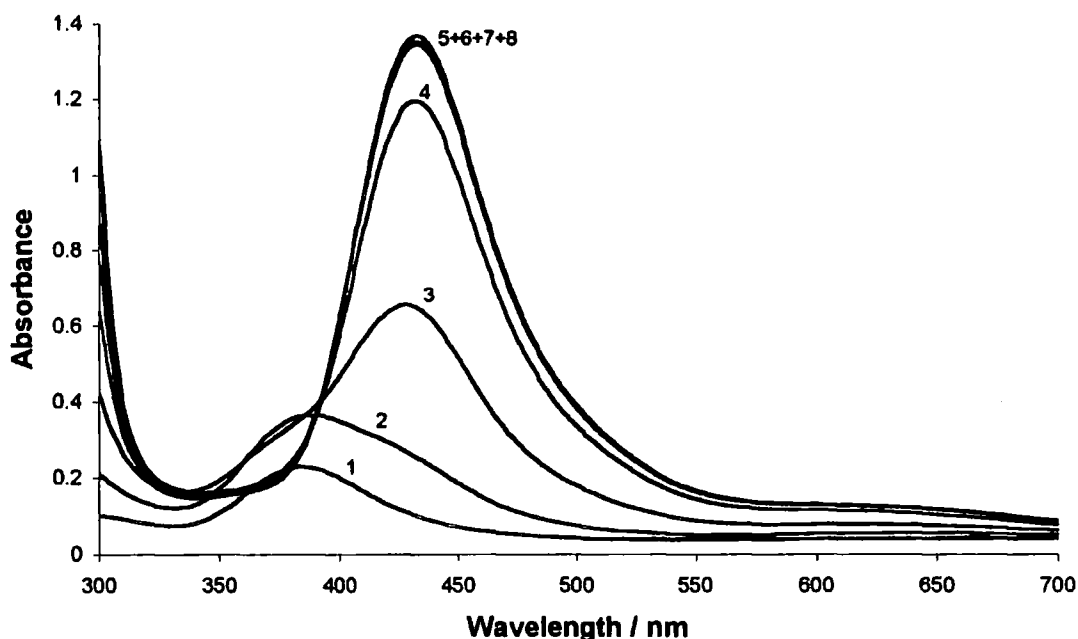
Figure 5.11 UV / Vis spectra of the solutions described in table 5.9.

The UV / Vis spectra show that a complex forms with an absorbance at 433 nm via an intermediate which absorbs at 384 nm. Average absorbance at 433 nm for solutions 5, 6, 7 and 8 is 1.353 which corresponds to the extinction co-efficient ε_{433nm} = 13 530 dm^3 mol^{-1} cm^{-1}. The UV / Vis spectra were unchanged by the presence of 0.15 M phosphate buffer (pH 7.4).

The possibility that MGD could reduce copper ions was investigated using the specific copper(+1) chelator neocuproine. The $\{Cu(I)(Neocuproine)_2\}^+$ complex has an absorbance maximum at 454 nm with an extinction co-efficient 7 950 dm^3 mol^{-1} cm^{-1}.[29] A solution was made up containing 2×10^{-3} M MGD, 1×10^{-3} M neocuproine and 2×10^{-4} M CuSO$_4$. The expected UV / Vis spectrum of the copper MGD complex was obtained. No copper(+1) appears to be generated from the reaction of MGD with copper(+2) ions. The proposed chemical reactions for copper complexation are shown in scheme 5.7.

$$Cu^{2+} + MGD \rightleftharpoons \{Cu(II)(MGD)\}^+ + MGD \rightleftharpoons \{Cu(II)(MGD)_2\}$$

Scheme 5.7 Proposed chemical reactions for the complexation of copper(+2) by MGD.

151

5.5.3. Product Analysis of the MGD Reaction with GSNO

It has been found that NO can be generated by the nitrosation of a dithiocarbamate. NO is oxidised in aerobic solutions at pH 7.4 and forms quantitative amounts of nitrite.[30,31] The Griess test was used as described in section 2.3.2 to determine how much nitrite was generated when MGD decomposed GSNO.

A solution containing $2x10^{-2}$ M MGD, $2x10^{-3}$ M GSNO and 0.15 M phosphate buffer (pH 7.4) was prepared. When the *S*-nitrosothiol had decomposed the nitrite concentration was measured. The nitrite yield from the reaction was 33 %. This suggested that the alcohol groups on the MGD reacted with the *S*-nitrosothiol as well so quantitative nitrite was not formed in the reaction.

The alcohol groups on the MGD could have reacted with GSNO to form an alkyl nitrite and thiol. (see scheme 5.8)

$$ROH \ + \ RSNO \longrightarrow RONO \ + \ RSH$$

Scheme 5.8 Chemical equation for the reaction between an alcohol and an *S*-nitrosothiol.

It has been shown that the reaction of MGD with GSNO cannot account for the transfer of NO from GSNO to the iron complex for two reasons. The reaction is too slow to account for the rapid transfer of NO and it does not generate quantitative amounts of NO from GSNO either.

5.6 The Reaction of GSNO with the Iron(+3) MGD Complex

Evidence has been obtained that GSNO can transfer NO to the iron(+2) MGD complex. (see section 5.3) GSNO was reacted with the iron(+3) MGD complex to establish whether a similar reaction could occur. The iron(+3) complex was prepared by reacting MGD with $FeCl_3$ in a 3 : 1 ratio and using concentrated TRIS buffer (pH 7.4) to give a final concentration of 0.15 M.

5.6.1 Initial Evidence that GSNO Reacted with the Iron(+3) MGD Complex

A solution containing 5×10^{-4} M {Fe(III)(MGD)$_3$} and an equimolar quantity of GSNO in the presence of 0.15 M TRIS buffer (pH 7.4) was prepared. The colour of the solution rapidly changed from brown to yellow. This suggested that the iron nitrosyl complex was forming and NO transfer was taking place. A UV / Vis spectrum of the iron complex solution was compared with one taken fifteen minutes after mixing with an equimolar quantity of GSNO. (see figure 5.12)
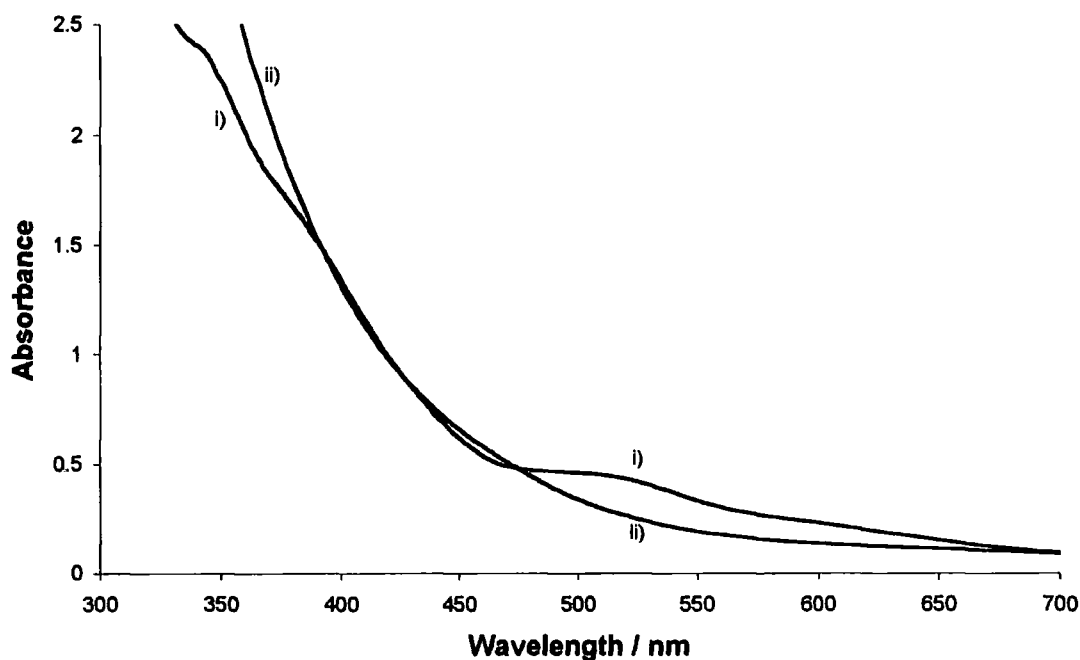
Figure 5.12 UV / Vis spectra of a {Fe(III)(MGD)$_3$} solution at the same concentration i) before and ii) fifteen minutes after a 1 : 1 reaction with GSNO.

A decrease in absorbance around 500 nm was observed when NO was reacted with the iron(+3) MGD complex.

One problem that did occur was precipitation in the iron complex stock solution so solutions were made up and analysed as quickly as possible. The precipitation did not occur in the sample solutions so the spectral data were not affected.

5.6.2 Kinetic Data for the Reaction of GSNO with the Iron(+3) MGD Complex

A spectral change was observed when GSNO was reacted with the iron(+3) complex (see figure 5.12), therefore the reaction could be followed using UV / Vis spectrometry. The decrease in absorbance at 511 nm was followed for a reaction solution containing 1×10^{-2} M GSNO, 5×10^{-4} M {Fe(III)(MGD)$_3$} and 0.15 M TRIS buffer (pH 7.4). Precipitation did not occur in the solution and the reaction profile is shown in figure 5.13.
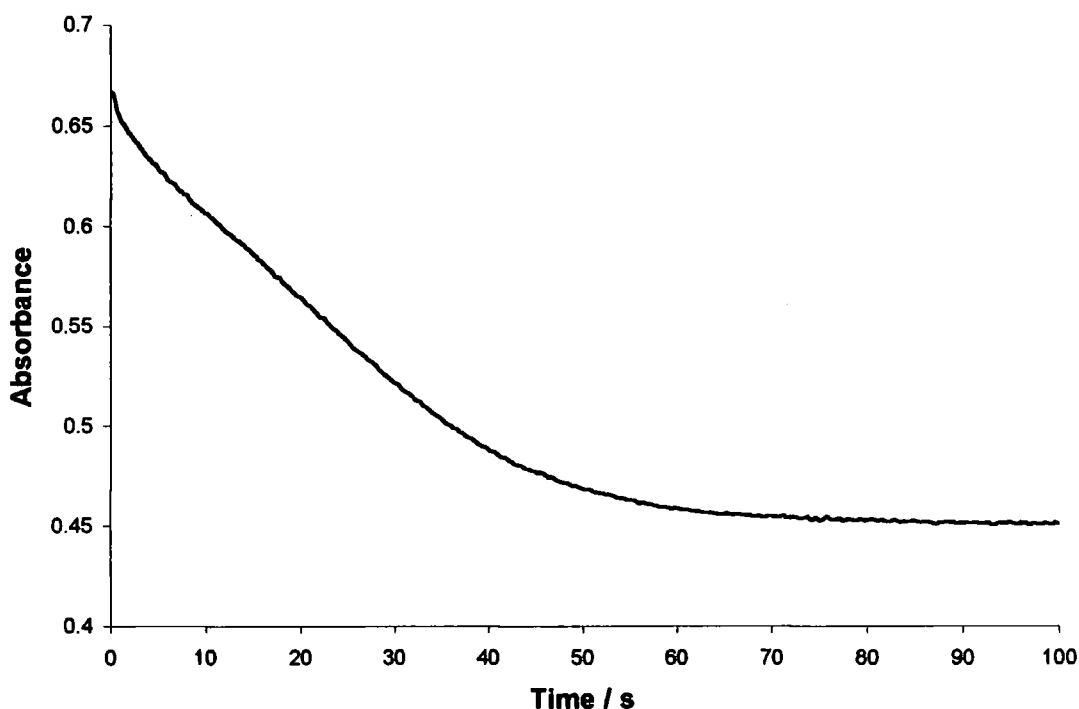
Figure 5.13 Absorbance at 511 nm measured over time for a solution containing 1×10^{-2} M GSNO, 5×10^{-4} M {Fe(III)(MGD)$_3$} and 0.15 M TRIS buffer (pH 7.4).

The reaction profile did not fit a first order model suggesting that the iron complex did not react with GSNO in the same way as the iron(+2) dithiol complex did in chapter 4. A rapid initial decrease could have been due to NO produced photolyticaly from GSNO in the stock solutions, which has been observed before.[32] The remainder of the profile was mostly linear with a tail off as the reaction went to completion. Linear reaction profiles are characteristic of zero order reactions, which suggested that the reaction did not involve the iron complex in the rate determining step.

5.6.3 HPLC Analysis of the GSNO Reaction with the Iron(+3) MGD Complex

The HPLC experiment described in section 5.3.2 was repeated in aerobic conditions using an iron complex solution containing 2×10^{-3} M $FeCl_3$ and 6×10^{-3} M MGD with 0.15 M TRIS buffer (pH 7.4). This was reacted with an equal volume of a solution containing 2×10^{-3} M GSNO and 0.15 M TRIS buffer (pH 7.4). Fifteen minutes after mixing took place the solution was analysed by HPLC.

Precipitation did occur more rapidly than expected in the reaction solution possibly due to the decomposition of iron(+3) complexes. The higher concentration of the iron(+3) MGD complex could have accelerated the process.

A GSNO solution was analysed using HPLC and three compounds were eluted. Two corresponded to GSNO and GSSG retention times. The third compound eluted at 3.3 minutes could have been nitrous acid / nitrite, the oxidised product of NO. This could have been because the GSNO used was impure due to decomposition during or after its preparation.

Fifteen minutes after mixing the reaction solution was analysed by HPLC. The reaction solution was found to contain significant quantities of GSNO and GSSG. Another compound eluted at 3.3 minutes that was believed to be nitrous acid / nitrite. If rusting was taking place in the solution the presence of nitrous acid could have been due to decomposition of an iron nitrosyl complex, oxidised NO or both of these factors.

The incomplete conversion of GSNO to GSSG could have been due to the rusting of the iron(+3) complex reactant. Despite this the experiment still showed significant formation of GSSG from GSNO.

When the experiment was complete the yellow solution was divided into two vessels, one was left open to the air and the other one was stoppered. Over time the solution in the stoppered flask turned green. A study has found that the nitrosyl iron(+3) MGD complex forms the nitrosyl iron(+2) MGD complex spontaneously in anaerobic conditions (see scheme 5.9).[18] Sealing the flask from the atmosphere may have brought about similar

reaction conditions if dissolved oxygen was being consumed by other reactions in the solution, eg. the rusting of iron(+3).

$$\{Fe(III)(MGD)_3(NO)\} \xrightarrow{+ e^-} \{Fe(II)(MGD)_2(NO)\} + MGD$$
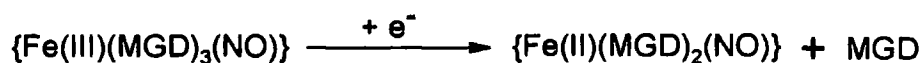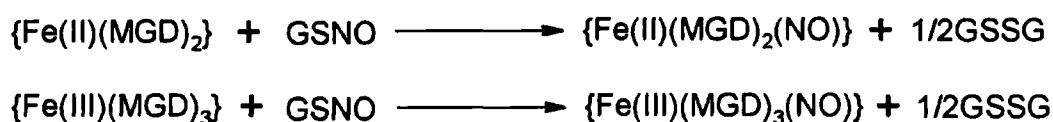
Scheme 5.9 Spontaneous reaction of the nitrosyl iron(+3) MGD complex in anaerobic conditions.

One explanation suggested for the spontaneous reaction is a reduction by NO present in the solution.[19] If this was the case then GSNO would have had to continue to decompose releasing NO in solution after the HPLC analysis. The kinetic analysis indicated that the reaction went to completion in a short period of time.

5.7 Discussion

Evidence has been found that GSNO can transfer NO to the metal centre of iron(+2) and iron(+3) MGD complexes. This work suggested that the oxidation state of iron in the complex was not a critical factor when NO transfer took place. The proposed reactions are shown in scheme 5.10.

$$\{Fe(II)(MGD)_2\} + GSNO \longrightarrow \{Fe(II)(MGD)_2(NO)\} + 1/2GSSG$$

$$\{Fe(III)(MGD)_3\} + GSNO \longrightarrow \{Fe(III)(MGD)_3(NO)\} + 1/2GSSG$$

Scheme 5.10 Proposed reactions of GSNO with iron MGD complexes at pH 7.4.

No evidence of NO^+ transfer was observed, as was the case for some reactions studied in chapter four when the organic product was the thiol. This could be due to the stability of the nitrosyl iron MGD complexes because no reducing agent was required to prevent oxidation of the complexes during their preparation.

The reaction of MGD with copper(+2) ions was studied but no evidence of copper(+1) formation was found. Kinetic data for the reaction of MGD with GSNO suggested that the reaction was metal ion independent and too slow to account for the NO transfer. The yield

of nitrite from the reaction was found to be 33 %, which suggested that quantitative formation of NO from GSNO does not occur in this reaction.

Kinetic data for the reaction involving the iron(+2) MGD complex with GSNO could not be obtained due to the sensitivity of the complex to oxidation. However, the relatively stable iron(+3) complex could be used to obtain some kinetic data. A zero order reaction profile indicated that a reaction between the complex and GSNO was not in the rate determining step.

It has therefore been proposed that the iron MGD complexes can weaken the sulfur nitrogen bond in GSNO. GSNO could form a bond with the iron complex at the NO co-ordination site leading to a nitrogen iron atom interaction. The sulfur nitrogen bond then homolyticaly cleaves releasing NO and the iron nitrosyl complex forms. (see scheme 5.11) Formation of disulfide could then occur via thiyl radical dimerisation or by reaction with S-nitrosothiol, which would also form another molecule of NO.
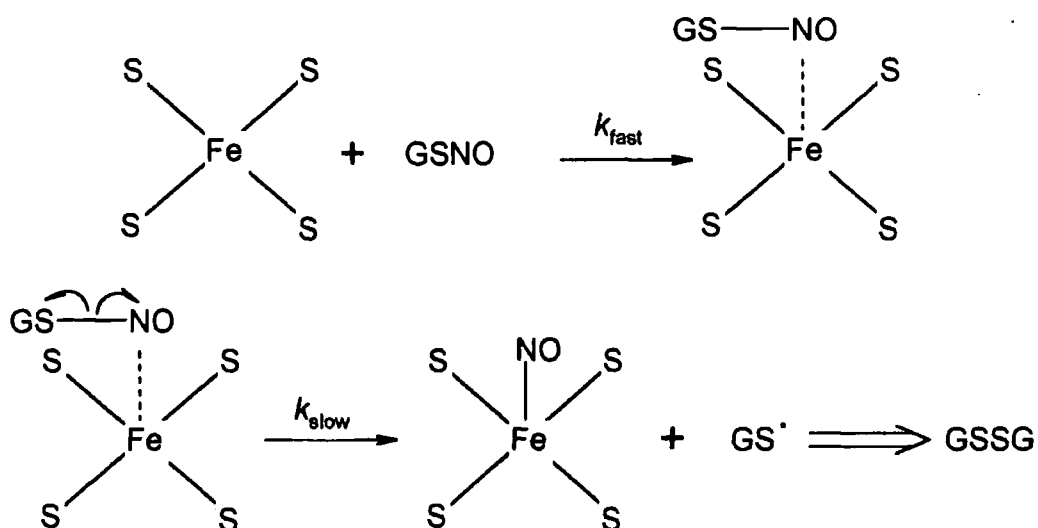
Scheme 5.11 Proposed mechanism for nitrosyl iron(+2) MGD complex formation using GSNO. (the dotted line represents atom interactions)

Proline dithiocarbamate has been used as another water soluble ligand for iron(+2) complex trapping of NO.[33] The compound was found to be very hygroscopic which hindered attempts to determine the purity of the compound and weigh out accurate masses.

5.8 References

1) D. Coucouvanis, *Prog. Inorg. Chem.*, 1970, **11**, 233.

2) D. Coucouvanis, *Prog. Inorg. Chem.*, 1979, **26**, 301.

3) J. P. Fackler Jr. and D. G. Holah, *Inorg. Nucl. Chem. Lett.*, 1966, **2**, 251.

4) M. Colapietro, A. Domenicano, L. Scaramuzza, A. Vaciago and L. Zambonelli, *Chem. Commun.*, 1967, 583.

5) B. Kalyanaraman, *Methods Enzymol.*, 1996, **268**, 168.

6) A. Komarov, D. Mattson, M. M. Jones, P. K. Singh and C. Lai, *Biochem. Biophys. Res. Commun.*, 1993, **195**, 1191.

7) Y. Kotake, T. Tanigawa, M. Tanigawa, I. Ueno, D. R. Allen and C. Lai, *Biochim. Biophys. Acta*, 1996, **1289**, 362.

8) V. D. Mikoyan, L. N. Kubrina, V. A. Serezhenkov, R. A. Stukan and A. F. Vanin, *Biochim. Biophys. Acta*, 1997, **1336**, 225.

9) G. M. Pieper and C. Lai, *Jpn. J. Pharmacol.*, 1999, **80**, 359.

10) A. F. Vanin, *Methods Enzymol.*, 1999, **301**, 269.

11) J. L. Zweier, A. Samouilov and P. Kuppusamy, *Biochim. Biophys. Acta*, 1999, **1411**, 250.

12) P. Tsai, S. Porasuphatana, S. Pou and G. M. Rosen, *J. Chem. Soc., Perkin Trans. 2*, 2000, 983.

13) A. L. Kleschyov, H. Mollnau, M. Oelze, T. Meinertz, Y. Huang, D. G. Harrison and T. Munzel, *Biochem. Biophys. Res. Commun.*, 2000, **275**, 672.

14) L. A. Shinobu, S. G. Jones and M. M. Jones, *Acta Pharmacol. et Toxicol.*, 1984, **54**, 189.

15) P. Giboreau and C. Morin, *J. Org. Chem.*, 1994, **59**, 1205.

16) N. N. Greenwood and A. Earnshaw, 'Chemistry of the Elements', 2nd Ed., Butterworth-Heinemann, Oxford, 1998, 1076.

17) S. Fujii, T. Yoshimura and H. Kamada, *Chem. Lett.*, 1996, **9**, 785.

18) A. F. Vanin, X. Liu, A. Samouilov, R. A. Stukan and J. L. Zweier, *Biochim. Biophys. Acta*, 2000, **1474**, 365.

19) S. Fujii and T. Yoshimura, *Coord. Chem. Rev.*, 2000, **198**, 89.

20) H. Büttner and R. D. Feltham, *Inorg. Chem.*, 1972, **11**, 971.

21) A. J. Holmes and D. L. H. Williams, *J. Chem. Soc., Perkin Trans. 2*, 2000, 1639.

22) P. H. Beloso and D. L. H. Williams, *J. Chem. Soc., Chem. Commun.*, 1997, 89.

23) E. E. Reid, 'Organic Chemistry of Bivalent Sulfur', Vol. 1, Chemical Publishing Company, New York, 1958, 294.

24) J. Buckingham, 'Dictionary of Organic Compounds', Vol. 2, Chapman and Hall, New York, 1982, 2365.

25) L. E. Lopatecki and W. Newton, *Can. J. Bot.*, 1952, **30**, 131.

26) G. L. Ellman, *Arch. Biochem. Biophys.*, 1959, **82**, 70.

27) D. R. Arnelle, B. J. Day and J. S. Stamler, *Nitric Oxide: Biol. Chem.*, 1997, **1**, 56.

28) S. C. Askew, D. J. Barnett, J. McAninly and D. L. H. Williams, *J. Chem. Soc., Perkin Trans. 2*, 1995, 741.

29) G. F. Smith and W. H. McCurdy, *Anal. Chem.*, 1952, 371.

30) D. A. Wink, J. F. Darbyshire, R. W. Nims, J. E. Saavedra and P. C. Ford, *Chem. Res. Toxicol.*, 1993, **6**, 23.

31) H. H. Awad and D. M. Stanbury, *Int. J. Chem. Kinet.*, 1993, **25**, 375.

32) D. J. Sexton, A. Muruganandam, D. J. McKenny and B. Mutus, *Photochem. Photobiol.*, 1994, **59**, 463.

33) S. V. Paschenko, V. V. Khramtsov, M. P. Skatchkov, V. F. Plyusnin and E. Bassenge, *Biochem. Biophys. Res. Commun.*, 1996, **225**, 577.

Chapter 6

Experimental Techniques

<u>**Chapter 6: Experimental Techniques**</u>

This chapter contains experimental details and general information on the research presented in this thesis.

<u>**6.1 Equipment**</u>

<u>6.1.1 UV / Vis Spectrophotometry</u>

A Shimadzu UV-2101PC, Perkin Elmer Lambda 2 and Perkin Elmer Lambda 12 UV / Vis spectrophotometers were used to obtain UV / Vis spectra. Reaction profiles could be recorded by following absorbance over time.

Solutions were analysed in quartz cuvettes with pathlength 1 cm and unless otherwise stated; the total volume of a solution in a cuvette was 2.5 ml. Spectrophotometers were zeroed using air as a reference or by using a cuvette filled with the solvent and buffer contained in the sample.

<u>6.1.2 Stopped Flow Spectrophotometry</u>

Some chemical reactions were so fast that when the sample cuvette was prepared and analysed the reaction was near completion. An Applied Photophysics DX.17MV stopped flow spectrophotometer was used in some cases to record reaction profiles so that rate constants for the reactions could be determined accurately.

Two syringes were filled with the chemical reagents required for a reaction and the solutions were transferred to two vessels in the spectrophotometer. Equal volumes of the two solutions were pushed into a cell using compressed air and absorbance of the reaction solution could be immediately measured over time.

6.1.3 Nitric Oxide Specific Electrode

Nitric oxide (NO) concentration in reaction solutions was measured using a World Precision Instruments ISO-NO MK II nitric oxide meter. A metal sleeve with a gas permeable membrane at the end surrounded the counter and working electrodes. The membrane allowed only small molecules to pass through into the electrolyte solution.

The electrode was calibrated before each experiment using the chemical equation shown in scheme 6.1. A 25 ml solution containing 0.1 M H_2SO_4 and 0.1 M KI was placed in a special glass vessel and nitrogen was bubbled through the solution for fifteen minutes. The vessel also contained the NO electrode and was sealed from the atmosphere by close fitting rubber stoppers. A magnetic stirrer was used to keep the solution agitated.

$$2KNO_2 + 2KI + 2H_2SO_4 \longrightarrow 2NO + I_2 + 2H_2O + 2K_2SO_4$$
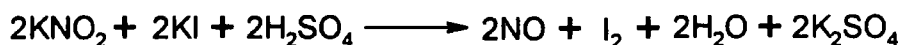
Scheme 6.1 Chemical reaction used to calibrate the NO electrode.

When the current detected from the electrode became constant, data for the calibration could be obtained and the nitrogen flow was stopped. The data collection program on the computer interfaced with the electrode was set to record the change in current. Using a syringe 50×10^{-6} dm^3 of a sodium nitrite solution was injected through a rubber seal. When the current had reached a plateau another 50×10^{-6} dm^3 of the sodium nitrite solution was added. This was repeated three further times so that the current dependence on NO concentration in the solution could be determined.

6.1.4 pH Meter

The pH of solutions was measured using a JENWAY 3020 pH Meter. Gelplas combination pH electrodes with a 12 mm or 6 mm diameter were used. The range of pH measurable was 0 – 14 with an error ± 0.02.

Calibration of the pH electrodes was performed using two buffers, one at pH 7 and the other at pH 4 or pH 10 depending on the pH being studied. The buffer solutions were thermostated at 25 °C when readings were taken.

6.1.5 Nuclear Magnetic Resonance

^{13}C and ^1H NMR spectra were recorded by the Durham University Chemistry Department analytical service.

6.1.6 Mass Spectrometry

Mass spectra were recorded by the Durham University Chemistry Department analytical service. Dr. Mike Jones compiled the experimental data.

6.1.7 High Pressure Liquid Chromatography

HPLC analysis was performed by the Durham University Chemistry Department analytical service. Mr. Len Lauchlan compiled the experimental data.

6.1.8 Elemental Analysis

Carbon, hydrogen and nitrogen elemental analysis was performed by the Durham University Chemistry Department analytical service. Mrs. Jaroslava Dostal compiled the experimental data.

6.1.9 Melting Point

The melting point of solid compounds was measured using Gallenkamp Melting Point Apparatus. (registered design no. 889339) The bottom of a melting point tube was covered with a sample and when the solid melted the temperature range at which it occurred was recorded using a thermometer.

6.1.10 Methods for Maintaining Anaerobic Conditions in Solutions

Solutions were deoxygenated by bubbling nitrogen through them for fifteen minutes. Suba·Seal rubber septa were placed in the tops of volumetric and conical flasks to seal the solutions from the atmosphere. Plastic tubing transported the nitrogen flow. Needles were

attached at one end to pierce the rubber septa so that the gas flow could enter the volumetric or conical flask. Two pieces of tubing were required for each solution, one supplying the nitrogen gas and the other removing the excess pressure caused by introducing a gas to a closed container. The end of the exhaust tube was placed in a beaker filled with water so that atmospheric air could not get back into the system.

When NO was reacted with a chemical compound two conical flasks with solutions in anaerobic conditions were used. One contained a 50 ml solution of 0.1 M ascorbic acid which had solid sodium nitrite added to it, the other contained the chemical compound in solution. The nitrogen flow was first bubbled through the flask containing the ascorbic acid and then the exhaust gas was transferred to the second flask. A second exhaust tube then lead to a beaker filled with water.

The mixing of solutions and the addition of solid to solutions in anaerobic conditions required the presence of a nitrogen atmosphere. A GLOVE BAG™ Inflatable Glove Chamber Evaluation Kit made by Instruments for Research and Industry, Inc. (I²R), model X-27-27H was used.

6.1.11 Methods for Accurate Measurement of Mass and Volume

Accurate small volumes of solutions were dispensed using a Pipetman made by Gilson or a βeta-Pette™ made by Continental Lab Products. A calibration was done before each experiment using water. For volumes greater than 1.5 ml graduated glass pipettes were used.

Masses of compounds measured in grams to four decimal places were obtained using an A&D enclosed balance model FX-40 that had a mass capacity of 41g. The balance was cleaned and calibrated using a 20g mass on a weekly basis. For larger masses a Sartørius open balance model PT 310 was used. Mass was measured in grams to two decimal places and the capacity was 310g.

6.2 Materials

6.2.1 Chemical Reagents

Chemicals used for the experimental work presented in this thesis were purchased from Sigma-Aldrich Company Ltd. unless stated otherwise.

S-Nitrosothiols were generated *in situ* when required for experimental purposes. A solution containing equimolar quantities of thiol and sodium nitrite with 0.02 M perchloric acid present was prepared. Solutions were used when the S-nitrosation reactions went to completion.

6.2.2 Preparation of Buffer Solutions

When reactions were studied at physiological pH (pH 7.4), phosphate or TRIS buffer was used to neutralise the acid required to nitrosate the thiol. When the buffer was made up the pH was corrected to within 0.02 of pH 7.40, which is the error range of the pH electrode.

Determining a rate constant dependence on pH required many rate constants to be obtained by following rate of reaction in the presence of different buffer solutions. Several buffers were prepared to cover the pH range required and the pH of the reaction solutions was measured to determine an accurate pH.

6.2.3 Preparation and Characterisation of Compounds

Compounds that were used in experiments that were not commercially available or more economical to prepare using synthetic methods in the literature are shown here.

6.2.3.1 N-Acetylpenicillamine Disulfide

N-Acetylpenicillamine disulfide was prepared in two stages using a method that is described in the literature.[1]

Part 1; A solution containing 1.4434 g of *N*-acetylpenicillamine in 15 cm³ methanol and 15 cm³ 1 M hydrochloric acid was made up. The reaction mixture was stirred until a suspension formed then 1.5 cm³ of concentrated sulfuric acid and 10 cm³ of concentrated hydrochloric acid was added to the agitated solution. The flask was then wrapped in foil and placed in an ice bath to minimise the decomposition of the *S*-nitrosothiol product via the thermal / photolytic pathway. Another solution was prepared by dissolving 1.0338 g of sodium nitrite in 15 cm³ of water. The sodium nitrite solution was added drop wise to the thiol solution, which was then stirred for thirty minutes. Crystals of the product *S*-nitroso-*N*-acetylpenicillamine (SNAP) formed in the solution and were removed using filtration and washed sparingly with water. The crystals were dried under vacuum in a desiccator in the dark overnight.
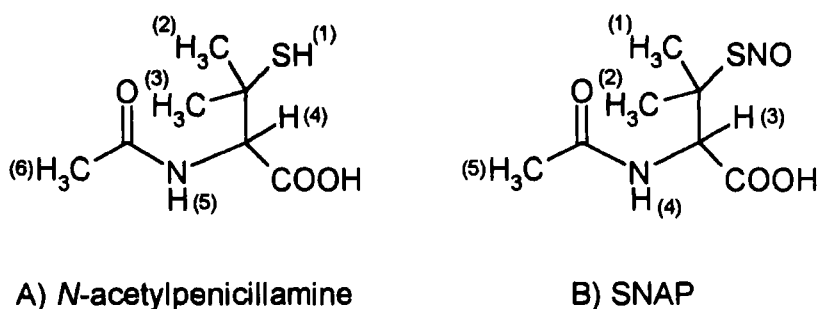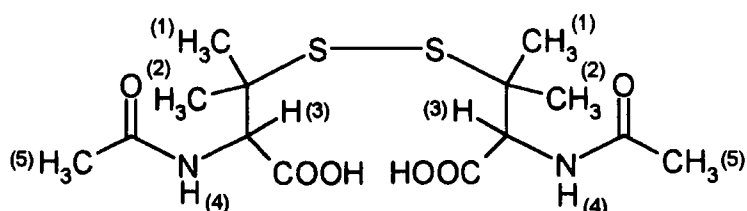

A) *N*-acetylpenicillamine   B) SNAP

Figure 6.1 Structure of A) *N*-acetylpenicillamine and B) SNAP.

A) δ_H / ppm (DMSO, 200 MHz), 8.72 (H-5, d, J = 9.0 MHz), 5.04 (H-4, d, J = 9.2 MHz), 3.95 (H-1, s), 3.13 (H-6, s), 2.01 + 2.00 (H-2 + H-3, s). B) δ_H / ppm (DMSO, 200 MHz), 8.55 (H-4, d, J = 9.6 MHz), 5.21 (H-3, d, J = 9.2 MHz), 2.01 + 1.98 (H-1 + H-2, s), 1.91 (H-5, s). Elemental analysis for $C_7H_{12}N_2O_4S$, expected C: 38.17, H: 5.49, N: 12.72, found C: 38.16, H: 5.55, N: 12.11. UV / Vis analysis, expected ϵ_{340nm} = 956 dm³ mol⁻¹ cm⁻¹,[2] found ϵ_{340nm} = 993 dm³ mol⁻¹ cm⁻¹.

The purity of SNAP was also analysed using mass spectrometry. When positive electrospray techniques were used a single peak at m/z = 403 was observed. This corresponded to *N*-acetylpenicillamine disulfide, which suggested that SNAP decomposed during the analytical process.

Part 2; A solution containing 0.5 g of SNAP in 20 ml methanol was made up and the solution was refluxed for four hours. The methanol was removed using a rotary evaporator leaving the product in a non crystalline form. Hot hexane was added and the oil obtained went opaque. A white solid was removed from the vessel after one week by which time the hexane had evaporated off.

N-Acetylpenicillamine disulfide

Figure 6.2 Structure of N-acetylpenicillamine disulfide.

δ_H / ppm (DMSO, 200 MHz), 8.21 (H-4, d, J = 8.8 MHz), 4.44 (H-3, dd, J = 8.6 MHz and 2.4 MHz), 1.97 (H-5, s), 1.39 + 1.36 (H-1 + H-2, s). $(M+Na)^+$, $C_{14}H_{24}O_6S_2N_2Na$, require m/z = 403, found m/z = 403.

6.2.3.2 N-Methyl-D-glucamine Dithiocarbamate

N-Methyl-D-glucamine dithiocarbamate (MGD) was prepared as described in the literature.[3]

A solution of 5 g of sodium hydroxide dissolved in 50 ml water was made up. The solution was stirred while 12.5 g of ice was added, then 24.4 g of N-methyl-D-glucamine was dissolved in the solution. An ice bath was used to keep the temperature of the reaction solution in the range 0 - 10 °C. Another solution was made up containing 12.5 ml carbon disulfide and 37.5 ml ethanol. The carbon disulfide solution was added drop wise to the solution containing N-methyl-D-glucamine while making sure the temperature of the reaction solution did not exceed 10 °C. After the addition was complete, 125 ml of methanol was added to the solution that contained a white precipitate and was then left covered overnight. The white solid was then removed using filtration and washed with methanol until the washings were not a yellow colour. The solid was dried in air.
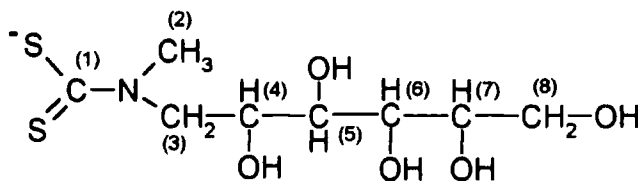
167

Figure 6.3 Structure of MGD.

Product) δ_C / ppm (D$_2$O), 212.80 (C-1), 74.78 (C-7), 73.72 (C-6), 73.62 (C-5), 72.56 (C-4), 65.26 (C-8), 61.48 (C-3), 47.28 (C-2). **Literature)** δ_C / ppm (D$_2$O), 210.0 (C-1), 72.1 (C-7), 71.0 (C-6), 70.9 (C-5), 69.8 (C-4), 62.8 (C-8), 58.8 (C-3), 44.6 (C-2).[4] (M)$^-$, $C_8H_{16}O_5S_2N$, require m/z = 270, found m/z = 270. Elemental analysis for $C_8H_{18}NO_6S_2Na$, expected C: 30.86, H: 5.83, N: 4.50, found C: 30.12, H: 5.89, N: 4.28.

Another peak at m/z = 194 was present in the mass spectrum. This corresponds to a decomposition product of MGD by cleavage of the carbon(1) nitrogen bond.

6.3 Quantitative Chemical Tests

6.3.1 Thiol

The thiol content in solutions was determined using the Ellmans test after an initial calibration was performed. The reagent used to react with thiol was 5,5'-dithiobis(2-nitrobenzoic acid) which was first dissolved in methanol so it would be soluble in aqueous conditions. The methanol solution formed 10 % of the final volume of the solution in the cuvettes. Fifteen minutes after cuvettes were prepared a UV / Vis spectrum was taken of the solutions.

6.3.2 Ammonia

The ammonia concentration in solutions was measured using the standard diagnostic kit sold by the Sigma-Aldrich Company Ltd. Ammonia concentration was measured by the reductive amination of 2-oxoglutarate using glutamate dehydrogenase (GLDH) and reduced

nicotinamide adenine dinucleotide phosphate (NADPH). (see scheme 6.2) The test can measure concentrations of ammonia up to 15 ug / ml. (8.8×10^{-4} mol dm^{-3})

$$\text{2-Oxoglutarate} + NH_3 + NADPH \xrightarrow{\text{GLDH}} \text{Glutamate} + NADP$$
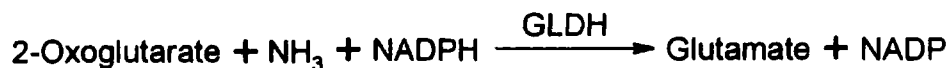
Scheme 6.2 Chemical reaction used in the ammonia test.

A UV / Vis spectrophotometer was zeroed with empty cuvette holders and set up so that the absorbance at 340 nm could be measured. The decrease in absorbance measured when ammonia was present was due to the oxidation of NADPH.

Two UV / Vis cuvettes were prepared, a BLANK and a SAMPLE while taking care not to shake the solutions too vigorously. The BLANK contained 2 ml ammonia assay solution and 0.2 ml of water and the SAMPLE contained 2 ml of ammonia assay solution and 0.2 ml of the solution being tested. The solutions were left to equilibrate for three minutes and then their absorbance at 340 mm was measured. 20×10^{-6} dm^3 of GLDH was added to both solutions and they were mixed gently. After five minutes the absorbance of the two solutions at 340 nm was measured again. The concentration of ammonia in the sample solution could then be calculated using the change in absorbance at 340 nm for the two cuvettes using equation 6.1.

Ammonia (µg / ml) = $(\Delta A_{SAMPLE} - \Delta A_{BLANK}) \times 30.3$

Equation 6.1 Mathematical equation for calculating the concentration of ammonia in a solution.

The ammonia test was first performed on an ammonia solution of known concentration so that the accuracy of the test could be determined. The calculated value was within 5 % of the ammonia concentration.

6.3.3 Nitrite

The concentration of nitrite in solutions was measured by the Griess test. N-(1-naphthyl)ethylenediamine (NNED) and sulfanilamide (SUL) were dissolved in 0.4 M

perchloric acid. The two acidic solutions made up 80 % of the total volume in the cuvettes. Sodium nitrite was dissolved in water and used at different concentrations to calibrate the test. The reactants were mixed in a specific order as described by Vogel.[5] The nitrite and SUL were mixed, NNED was added after five minutes, and a UV / Vis spectrum was taken after a further ten minutes.

6.4 Mathematical Equations and Derivations

6.4.1 First Order Rate Equation

Reactions were followed by recording absorbance at a particular wavelength over time. The reaction solutions were kept at 25 °C using a thermostat unless stated otherwise. A first order model was used in most cases to determine rate of reaction and it can be derived using the following simple first order reaction shown in scheme 6.3.

$$A \longrightarrow B$$

Scheme 6.3 A simple first order reaction.

The rate of reaction is governed by the rate equation shown in equation 6.2.

$$-\frac{d[A]}{dt} = \frac{d[B]}{dt} = k_1[A]$$

Equation 6.2 Rate equation for a simple first order reaction.

The rate equation can be rearranged and integrated from time t = 0 corresponding to an initial concentration [A_o] to time t corresponding to a lower concentration [A]. The integrated equation can then be rearranged to give the integrated first order equation shown in equation 6.3.

$$[A] = [A_o]e^{-k_1 t}$$

Equation 6.3 Integrated first order equation.

Plots of absorbance against time were fitted to this equation using the mathematical modelling package Scientist[6] or a program on the computer interfaced with the stopped flow spectrophotometer. Absorbance is proportional to the concentration of a compound so rate constants could be obtained from the data.

6.4.2 Determination of Rate Constants Using the Isolation Method

Rate constants for reactions with a higher order than one were determined using the isolation method. In a case where A reacts with B in the rate limiting step to form a product then the rate equation shown in scheme 6.4 is valid.

Rate = k_2[A][B]

Equation 6.4 Rate equation for a second order reaction.

If the reaction is performed with B in greater or equal to a ten fold excess of A then the rate equation is simplified to the one shown in equation 6.5, where k' is the pseudo first order rate constant.

Rate = k'[A]

Equation 6.5 Rate equation when A is reacted with B in excess in a second order reaction.

The equations for rate of reaction shown in equation 6.4 and 6.5 can be combined to give an equation that gives a relationship between the pseudo first order rate constant and the concentration of B. (see equation 6.6) Therefore a plot of pseudo first order rate constant against concentration of B should give a straight line with a gradient equal to the second order rate constant.

$k' = k_2$[B]

Equations 6.6 Mathematical equation used to determine second order rate constants.

6.4.3 Equation for Rate Constant Dependence on pH for a Nucleophile

If the sulfonate group on the DMPS molecule is ignored, because it does not react with an S-nitrosothiol then there are three possible forms of the dithiol that are present in solution. The different forms of DMPS are H_2DM, HDM^- and DM^{2-} and the concentration of these in solution at a particular pH is governed by the acid dissociation constants K_1 and K_2 and the total amount of DMPS added. The rate equation for the reaction of the three forms of DMPS with an S-nitrosothiol is shown in equation 6.7.

$$\text{Rate} = k_{H_2DM}[H_2DM][RSNO] + k_{HDM^-}[HDM^-][RSNO] + k_{DM^{2-}}[DM^{2-}][RSNO]$$

Equation 6.7 Rate equation for the three forms of DMPS reacting with an S-nitrosothiol.

Using equations for the two acid dissociation constants a rate equation can be derived in terms of the concentration of H_2DM. (see equation 6.8)

$$K_1 = \frac{[HDM^-][H^+]}{[H_2DM]} \Rightarrow [HDM^-] = \frac{K_1[H_2DM]}{[H^+]} \qquad K_2 = \frac{[DM^{2-}][H^+]}{[HDM^-]} \Rightarrow [DM^{2-}] = \frac{K_2[HDM^-]}{[H^+]}$$

$$\text{Rate} = \left(k_{H_2DM}[H_2DM] + \frac{k_{HDM^-} \cdot K_1[H_2DM]}{[H^+]} + \frac{k_{DM^{2-}} \cdot K_1K_2[H_2DM]}{[H^+]^2} \right)[RSNO]$$

Equation 6.8 Modified rate equation for DMPS reacting with S-nitrosothiols.

Second order rate constants were calculated experimentally using the total DMPS concentration in solution. Therefore the concentration of H_2DM had to be expressed in terms of total DMPS concentration and this is shown in equation 6.9.

$$[DMPS]_T = [H_2DM] + [HDM^-] + [DM^{2-}] \Rightarrow [DMPS]_T = [H_2DM]\left(1 + \frac{K_1}{[H^+]} + \frac{K_1K_2}{[H^+]^2} \right)$$

$$[H_2DM] = \frac{[DMPS]_T[H^+]^2}{[H^+]^2 + K_1[H^+] + K_1K_2}$$

Equation 6.9 Equation for concentration of H_2DM in terms of total concentration of DMPS present.

Equation 6.9 can be substituted into equation 6.8 to give the rate equation (see equation 6.10) for the reaction of DMPS with S-nitrosothiols in terms of the reactivity of the three different forms of DMPS.

$$\text{Rate} = [\text{DMPS}]_T [\text{RSNO}]\left(\frac{k_{\text{H}_2\text{DM}}[\text{H}^+]^2 + k_{\text{HDM}}\cdot K_1[\text{H}^+] + k_{\text{DM}^{2-}}\cdot K_1 K_2}{K_1 K_2 + K_1[\text{H}^+] + [\text{H}^+]^2} \right)$$

Equation 6.10 Rate equation for the reaction of DMPS with S-nitrosothiols in terms of the reactivity of the three different forms of DMPS.

The rate constant dependence on pH for the reaction of cysteine with S-nitroso-1-thio-β-D-glucose tetraacetate was derived in a similar way.

6.4.4 Error Analysis

Physical constants reported in this thesis were determined using five or more experimental points. The data analysis produced a value for the standard deviation and correlation coefficient r for the fit. Errors quoted are the standard deviations found. The r^2 value in every case was greater than or equal to 0.95.

Constants that were found by following a linear trend were analysed using the linear regression function in Excel. For more complicated trends the mathematical modelling package Scientist[6] was used and statistical values could be obtained using the statistics function.

6.5 Nomenclature

6.5.1 Abbreviations

The following abbreviations were used in this thesis.

BCS   bathocuproine sulfonate
cGMP   guanosine 3',5'-cyclic monophosphate

DETC	diethyldithiocarbamate
DM^{2-}	DMPS with no protonated thiol groups
DMPS	2,3-dimercapto-1-propanesulfonic acid
DTE	dithioerythritol
DTNB	5,5'-dithiobis(2-nitrobenzoic acid)
DTT	dithiothreitol
EDRF	endothelium derived relaxing factor
EDTA	ethylenediaminetetraacetic acid
EPR	electron paramagnetic resonance
GLDH	glutamate dehydrogenase
GPSNO	2-acetamido-2-deoxy-S-nitroso-1-thio-β-D-glucopyranose-3,4,6-triacetate
GSH	glutathione
GSNO	S-nitrosoglutathione
GSSG	glutathione disulfide
H_2DM	DMPS with two protonated thiol groups
HDM^-	DMPS with one protonated thiol group
HPLC	high pressure liquid chromatography
MGD	N-methyl-D-glucamine dithiocarbamate
NADPH	reduced nicotinamide adenine dinucleotide phosphate
NAP	N-acetylpenicillamine
NMR	nuclear magnetic resonance
NNED	N-(1-naphthyl)ethylenediamine
NOS	nitric oxide synthase
R	part of a chemical compound
$R'NH_2$	primary amine
R'Se-SeR'	diselenide
RB	Rose Bengal photosensitiser
RIG200	N-(S-nitroso-N-acetylpenicillamine)-2-amino-2-deoxy-1,3,4,6-tetra-O-acetyl-β-D-glucopyranose
RN_2^+	diazonium ion
RONO	alkyl nitrites
RSH	thiol

RSNO	S-nitrosothiol
RSSR	disulfide
SNAC	S-nitroso-N-acetylcysteine
SNAG	S-nitroso-1-thio-β-D-glucose tetraacetate
SNAP	S-nitroso-N-acetylpenicillamine
SNGP	S-nitroso-β-D-galactopyranose
SNOCAP	S-nitrosocaptopril
SNTG	S-nitroso-β-D-thioglucose
SUL	sulfanilamide
TNB	2-nitro-5-thiobenzoic acid
TRIS	tris(hydroxymethyl)aminomethane
UV	ultraviolet
Vis	visible
X^-	halide anion or a nucleophile

6.5.2 Definition of Symbols

The following symbols were used in this thesis.

$\triangle H^{o\ddagger}$	enthalpy of activation
$\triangle S^{o\ddagger}$	entropy of activation
[A]	concentration of A
Abs.	absorbance
c	concentration
h	Planck's constant
k	rate constant
K	equilibrium constant
K_a	acid dissociation constant
k_B	the Boltzman constant
k_{obs}	observed rate constant
l	pathlength of the cell
M	mol dm^{-3}

R	the gas constant
s	second
T	temperature
ε	extinction co-efficient
λ	wavelength

$pH = -\log_{10}([H^+] / mol\ dm^{-3})$

$pK_a = -\log_{10}(K_a / mol\ dm^{-3})$

6.5.3 Chemical Structures Not Shown Previously

The chemical structures shown in table 6.1 are of chemicals used in the research presented in this thesis that are not shown elsewhere.

Chemical Name	Chemical Structure
EDTA	
Neocuproine	
SNAC	
S-Nitroso-1-amino-2-methyl-2-propane thiol	
SNOCAP	

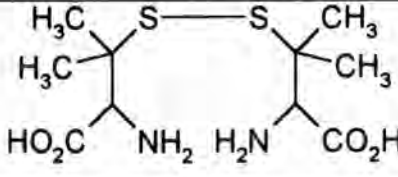| Penicillamine disulfide | |

Table 6.1 Chemical structures not shown previously.

6.6 References

1) L. Field, R. V. Dilts, R. Ravichandran, P. G. Lenhert and G. E. Carnahan, *J. Chem. Soc., Chem. Commun.*, 1978, 249.

2) D. J. Barnett, Ph.D. thesis, University of Durham, 1994, 77.

3) L. A. Shinobu, S. G. Jones and M. M. Jones, *Acta Pharmacol. et Toxicol.*, 1984, **54**, 189.

4) P. Giboreau and C. Morin, *J. Org. Chem.*, 1994, **59**, 1205.

5) A. Vogel, 'Textbook of Quantitative Inorganic Analysis', Longman, London, 1978, 755.

6) Scientist, version 2.02, Micromath Scientific Software, Salt Lake City, UT, USA. www.micromath.com

Chapter 7

Appendix

Chapter 7: Appendix

7.1 Conferences Attended

i. Royal Society of Chemistry Organic Reaction Mechanisms Group. 3rd October 2000 at Bracknell. Presented a talk called, "Direct NO Transfer Between S-Nitrosothiols and an Iron Complex".

ii. Postgraduate Winter School on Organic Reactivity. (WISOR X) 7th – 14th January 2001 at Bressanone, Italy. Presented a poster called, "Direct NO$^+$ Transfer Between S-Nitrosothiols and an Iron Complex".

iii. 8th European Symposium on Organic Reactivity. (ESOR 8) 1st – 6th September 2001 at Cavtat, Croatia. Presented a poster called, "Direct NO Transfer Between S-Nitrosothiols and Iron Complexes".

iv. Royal Society of Chemistry Organic Reaction Mechanisms Group. 28th September 2001 at Liverpool. Presented a talk called, "An Investigation into a 1,2-Dithiol-Induced S-Nitrosothiol Decomposition".

7.2 Durham University Chemistry Department PhD Induction Courses

i. Safety. (Fire fighting, breathing apparatus, COSHH and departmental safety rules)
ii. Handling heavy equipment.
iii. Library resources.
iv. Research resources and search methods.
v. Computing.
vi. Glassblowing techniques.
vii. Analytical Services. (Mass spectrometry, nuclear magnetic resonance spectroscopy, elemental analysis and chromatography)